SANDIA REPORT
SAND2023-09936R
Printed September 2023

Sandia National Laboratories

Self-healing, self-assembling islanded power systems using only local measurements

Michael E. Ropp, Olga Lavrova, Matthew J. Reno, Elijah Silva, McKendree A. Densel, Lara N. Kassabian, Milan Biswal, Ada Ramoko, Satish J. Ranade

Prepared by
Sandia National Laboratories
Albuquerque, New Mexico
87185 and Livermore,
California 94550

Issued by Sandia National Laboratories, operated for the United States Department of Energy by National Technology & Engineering Solutions of Sandia, LLC.

Available to DOE and DOE contractors from
U.S. Department of Energy
Office of Scientific and Technical Information
P.O. Box 62
Oak Ridge, TN 37831

Telephone: (865) 576-8401
Facsimile: (865) 576-5728
E-Mail: reports@osti.gov
Online ordering: http://www.osti.gov/scitech

Available to the public from
U.S. Department of Commerce
National Technical Information Service
5301 Shawnee Rd
Alexandria, VA 22312

Telephone: (800) 553-6847
Facsimile: (703) 605-6900
E-Mail: orders@ntis.gov
Online order: https://classic.ntis.gov/help/order-methods/

ABSTRACT

This SAND report collects the results from the LDRD project "SHAZAM", which aimed to push the limits of performance for self-healing, self-assembling power systems whose sectionalizing and load-control agents rely on local measurements only (i.e., only what they can measure at their own terminals, with no data sharing between agents). This work includes self-networking microgrids. The key objectives of this work were a) to demonstrate how high the performance of local-measurement-only self-assembling power systems can be; and b) to solve certain technical problems associated with such systems, such as their inability to prevent the accidental formation of closed loops and their tendency to thermally overload some conductors.

"SHAZAM" investigators a) demonstrated that the performance of such systems can be surprisingly high, b) demonstrated that such systems are quite robust to all kinds of variations, and c) developed and demonstrated solutions to several key challenges associated with this type of system.

ACKNOWLEDGEMENTS

The authors would like to acknowledge Ray Byrne (Sandia) and Satish Ranade (New Mexico State University) for their support of and creative input into the SHAZAM project.

CONTENTS

LIST OF FIGURES

LIST OF TABLES

EXECUTIVE SUMMARY

Self-healing power systems can be exceptionally robust during severe events, and are thus desirable elements of an electric power resilience strategy. Self-healing power systems must be controlled and protected, like any other power system. However, if the power sources in such a system are a) geographically distributed and b) inverter-based, then that control and protection face some serious challenges. Solutions to these challenges exist today, but nearly all of these involve sharing of data between power system elements, and the communications systems required for that data sharing create significant challenges of their own.

This report documents the learning and results from a project called "SHAZAM", an LDRD-funded project at Sandia National Laboratories. SHAZAM sought to push the performance boundaries of self-healing power systems whose elements rely on *local measurements only*, and thus do not require a data-sharing communications system. SHAZAM resulted in a collection of techniques, some existing and some all-new, to create self-healing power systems relying only on local measurements but exhibiting very high performance and exceptional robustness. Results reported herein include the following.

1. A large number of transient simulation tools were developed, and are described here.
2. SHAZAM includes techniques for basic functions such as automatic load-generation balancing and fault isolation. These functions were successfully demonstrated.
3. Black-start and post-fault self-assembly of power systems were demonstrated for a wide array of scenarios. In all contingency cases tested, the final operating state of the power system using SHAZAM techniques had the maximum amount of load energized, and all faults were isolated.
4. A technique was developed to ensure that self-healing power systems using local measurements only will not unintentionally self-assemble into a closed loop. This technique was demonstrated in transient simulation.
5. A technique was developed to enable self-healing systems using only local measurements to avoid thermal overloading of conductors when transferring loads from one circuit to another.
6. A technique was developed to ensure that no two adjacent relays have the exact same closing time. This ensures that when adjacent microgrids spontaneously network with each other during self-assembly, an asynchronous connection will be prevented.

ACRONYMS AND TERMS

Acronym/Term	Definition
FLISR	Fault Location, Isolation, and Service Restoration
GFL	Grid Following
GFM	Grid Forming
IBR	Inverter-Based Resource
IEEE	Institute for Electrical and Electronics Engineers
LDRD	Laboratory-Directed Research and Development
MAE	Mean Absolute Error
MBR	Microgrid Boundary Relay
SHAZAM	Self-Healing Adaptive Zeta-Alpha Microgrid
SHePS	Self Healing Power System
SST	Solid State Transformer
UFLS	Under Frequency Load Shedding
UVLS	Under Voltage Load Shedding
UVOC	Under Voltage supervised Over Current

1. INTRODUCTION

A self-healing power system (SHePS) has the ability to automatically detect that it is not operating properly and restore as much of the system as possible to normal operation [1]. Future SHePS will be energized by grid-forming (GFM) inverter-based resources (IBRs) or solid-state transformers (SSTs).

A SHePS must be able to perform a) protection, or detection and isolation of a fault; and b) restoration, in which all of the healthy parts of the system are re-energized. A great deal of work has been done on SHePS [2], [3], [4], [5], [6] and FLISR-type SHePS [7] are commercially available (for example, see [8] and [9]).

Today's SHePS tend to have three significant drawbacks.

1. They generally rely on sharing of data via high-speed communication networks [10]. Communications improve performance under "blue-sky" conditions, but a) they are expensive, often to the point of rendering projects unfeasible; b) they can become unreliable during "black-sky" events; and c) they introduce cyber vulnerabilities. Maurer et.al. wrote in 2012: "Communications is the Achilles' Heal (sic) of any self-healing system. No matter what type of self-healing system you select—centralized, substation-based, or distributed intelligence—that fact is still true." [11]
2. They cannot perform self-assembly or form ad-hoc networked microgrids, which forces each individual system to remain entirely reliant on its own resources, limiting resilience benefits. One reason is that the formation of unintentional meshes or loops must be avoided. Intentional loops can increase reliability [12] but if circuits not designed to be operated as a closed loop are inadvertently connected in that way, large circulating currents can cause tripping of protection, potential damage to equipment, and difficulties in voltage regulation.
3. Because they tend to rely on algorithms using shared data from many endpoints, attempting to apply them to large systems results in a nearly exponential explosion of data and communications endpoints. Thus, they tend not to be very scalable.

In order to overcome these obstacles, there is a need for SHePS technology that relies on local measurements only. However, when one relies only on local measurements, two additional challenges appear: one related to the current limitations of IBRs, and the other related to the geographic distribution of grid-forming sources.

- With IBRs, time-overcurrent protection, which is the most-used protection tool [13], becomes ineffective due to the fault current limitations of the power electronics [14]. Directional elements would generally be the next tool used, followed by distance relays, but these too become unreliable with geographically-distributed GFM IBRs. In addition, when time-overcurrent cannot be used, thermal overload protection of conductors becomes difficult, which is a problem that no communications-free method has solved to date.
- Today's restoration procedures are designed around a centralized system architecture [3]. System restoration is a complex process that involves coordinating black-start resources, identifying critical paths, estimating surge loads during re-energization, and understanding the dynamics of the system at each step of the restoration process [15]. It is widely recognized that distributed resources can assist with system restoration, but most proposed techniques for achieving this still rely on centralized communication and control [15], [16].

This report details the results from a Lab-Directed Research and Development (LDRD) project called "SHAZAM", which stands for "Self-Healing Adaptive Zeta-Alpha Microgrid"[1]. SHAZAM facilitates allowing off-grid power systems energized by geographically-distributed GFM IBRs to be self-healing and self-assembling, using **local measurements only**. The various parts of the SHAZAM concept are described in the following sections.

The process envisioned in SHAZAM is an application to power systems of the concept of "self-assembly" [17], [18], a term borrowed from chemistry, biology, and materials science [19], [20] in which larger, more complex structures are formed spontaneously, without centralized direction. Self-assembling power systems could have major resilience benefits. They could be used by themselves, providing a minimum-cost high-flexibility option that avoids the problems associated with communications-dependent systems described above, or they could be used as backups to communications-based systems.

[1] In the original version of this concept, zeta was the undervoltage trip threshold and alpha was the underfrequency trip threshold. The concept has evolved considerably since then, but the name has stuck.

2. GENERATION-LOAD BALANCING

Automatic generation-load balancing in an off-grid power system energized by GFM IBRs is achieved in SHAZAM using a prioritized UFLS function in each load relay, along with a linear power-frequency (P-f) droop that is the same in each GFM IBR. This common P-f droop characteristic allows the load relays to use the system frequency as a measurement of how loaded the sources are. The P-f droop used in this work is shown in Figure 1. When the frequency reaches 59.5 Hz, all available GFM IBRs are at 90% loading. At 50% loading the frequency is 60.0 Hz.

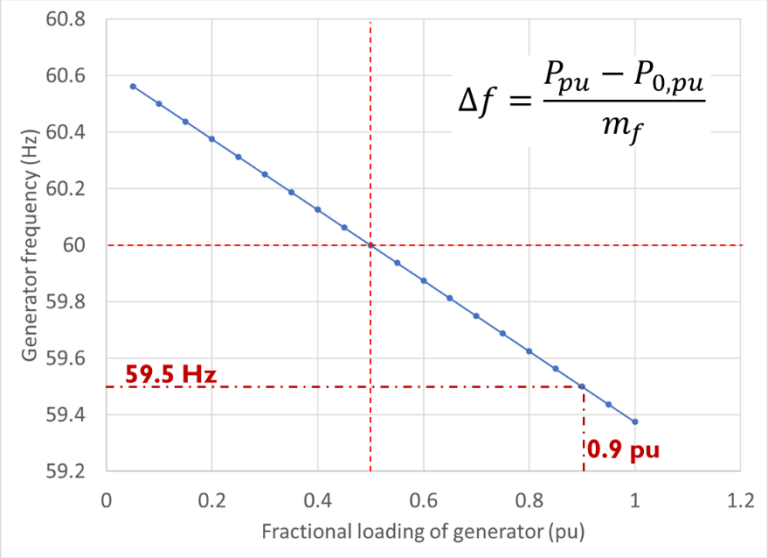

Figure 1. Power-frequency droop used in GFM IBRs in SHAZAM.

Loads are prioritized into three Groups. Group A loads are the most critical and will be de-energized only as a last resort. As a general design rule, in a power system designed to use SHAZAM, the GFM IBRs should be collocated with the Group A loads to the greatest extent possible. Group C loads are the least critical. These will be shed first, and will be brought back online last. Group B falls in-between. If more granularity in load prioritization is desired, more Groups can be defined.

The load relays also employ a time-underfrequency characteristic that will lead to UVLS if the inverters become sufficiently overloaded that they reach their current limits. The time-underfrequency characteristics for all three load Groups are shown in Figure 2. The time delays used in the time-voltage functions employ two parts: a fixed time delay, plus a random time delay whose maximum value is ±10% of the fixed time delay. The random time delay is intended to avoid having any two load relays trip at exactly the same time, the idea being to increase the possibility of preserving some of the loads in the event of an overload by not tripping the entire load Group all at the same time. The total time delays (fixed plus random part) for each load Group and voltage level are shown by the dashed lines in Figure 2.

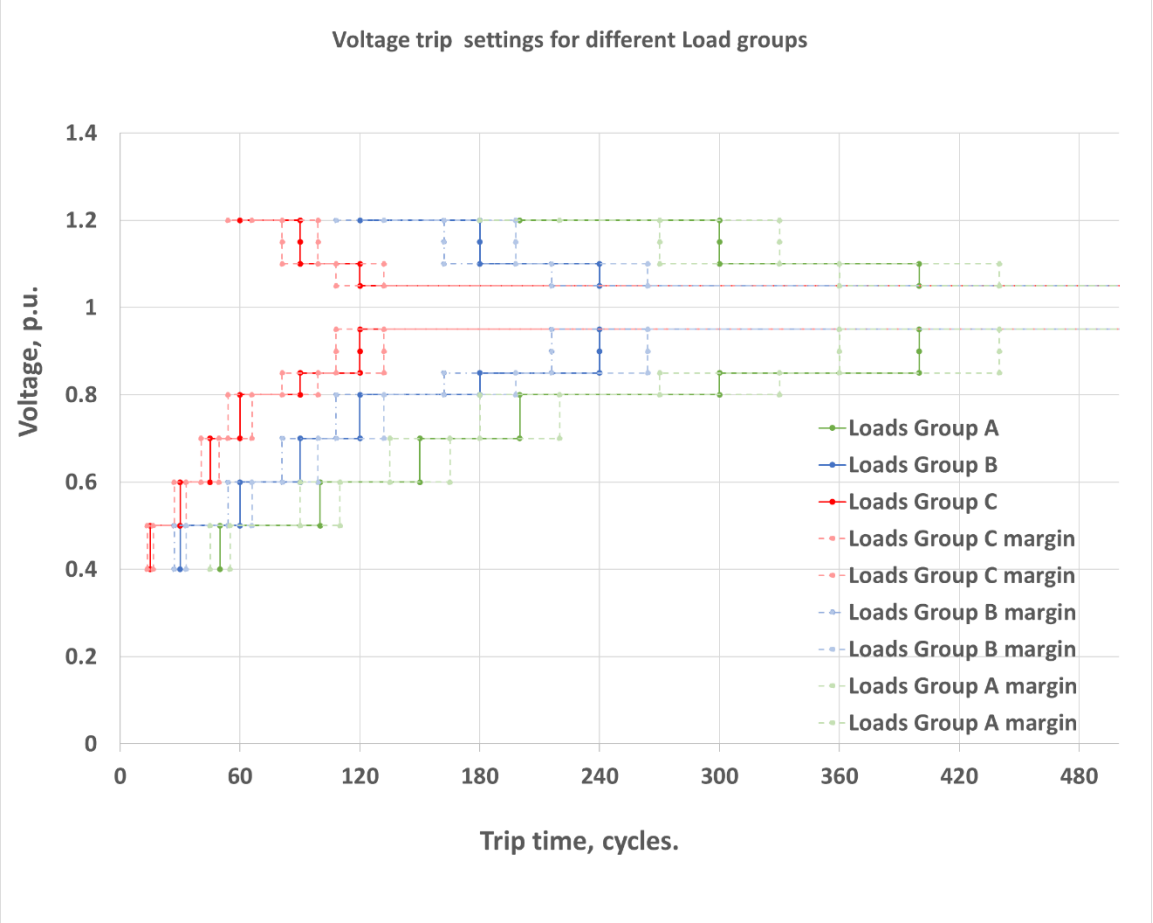

Figure 2. Figure showing the voltage-time tripping characteristic used in SHAZAM load relays. The green lines are for Group A, blue for Group B, and red for Group C.

The reason why both UFLS and UVLS are used in SHAZAM is because experiments conducted during the SHAZAM LDRD indicated that frequency measurements may cease to be a reliable indicator of source loading levels when GFM IBRs reach their current limits, because not all IBRs maintain a P-f droop characteristic when current limiting. The UFLS function maintains generator-load balancing under normal loading conditions, and the UVLS works during severe overloads, including faults.

It should also be noted that some GFM IBRs produce nonsinusoidal current outputs when they are in current-limiting mode. There are several ways in which this can happen. For example, some IBRs achieve current limiting by simply hard-limiting or "clipping" the current waveform. Some others simply seem to struggle with waveform quality during current limiting, and these can produce a variety of waveform distortions. Experience gained during the SHAZAM project suggests that IBRs that do not produce sinusoidal currents when current-limiting should be avoided for off-grid use, because the nonsinusoidal waveforms lead to voltage, current, and frequency measurement errors that can cause unpredictable, and in some cases highly undesirable, system behavior.

3. FAULT LOCATION, ISOLATION, AND SERVICE RESTORATION

3.1. Description

One of the most basic functions that a SHePS must be able to perform is to locate and isolate shunt faults, and then restore as much of the system as possible to normal operation. This process of Fault Location, Isolation, and Service Restoration is commonly referred to as "FLISR". As discussed above, the FLISR process can become more difficult in off-grid power systems that a) are energized only by GFM IBRs, or b) are energized by sources at multiple source buses, and the specific sources active during any event will not be known in advance. SHAZAM aims to create a highly robust FLISR algorithm that:

- Enables fault isolation when the system is energized by distributed GFM IBRs (in other words, *both* conditions a) and b) above are met), when it is not known in advance which combination of GFM IBRs is active in any specific situation;
- Robustly detects and isolates faults in any part of the system;
- Preserves as much of the load as possible.

The way this is handled in SHAZAM is described by the following sequence of events. Consider a system consisting of two adjacent distribution circuits designed to be a SHAZAM SHePS (Figure 3(a)). This system includes both grid-forming (blue) and grid-following (green) IBRs, including an IBR on the subtransmission circuit serving both distribution transformers. Red squares indicate closed relays, and green squares indicate open relays. In Figure 3(a), note that the breakers on the subtransmission system are both green (open), indicating that the portion of the system shown is operating off-grid. This off-grid system has been designed according to the SHAZAM rule that each Group A load has a GFM IBR.

Figure 3(a): the system is operating in steady state. All IBRs are operating and there is sufficient source capacity that all loads are being served.

Figure 3(b): A persistent shunt fault occurs on one of the laterals from feeder FDR_1. The GFM IBRs reach their current limits, and the voltage collapses across the system. At each feeder head-end, there is a Microgrid Boundary Relay (MBR) that opens quickly on undervoltage, thus isolating the faulted feeder from, and preventing load shedding in, the rest of the system.

Figure 4(a): UVLS initiates on FDR_1. Group C loads shed first, as indicated by load relay blocks turning green. The timing of the Group C load shedding is determined by the red time-undervoltage curves shown in Figure 2. Typically, all of the Group C loads are shed by ~ 0.5 s post-fault.

Figure 4(b): shedding Group C does not resolve the undervoltage on FDR_1. Because there is a fault, Group C load shedding does not clear the undervoltage condition. Group B loads are then shed, as indicated by load relay blocks turning green, with timing according to the blue time-undervoltage curves shown in Figure 2. Typically, shedding of the Group B loads is completed by ~1.0 s post-fault.

Figure 5(a). Shedding Groups B and C has not cleared the undervoltage. At this point, all of the line relays on FDR_1 open, causing the system to retreat to within the boundaries of a few "core microgrids" centered around GFM IBRs, as indicated by the dashed green lines. (Note that if there

were Group A loads outside of these "core microgrid" boundaries, those Group A loads would lose power at this point.) The line relays typically open by about 1.5 s post-fault[2].

Figure 5(b): system reassembly begins. The border of each "core microgrid" includes a line relay that now detects in-range voltage on one side only. Those breakers are allowed to reclose after a time delay, and the energized-system boundaries (green dashed lines) expand. The reclose time delay is

$$t_{reclose} = t_{fixed} + t_{rand} + t_{tagged} \quad (1)$$

$$t_{tagged} = t_{inc} \times k \quad (2)$$

where $t_{reclose}$ is the reclose delay applied for in-range voltage on one side only, t_{fixed} is a fixed delay (typically 2-5 seconds), t_{rand} is a random time element similar to that described above for the load relays, t_{tagged} is a "tagged time", t_{inc} is a pre-selected timing increment that is much shorter than t_{fixed} (in this work, t_{tagged} = 300 ms), and k is a "tag" used to determine the "tagged time". The tag and tagged time are explained below in Section 4.

Figure 6(a): self-assembly continues. The next set of line relays that detect good voltage on one side only are allowed to reclose after a time delay, and the energized-system boundaries expand again. Note that there is now a line relay at the center of FDR_1 that detects in-range voltage on both sides. That line relay will thus reclose on sync check (IEEE function 25 [21]). Note also that toward the top of FDR_1, there are two adjacent line relays that are on the boundaries of adjacent energized systems. Each of these line relays detects in-range voltage on one side only, but it is imperative that they not be allowed to reclose at the same time, or else an asynchronous connection of the two energized islands is likely. In SHAZAM, the random and tagged timing elements in Equations (1) and (2) provide this temporal separation between the line relays, as is discussed further in Section 4.

Figure 6(b): self-assembly continues. The line relays that were on the boundaries between adjacent microgrids have closed. However, the line relay on the faulted lateral has also reclosed onto the fault. That line relay sees a voltage collapse immediately after its closure, accompanied by high current. The UVOC function becomes active.

Figure 7(a): about 250-300 ms after Figure 6(b), UVOC opens and locks out the line relay on the faulted lateral. This isolates the fault.

Figure 7(b): self-assembly continues. The last line relays on FDR_1 reclose.

Figure 8(a): the load relays on FDR_1 detect in-range voltage and begin to reclose, in load-priority order with Group B being energized first and Group C later. In this case, the faulted lateral did not contain any GFM IBRs, so all of the loads on FDR_1 can be served. If this were not the case, then the frequency would begin to droop as load is picked up according to Figure 1, and if the frequency becomes too low, relays on some of the Group C loads do not reclose, preventing an overload.

Figure 8(b): final system state. Eventually the MBR at the head end of FDR_1 recloses, and the grid-following (GFL) assets on FDR_1 restart. The system returns to steady state. The time between Figure 3(b) and Figure 8(b) is typically on the order of 15 to 20 seconds in this system.

[2] Utility advisors to this project indicated that a maximum definite fault clearing time of 2 s is desirable, so this was used as an upper limit on the SHAZAM timing.

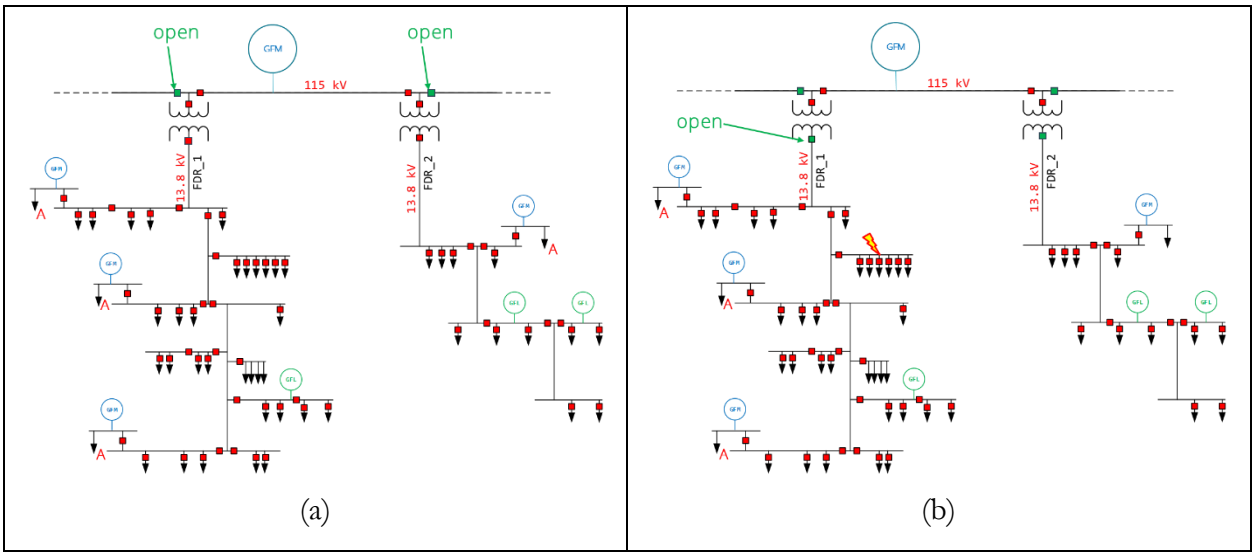

Figure 3. SHAZAM FLISR example, part 1. (a) Initial steady state operation. (b) A fault occurs on FDR_1.

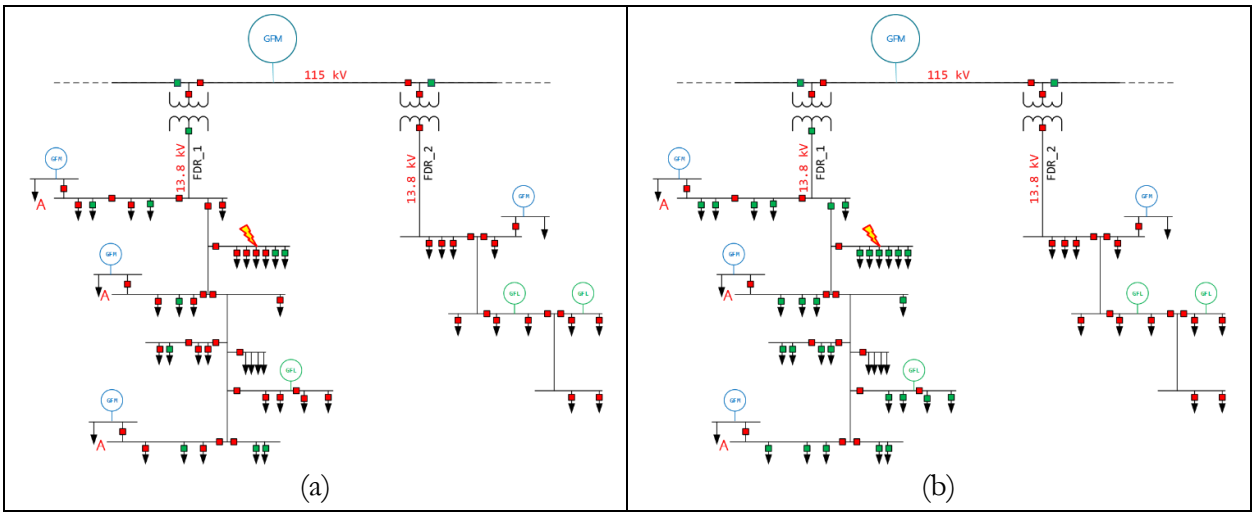

Figure 4. SHAZAM FLISR example, part 2. UVLS. (a) Group C loads are shed. (b) Group B loads are shed.

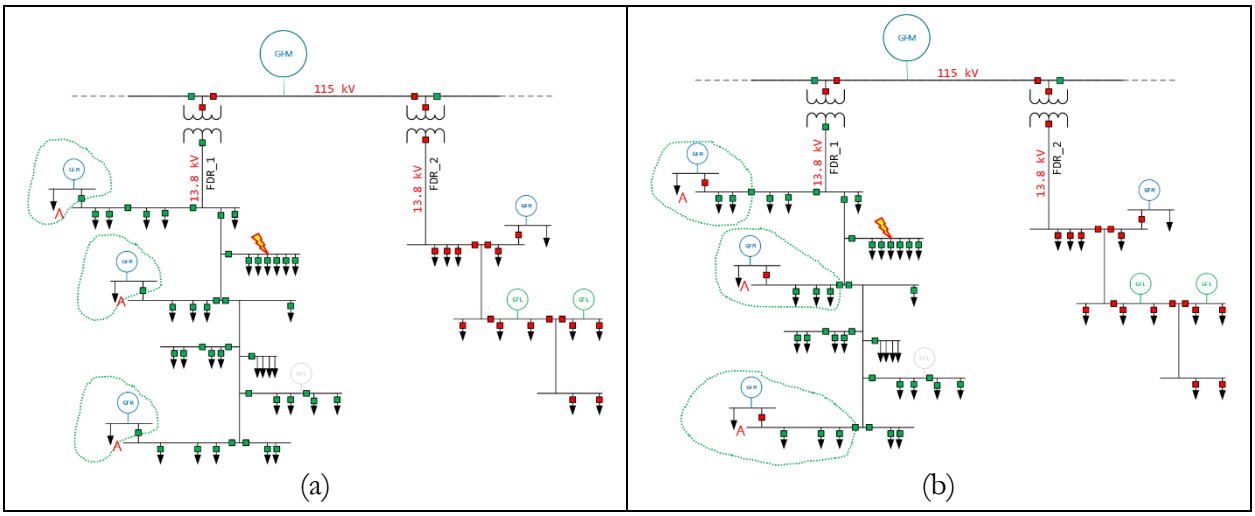

Figure 5. SHAZAM FLISR example, part 3. (a) UVLS has not resolved the undervoltage, so all line relays open. The system retreats back to a set of "core microgrids" centered on each GFM IBR, as shown by the green dashed boundaries. (b) First step in reassembly. Line relays begin reclosing on one-sided voltage.

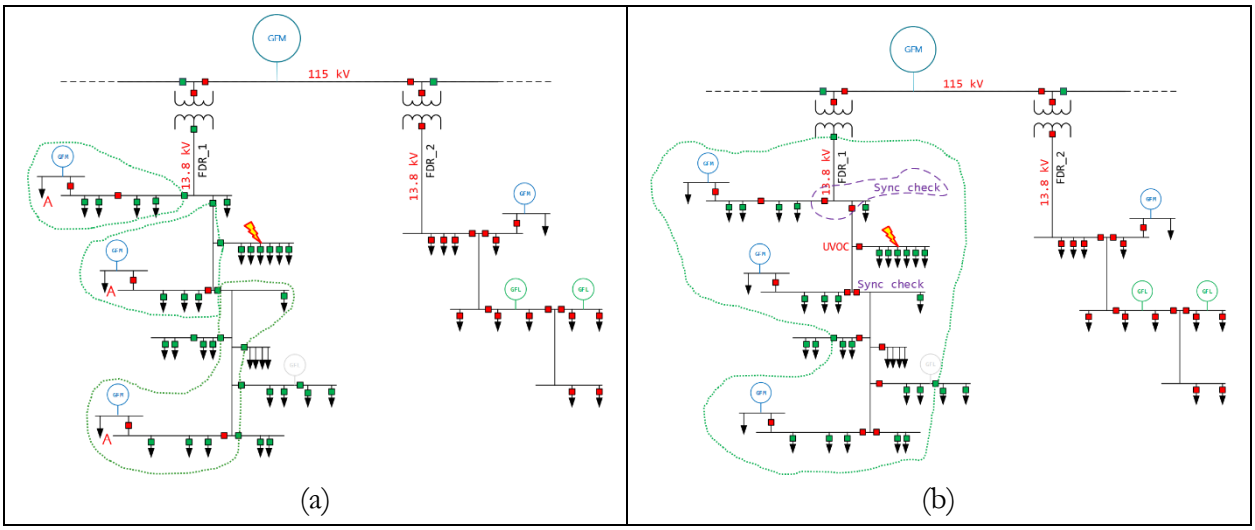

Figure 6. SHAZAM FLISR example, part 4. (a) Self-assembly continues. The microgrid boundaries continue to expand. (b) The line relay in the center of FDR_1 detects in-range voltage on both sides, and thus closes on sync check. Similarly, the two line relays in the purple boundary near the top of FDR_1 are time-separated; one closes first and then the other closes on sync check. Also, note that a line relay has reclosed onto the fault. Thus, that line relay detects a voltage collapse and high current immediately after its closure. UVOC is activated.

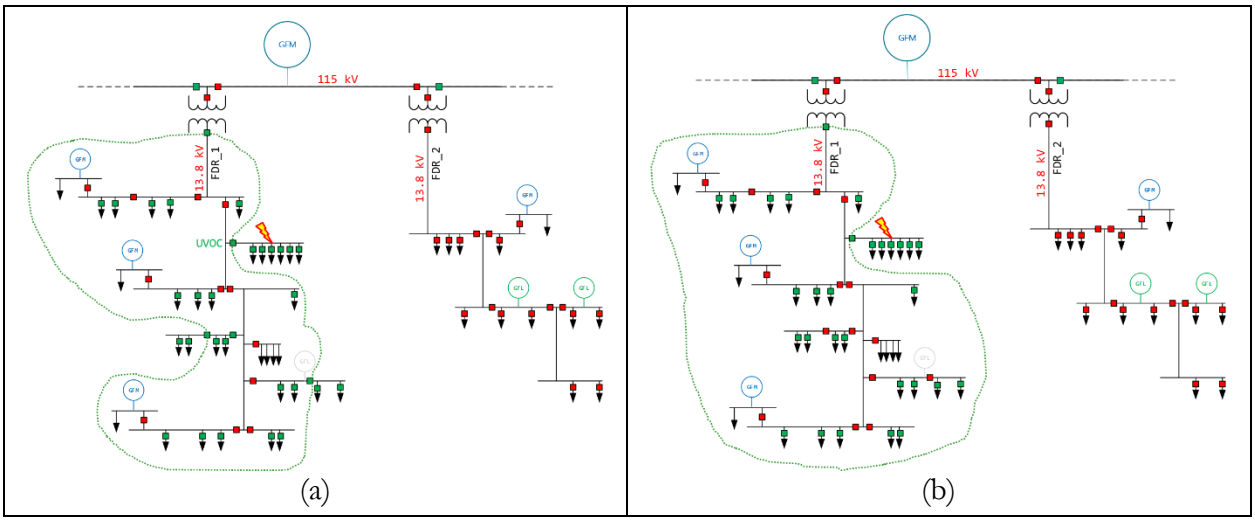

Figure 7. SHAZAM FLISR example, part 5. (a) UVOC re-opens and locks out the breaker that closed onto the fault. The fault is now isolated. (b) The last of the line relays on FDR_1 recloses.

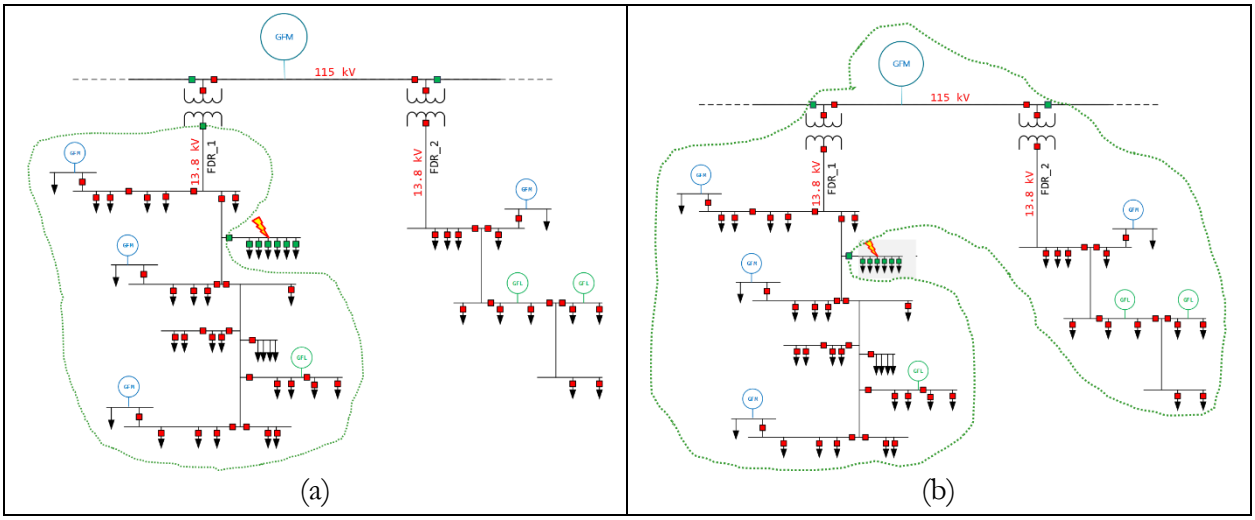

Figure 8. SHAZAM FLISR example, part 6. (a) Load relays see in-range voltage and begin to reclose according to their load Group, with Group C being picked up last. The frequency drops as loads come online, and if the frequency drops below a load's underfrequency limit it will not close its load relay. (b) Final system state. The fault is isolated, the two feeders are rejoined into one microgrid, and all loads outside of the faulted zone are being served.

3.2. Demonstrations

This section provides results from demonstrations of the SHAZAM self-assembly concept using a model of the IEEE 13-bus distribution test circuit shown in Figure 9. Table 1 shows the tagged timer values[3] for each of the line relays, and Table 2 shows the Load Group assignment for each of the loads.

[3] Tagged timers are discussed in Section 4.2.

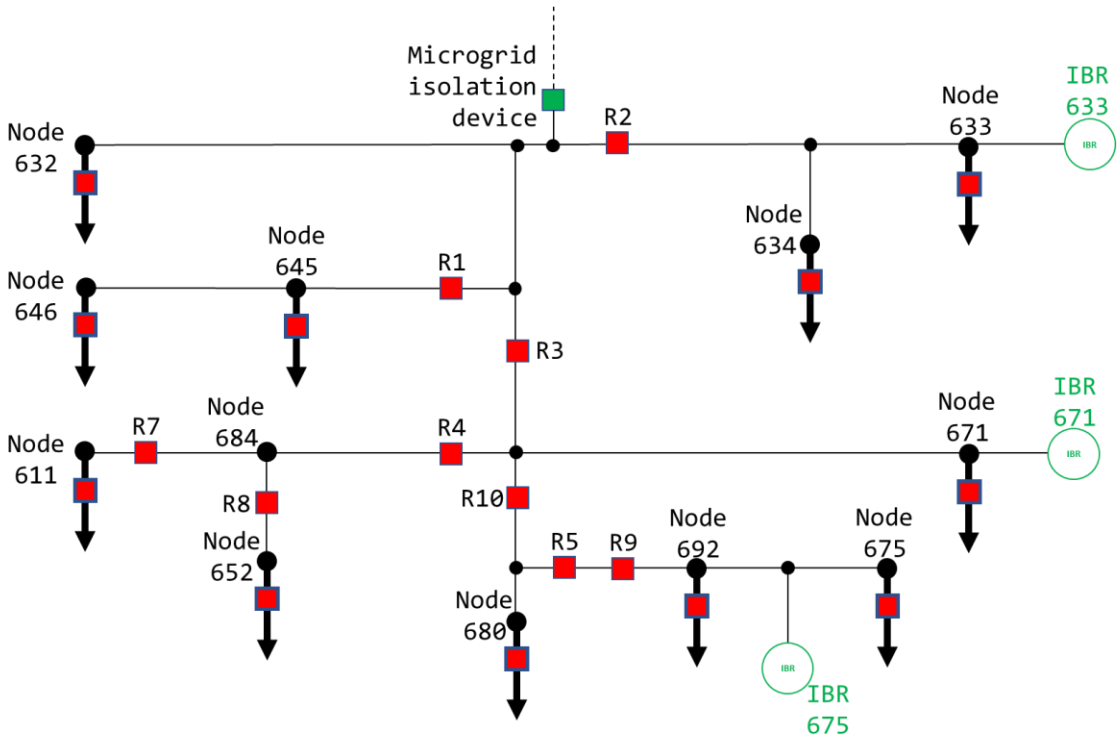

Figure 9. One-line diagram of the IEEE 13-bus system, operating off-grid, with three grid-forming IBRs (in green at the right).

Table 1. Tag values used in each line relay.

Line Relay	R1	R2	R3	R4	R5	R6	R7	R8	R9	R10
Tag Value	1	1	0	0	1	1	1	1	0	0

Table 2. Load group assignments.

Load number	632	675	680	671_2	692	611	652	645	646	671	634	671LL
Load Group	A	B	C	A	B	C	A	B	C	A	B	C

3.2.1. Results using manufacturer-specific inverter models

This section includes SHAZAM self-assembly demonstrations when the 13-bus model is energized by three grid-forming IBRs represented using a manufacturer-specific, code-based PSCAD model. These inverters are each rated at 3.95 MVA.

3.2.1.1. Black Start

The black-start case is shown in Figure 10. This figure shows the PSCAD model of the 13-bus system, off-grid, with the three grid-forming IBRs. The colored lines show the boundaries of the sub-microgrids at different stages along the black-start process. At the beginning of the black-start case, all line and load relays are open, which creates a set of isolated core microgrids centered around each IBR indicated by the **red** boundaries in **Error! Reference source not found.**. At the edge of each c ore microgrid is an open line relay that sees in-range voltage on one side, and 'zero' voltage on the other side. These line relays are allowed to close after their time delay has elapsed. The line relays with a tag value of zero (Table 1) close first, expanding the microgrid boundaries to the **blue** lines in Figure 10.

Note that there is not a blue microgrid boundary near IBR 633 (the one at the top of Figure 10). That is because the line relay at the boundary of that microgrid, line relay R2, sees good voltage on one side only but it has a tag value of 1. Thus, it has a longer reclose delay t_{close} and does not close with the rest of the 'blue' group.

The next set of line relays then close, moving the microgrid boundaries to the **green** line**s** in Figure 10. All of these close due to seeing in-range voltage on one side only, except for R2, which is between microgrids 633 and 671. At this step in the process, R2 sees in-range voltage on both sides, and it closes after synchronization check and loop-prevention functions are satisfied.

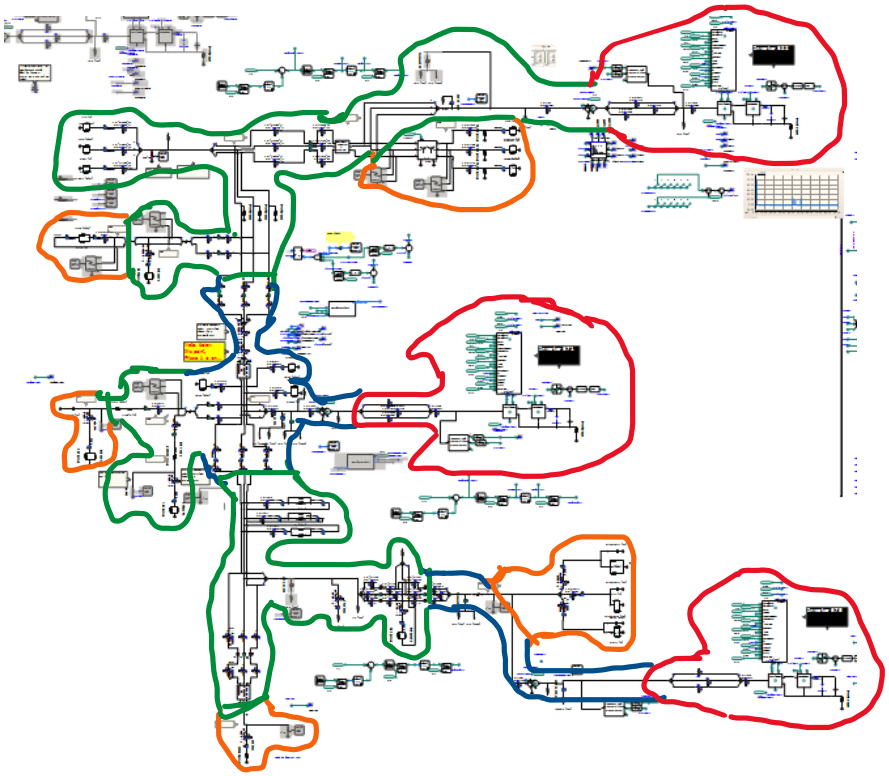

Figure 10. Diagram showing propagation of microgrid boundaries during the black-start case

At this point, all of the line relays are closed. Load relays will begin closing according to their group-specific closure delays (Table 2) as soon as they are supplied with in-range voltage. In this example, the final group of load relays closes to move the microgrid boundaries to the orange lines in Figure 10. In this scenario there are sufficient resources to carry all of the loads, so the frequency does not drop below the load relay underfrequency thresholds, and in the final system state all of the loads are energized.

3.2.1.2. A-B fault at load 632

In this use case, a phase-to-phase fault occurs at node 632 at $t = 15$ s. When the fault occurs, the IBRs reach their current limits, the voltage collapses, and the system begins to shed load following the time-undervoltage function in Figure 2. The load-shedding process is illustrated in Figure 11. The loads marked by **red** X's, all in group C, trip within the first 1 s after the fault occurs. The undervoltage persists, so the next set of loads, marked by **blue** X's, are shed between 1 and 1.5 s post-fault. Then, between 2 and 2.5 s post-fault, all loads in group A trip, marked by **green** X's. Finally, at 2.5 s post-fault, all of the line relays (R1, R4, R6, R7, and R8) end up tripping, marked by **orange** X's.

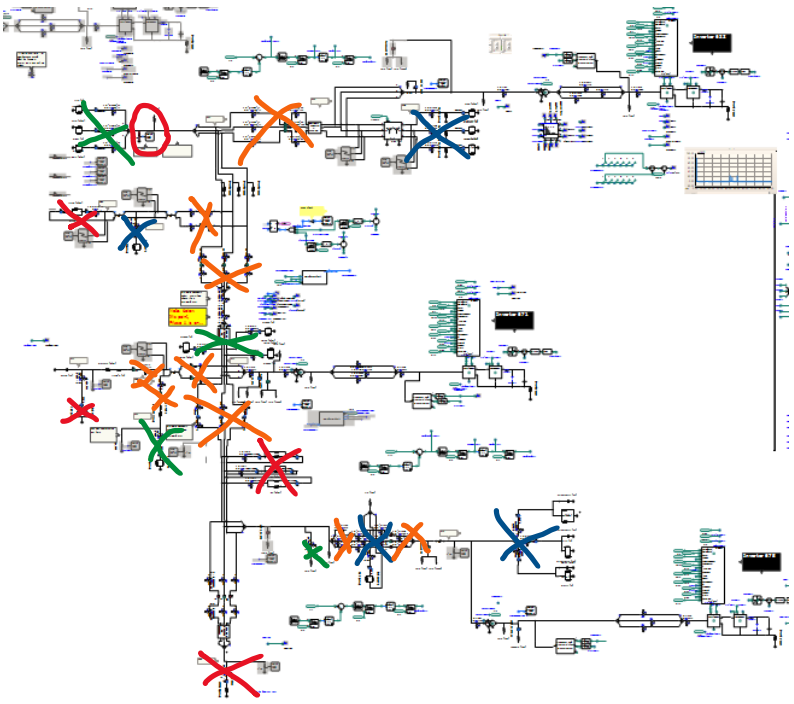

Figure 11. Load shedding following an A→B fault at node 632.

When load shedding is completed, the fault persists and thus the undervoltage persists. At that point, about 3 s post-fault, all of the remaining line relays open, forming the three 'core microgrids' whose boundaries are the **red** lines in Figure 12.

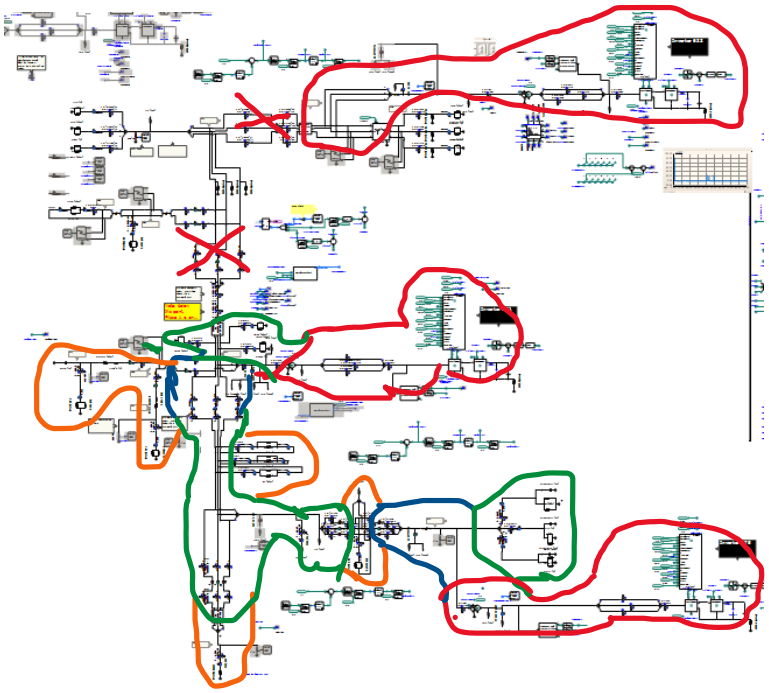

Figure 12. System reassembly following A→B fault at node 632.

The reassembly process is illustrated in Figure 12, and proceeds similarly to the black-start case. The first line-relay reclosure moves the boundaries of microgrids 671 and 675 to the **blue** boundaries, over an interval stretching from about 3.454 s after the fault. Also, line relay R3 closes onto the fault at 3.469 s post-fault, then re-opens and locks out on UVOC, as indicated by the red X near the center of Figure 12. Similarly, at 3.93 s post-fault, R2 recloses onto the fault, then re-opens and locks out on UVOC, indicated by the red X toward the upper left corner of Figure 12. At roughly 8 s post-fault, the system has reached its final state: microgrid 633 is operating in isolation, microgrids 671 and 675 have reconnected, the faulted zone around node 632 is isolated, and all of the loads outside of the faulted zone are being served. The load and line relay reclosing times are given in Table 3 and Table 4, respectively. Load relays 632 and 634 remain open because they are in the faulted zone.

Table 3. Load relay closing times (post-fault) for the AB fault at node 632. NT = never tripped; RO = remains open.

Load	632	675	680	671_2	611	692	652	645	646	671	634	671LL
Closing time (s)	RO	4.87	6.96	4.2	6.826	5.47	5.34	RO	RO	4.384	RO	5.63

Table 4. Line relay closing times (post-fault) for the AB fault at node 632. RO = remains open.

Line Relay	R1	R2	R3	R4	R5	R6	R7	R8	R9	R10
Closing Time (s)	RO	3.73; UVOC lockout at 3.93	3.469; UVOC lockout at 3.54	3.452	5.657	4.847	4.846	4.843	3.453	3.454

3.2.1.3. A-G fault at load 633

In this use case, a phase A-to-ground fault occurs at node 633. IBR 633 is in the faulted zone. As before, the load relays open on time-undervoltage as shown in Figure 13. First to open are the group C loads marked with **red** X's, all within 1 s post-fault. The group B loads marked with **blue** X's open between 1 and 1.5 s post-fault, and the last group of loads to trip, all group A, are marked with **green** X's and trip around 2.5 s post-fault. Lastly line relays trip between 2.5 and 3 seconds, marked with **orange** X's**.**

The system then self-assembles as shown in Figure 14. At first, the boundaries of the energized microgrids are the **red** lines. The first set of line relays closes, extending the boundaries to the **blue** lines, then to the **green**, and then to the **orange**. The load and line relay closure times post-fault are given in Table 5 and Table 6, respectively.

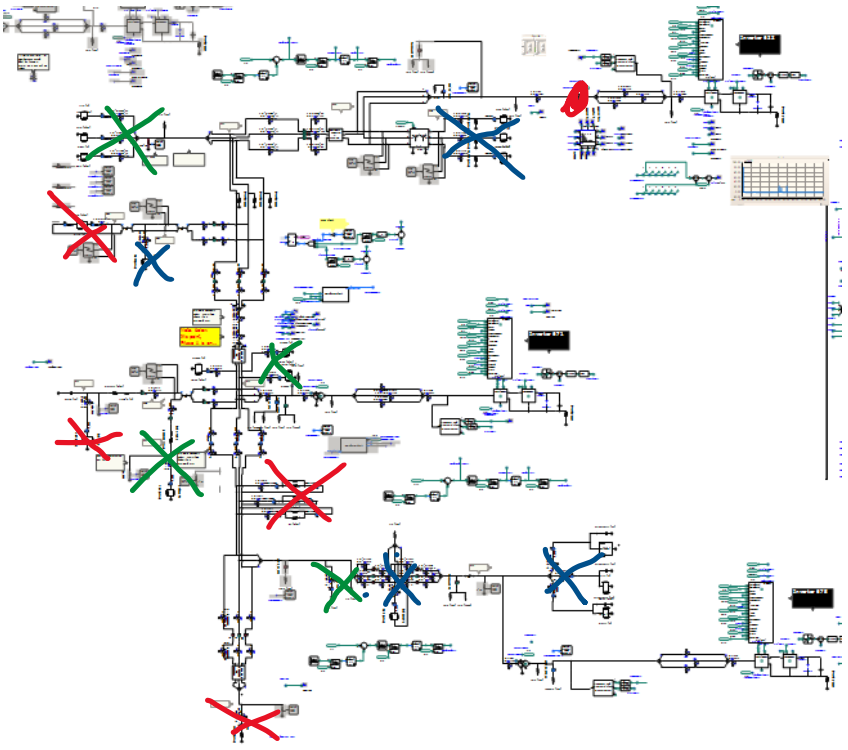

Figure 13. System diagram showing the order of line relay opening for the case of a 1LG fault at node 633.

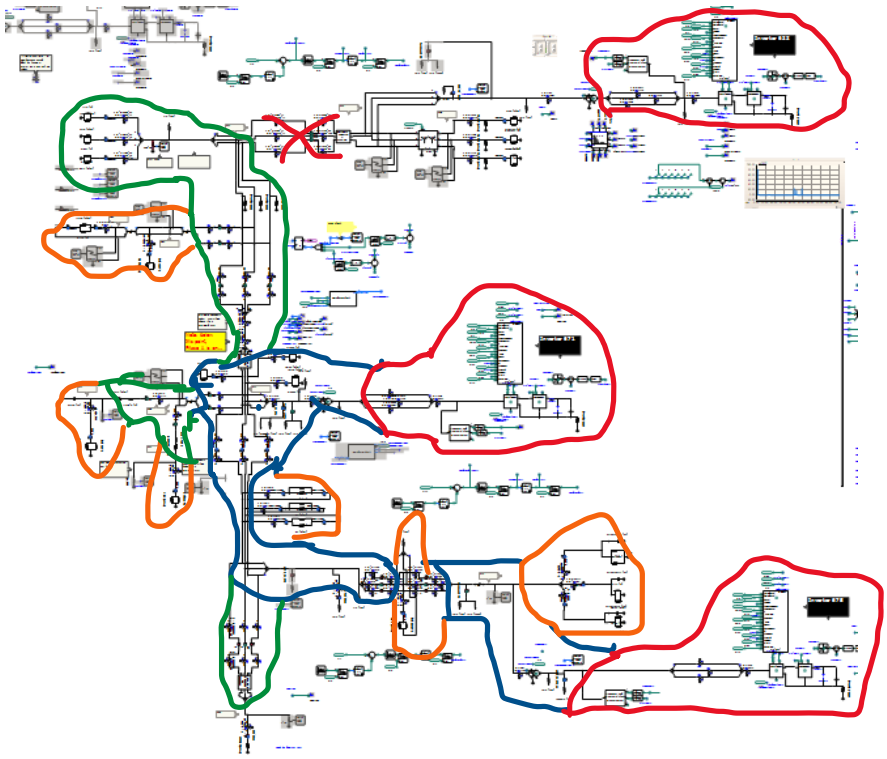

Figure 14. Reassembly of the 13-bus system after the 1LG fault at node 633.

Table 5. Load relay closing times (post-fault) for the AG fault at node 633. NT = never tripped; RO = remained open.

Load	632	675	680	671_2	611	692	652	645	646	671	634	671LL
Closing time (s)	4.4	6.44	8.38	4.35	8.248	7.42	7.70	8.15	3.62	3.619	RO	8.558

Table 6. Line relay reclose times (post-fault) for the AG fault at node 633.

Line Relay	R1	R2	R3	R4	R5	R6	R7	R8	R9	R10
Closing Time (s)	6.2	4.7; UVOC lockout at 4.899	3.49	3.54	3.62	6.2	6.198	6.193	3.485	3.484

3.2.1.4. A-G fault at load 611

In this case a fault was placed at load 611, marked with a **red** dot in Figure 15. Node 611 is on a single-phase lateral, which creates an increased chance that the SHAZAM logic will preserve parts of the system closer to the sources.

Load relays open on time-undervoltage as shown in Figure 15. First to open are the Group C loads marked with **red** X's, all within 1 s post-fault. One Group B load, load 675, falls in the early part of

the Group B trip range and trips at close to t = 1 second. Group B loads marked with **blue** X's open between 1 and 1.5 s post-fault, and the last group of loads to trip, all group A, are marked with **green** X's and trip around 2.5 s post-fault. Lastly, line relays trip between 2.5 and 3 seconds, marked with **orange** X's**.**

The system then self-assembles as shown in Figure 16. At first, the boundaries of the energized microgrids are the **red** lines. The first set of line relays closes, extending the boundaries to the **blue** lines, then to the **green**, and then to the **orange**. The load and line relay closure times post-fault are given in Table 7 and Table 8, respectively.

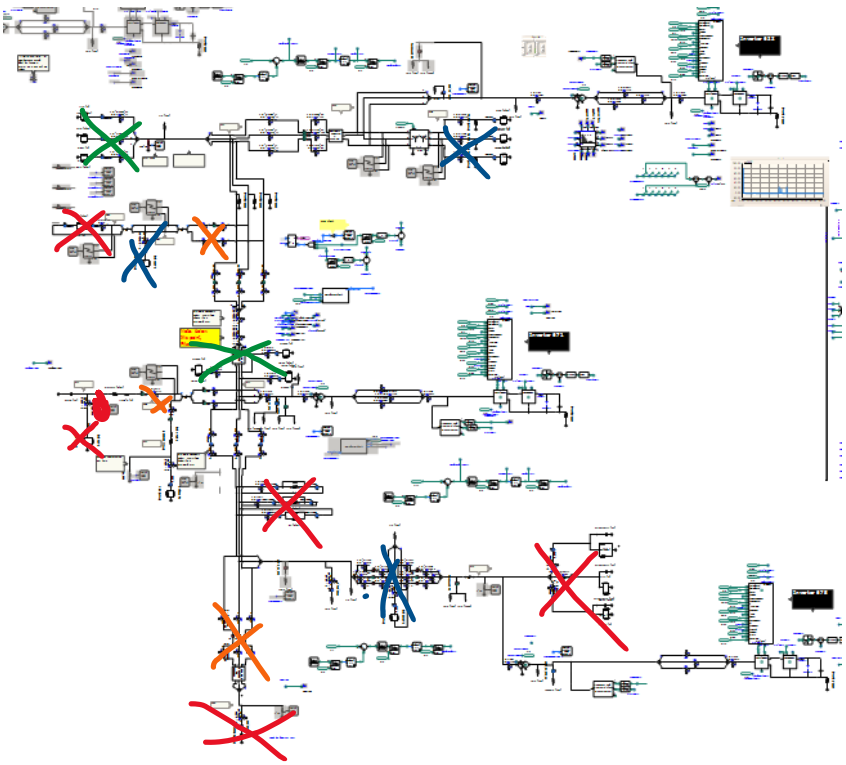

Figure 15. System diagram showing the order of line relay opening for the case of a 1LG fault at node 611.

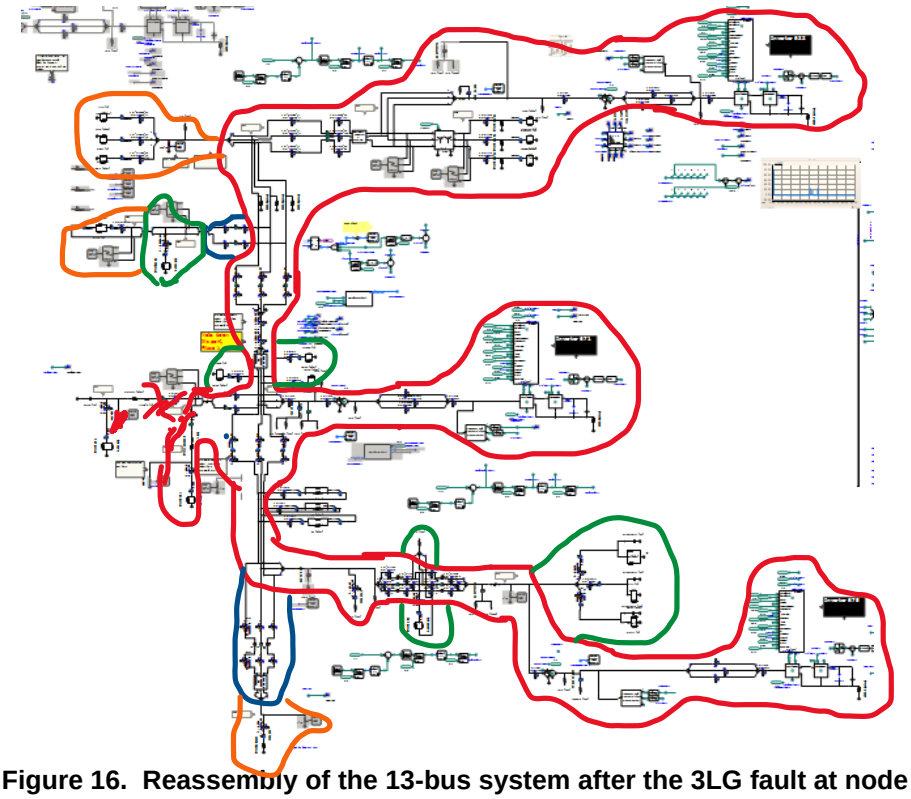

Figure 16. Reassembly of the 13-bus system after the 3LG fault at node 680.

Table 7. Load relay closing times (post-fault) for the AG fault at node 611. NT = never tripped; RO = remained open.

Load	632	675	680	671_2	611	692	652	645	646	671	634	671LL
Closing time (s)	.81	3.02	5.45	NT	RO	2.35	NT	2.45	5.07	.987	4.014	4.829

Table 8. Line relay reclose times (post-fault) for the AG fault at node 611.

Line Relay	R1	R2	R3	R4	R5	R6	R7	R8	R9	R10
Closing Time (s)	NT	NT	NT	0.56	NT	.904; UVOC lockout at.906	NT	NT	NT	NT

3.2.1.5. A-B fault at load 680

In this use case, an LL fault occurs at node 680. As before, the load relays open on time-undervoltage as shown in Figure 17. First to open are the Group C loads marked with **red** X's, all within 1 s post-fault. The Group B loads marked with **blue** X's open between 1 and 1.5 s post-fault, and the last group of loads to trip, all Group A, are marked with **green** X's and trip around 2.5 s post-fault. Finally, the line relays trip between 2.5 and 3 seconds, marked with **orange** X's.

The system then self-assembles as shown in Figure 18. At first, the boundaries of the energized microgrids are the **red** lines. The first set of line relays closes, extending the boundaries to the **blue** lines, then to the **green**, and then to the **orange**. The load and line relay closure times post-fault are given in Table 9 and Table 10, respectively.

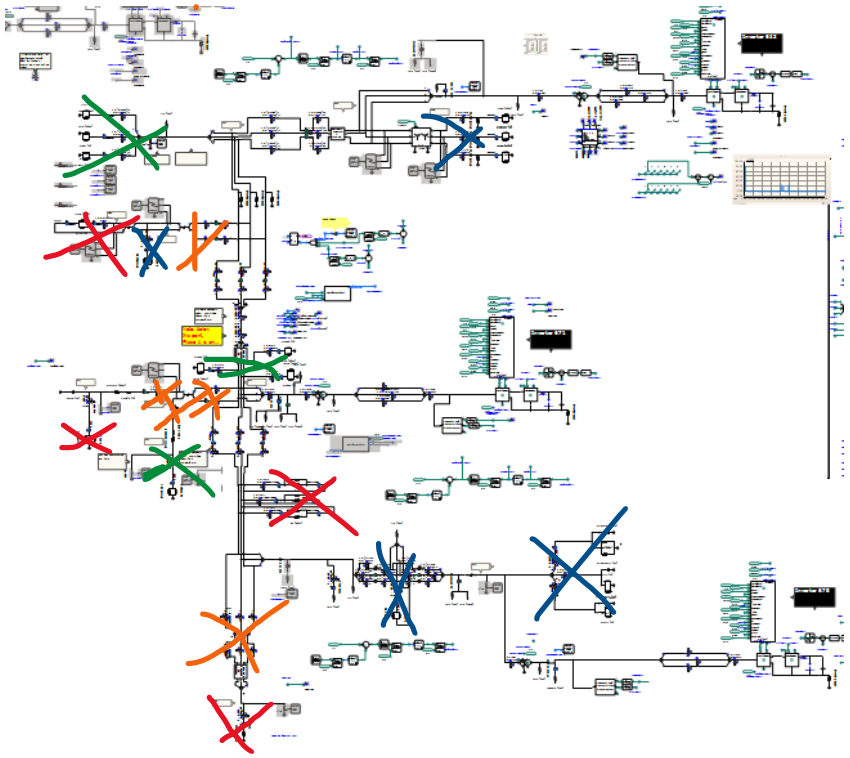

Figure 17. System diagram showing the order of line relay opening for the case of a 1LG fault at node 680.

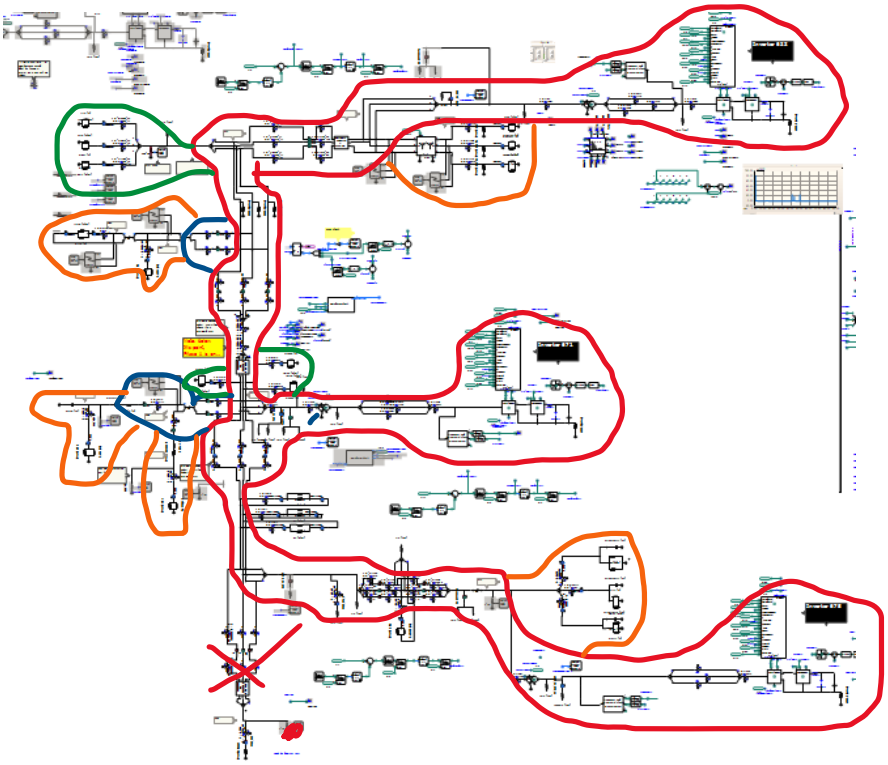

Figure 18. Reassembly of the 13-bus system after the 1LG fault at node 680.

Table 9. Load relay closing times (post-fault) for the AG fault at node 680. NT = never tripped; RO = remained open.

Load	632	675	680	671_2	611	692	652	645	646	671	634	671LL
Closing time (s)	1.2	4.4	RO	NT	6.07	4.53	1.02	3.38	5.03	4.53	4.51	5.12

Table 10. Line relay reclose times (post-fault) for the AG fault at node 680.

Line Relay	R1	R2	R3	R4	R5	R6	R7	R8	R9	R10
Closing Time (s)	.948	NT	NT	0.959	NT	0.959; UVOC lockout at .968	1.905	1.802	NT	NT

3.2.2. Results obtained using generic inverter model

In this section, results are presented for PSCAD modeling demonstrations of SHAZAM self-assembly when the 13-bus system is energized by three GFM IBRs represented by a generic inverter model.

The Load Group assignments used in this portion of the work are listed in Table 11.

Table 11. Load group assignments (Generic model).

Load number	632	675	680	671_2	692	611	652	645	646	671	634	671LL
Load Group	C	C	A	B	B	A	C	C	C	C	C	C

3.2.2.1. A-B fault at load 632

In this use case, a LL fault occurs at node 632 at 40s. Along with the manufacturer specific model testing was also done on a generic model for the inverters. This is an example of the previous fault tested using the generic model instead. The areas where the inverters vary the most is their respective droop controls, the generical model controls operated slow and would case chattering within the system in some cases. The other key difference was also caused by the controls, since the generic model operated slower it also would cause overcurrent to build up more during these switching operations making UVOC easier to detect. While simulating the generic model it was also difficult to maintain load priority and although it did influence when loads would close this was mostly influenced by location in proximity to the inverters. The manufacturer specific model is able to ramp up voltage fast enough that this isn't an issue. Lastly the generic model system had a magnitude mismatch at R5 which effectively isolated it from the rest of the system in this case.

As before, the load relays open on time-undervoltage as shown in Figure 16. First group to open are marked with **red** X's, all within 1 s post-fault. The second group of loads, marked with **blue** X's open between 1 and 1.5 s post-fault, and the last group of loads to trip, are marked with **green** X's and trip around 2.5 s post-fault. Lastly line relays trip between 2.5 and 3 seconds, marked with **orange** X's**.**

The system then self-assembles as shown in Figure 14. At first, the boundaries of the energized microgrids are the **red** lines. The first set of line relays closes, extending the boundaries to the **blue** lines, then to the **green**, and then to the **orange**. The load and line relay closure times post-fault are given in Tables 6 and 7, respectively.

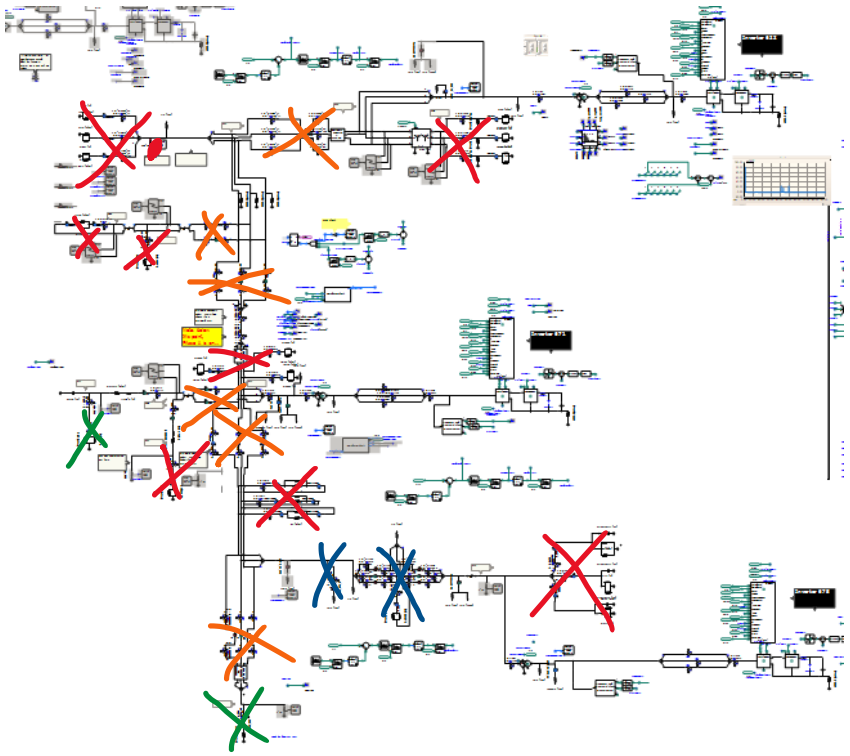

Figure 19. System diagram showing the order of line relay opening for the case of a 1LG fault at node 633.

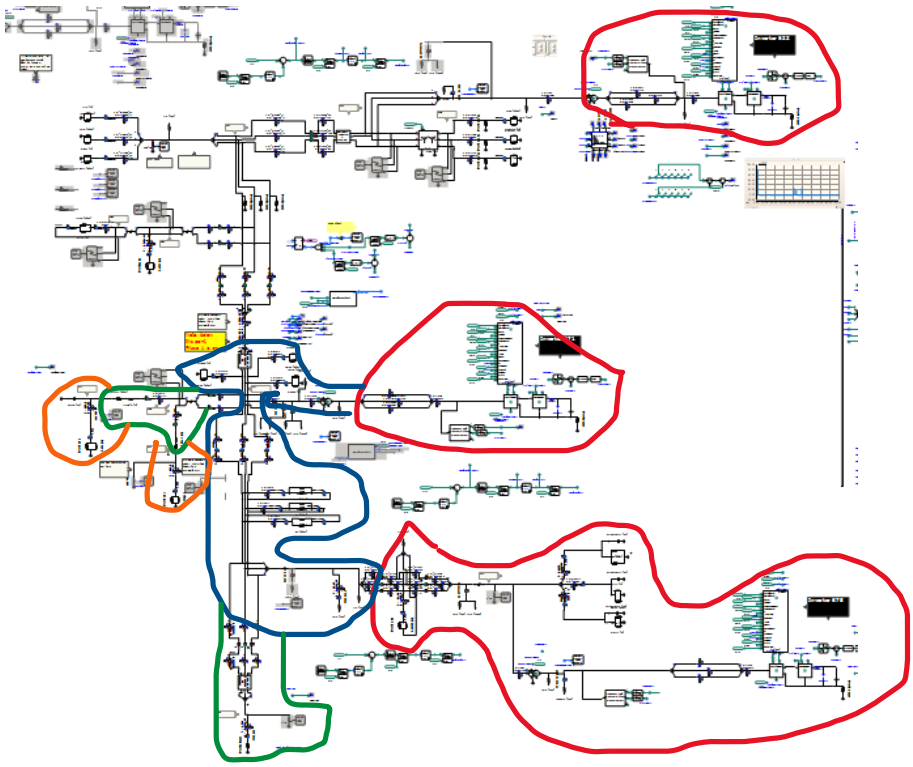

Figure 20. Reassembly of the 13-bus system after the 1LG fault at node 632.

Table 12. Load relay closing times (post-fault) for the AG fault at node 632. NT = never tripped; RO = remained open.

Load	632	675	680	671_2	611	692	652	645	646	671	634	671LL
Closing time (s)	RO	-	14.3	11.85	17.31	-	17.75	RO	RO	8.59	8.45	12.58

Table 13. Line relay reclose times (post-fault) for the AG fault at node 632.

Line Relay	R1	R2	R3	R4	R5	R6	R7	R8	R9	R10
Closing Time (s)	R0	10.744; UVOC lockout at 10.764	10.73; UVOC lockout at 10.75	RO	-	13.73	13.79	11.23	NT	10.718

4. PREVENTING SIMULTANEOUS CLOSURE OF ADJACENT LINE RELAYS

4.1. Random time delays

[Discuss random time element. Include here Olga's analysis of the likelihood of any two adjacent line relays choosing the same random element, as a function of granularity of the random numbers.]

4.2. Tagged timers

4.2.1. Introduction

Figure 21 shows a one-line diagram of the IEEE 13-bus distribution test circuit [21] configured to operate as a microgrid. The red blocks are closed relays. Each load has a load relay, and there are ten line relays, R1 through R10. This system has a microgrid isolation device, which is shown as green indicating that it is open and this system is off-grid.

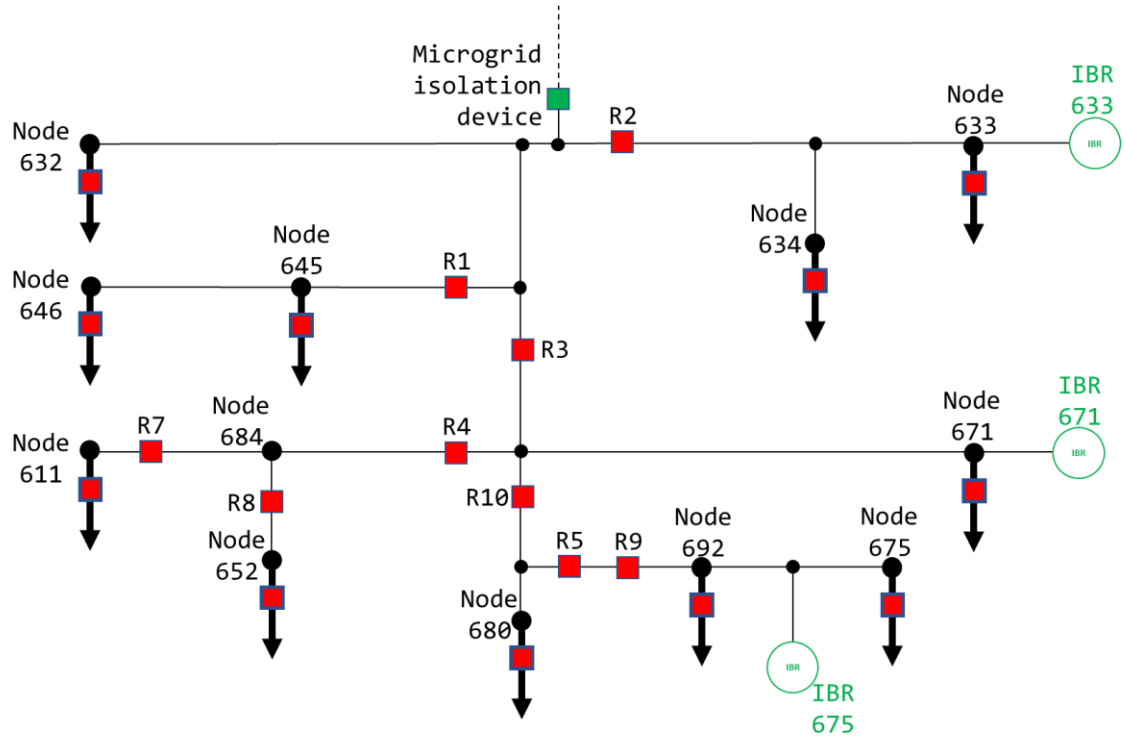

Figure 21. IEEE 13-bus distribution test circuit configured to operate as three microgrids, with an IBR (green) in each microgrid.

Consider a case in which a fault occurs near node 645, as shown in Figure 22. As discussed above, the IBRs hit their current limits and the entire system enters into an undervoltage condition. As discussed above, the first step toward restoring the system is undervoltage load shedding (UVLS, IEEE function 27TD [21]) according to load priority. In Figure 22 (left), the first group of loads (least

critical) has been shed, as indicated by the green-filled load relays. The fault persists, so the undervoltage remains, and some time later the second group of loads is shed on UVLS, as shown in Figure 22 (right). The fault persists, and the undervoltage condition remains. At this point, after UVLS has been exhausted, the line relays' time-undervoltage (27TD) functions then disassemble the SHePS into local intentional islands, each centered around a grid-forming IBR, as shown in Figure 23. The green dashed lines in Figure 23 show the boundaries of the three microgrids. There is a line relay on the boundary of each microgrid—for example, the boundary of Microgrid 633 includes line relay R2, and the boundary of Microgrid 671 includes line relay R3. When a line relay sees an in-range voltage on one side that remains stable for a preset length of time, then that line relay can reclose. In Figure 24 (left), line relays R2, R3, R4, R9 and R10 each sees an in-range voltage on one side, and they can all reclose, resulting in the new microgrid boundaries shown in Figure 24 (left). At this point, R1, R7 and R8 each see in-range voltage on one side only and can reclose on a timer, as shown in Figure 24 (right). Now, line relay R5 sees in-range voltage on both sides and will only reclose when two conditions are met: a) a synchronization check function (IEEE function number 25 [21]) has verified that the voltages on each side of the relay are sufficiently similar in magnitude and the phase angle difference between them is sufficiently small; and b) the unintentional loop detection function has verified that closure of that relay will not create a closed loop in a system designed to be operated radially [23]. In Figure 24 (right), note that line relay R1 has reclosed onto the fault. When this happens, the system voltage collapses again, and line relay R1 sees significant fault current immediately upon its closure. At this time, a windowed undervoltage-supervised overcurrent function (UVOC, IEEE function number 51TV [21]) asserts itself: if a line relay, having reclosed due to in-range voltage on one side only, sees a voltage collapse accompanied by high current within a short time window (here, 300 ms) after its closure, that line relay re-opens and locks out. In this way, the fault is isolated (Figure 25, left). The UVOC or 51V function timing must be long enough that it is not activated by the various inrush currents associated with cold load pickup. Eventually the synchronization check function (function 25) in line relay R5 is satisfied, and it recloses. No generation has been lost, so there is sufficient capacity to recover all of the loads, and the final system state is as shown in Figure 25 (right).

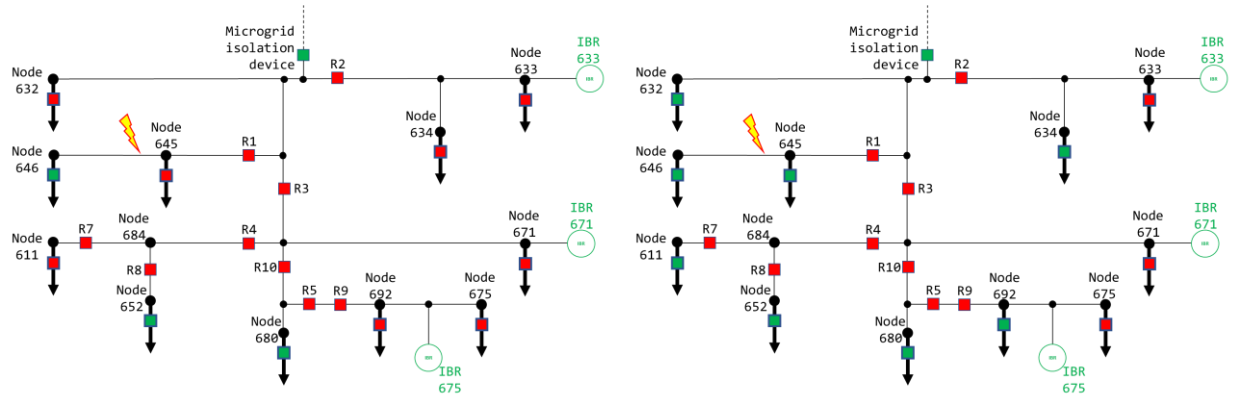

Figure 22. The system in Figure 21, undergoing a fault. Left : system after the first phase of UVLS (shedding Priority C loads). Right : system after the second phase of UVLS (shedding Priority B loads).

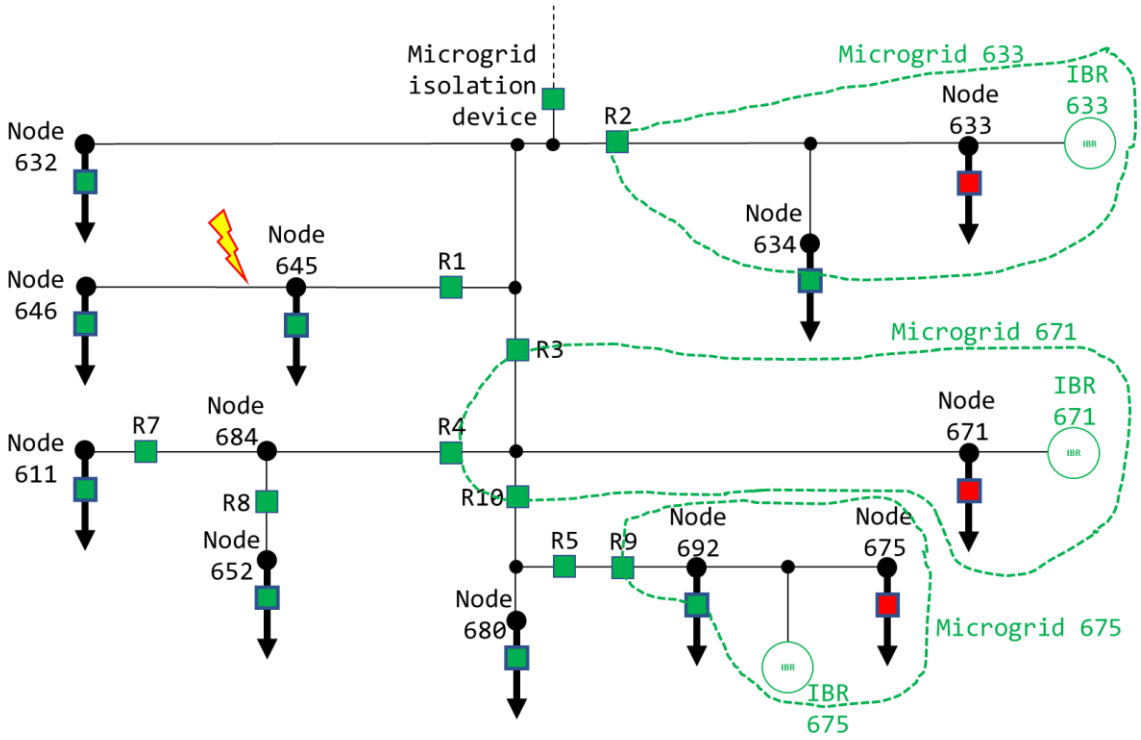

Figure 23. After UVLS has been exhausted, the line relays all open on undervoltage, creating three isolated microgrids each centered around a grid-forming IBR. The microgrid boundaries are shown in dashed green.

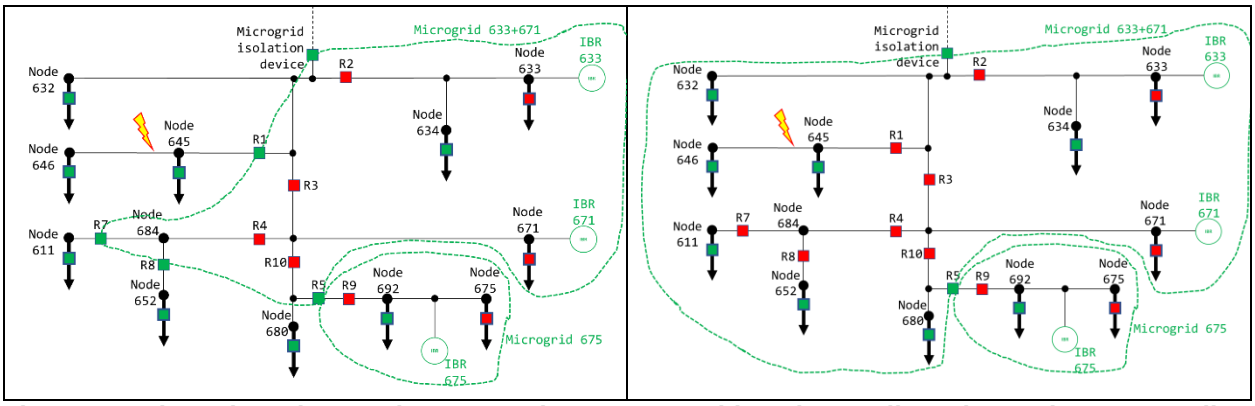

Figure 24. Line relays that see in-range voltage on one side only are allowed to reclose, expanding the microgrid boundaries. Left : R2, R3, R4, R9, and R10 close. Right : R1, R7 and R8 close (note that R1 closes onto the fault).

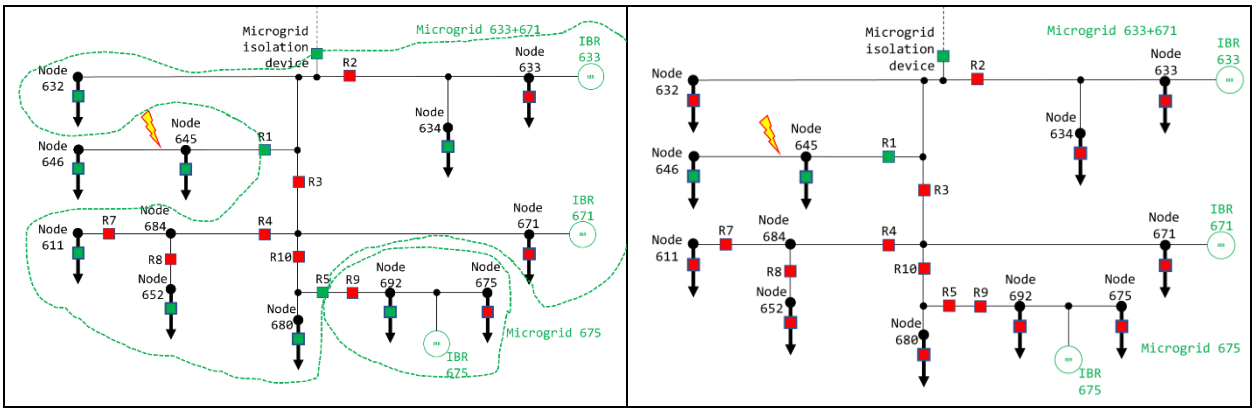

Figure 25. Left : Line relay R1 re-opens on UVOC, and locks out to isolate the fault. Right : Final system state after self-assembly has been completed.

4.2.2. Problem Statement

During self-assembly of multi-source microgrids, one condition that must be avoided is an asynchronous connection of two adjacent microgrids. In Figure 25 (left), line relay R5 is on the boundary between microgrid 675 and the combined microgrid 633+671, and it sees in-range voltage on both sides. If there is a significant difference in the magnitudes or phase angles of the voltages on either side of R5 when it closes, then large currents could surge back and forth between the microgrids, potentially leading to transient instability in the microgrids and likely triggering the UVOC function in relay R5. To avoid such an asynchronous connection, the line relays all incorporate a standard synchronization check or "sync-check" function (IEEE function number 25 [21]) in which the relay will not close until the magnitudes and phase angles of the voltages on either side of the relay are within preset tolerances. For IBR-energized systems, the required values of these tolerances will be set by the need to avoid damage to rotating loads in the microgrids.

However, in Figure 23, the boundary between microgrids 633 and 671 passes between line relays R2 and R3. Thus, in this situation, R2 and R3 together form the border between microgrids 633 and 671, and they must not be allowed to close simultaneously because this could create an asynchronous connection between microgrids 633 and 671. Because the line relays are using local measurements only, it is not possible to block one relay or the other via shared data. Thus, the timers used to close the line relays when they see in-range voltage on one side only must be configured such that no two adjacent line relays have exactly the same timing interval. In this way, one of the two line relays will always close first, and the other will then see in-range voltage on both sides and go to its synch-check function, preventing the asynchronous connection.

One method for differentiating the line relay closure timers would be to add a random element to the timers. However, there is still a finite possibility that two adjacent line relays could choose the same random delay, and if the resolution of the random timers is relatively coarse, which it would have to be to ensure that there is a sufficient time delay between any two adjacent line relays, then the probability that two adjacent line relays can choose the same random delay becomes significant [18]. As will be demonstrated below, the random time element is often not sufficient to guarantee prevention of asynchronous closure.

4.2.3. Tagged Timers Concept

The solution proposed is to add to the line relay closure time a 'tagged time', which is calculated as follows:

$$t_{reclose} = t_{fixed} + t_{tagged} \quad (3)$$

$$t_{tagged} = t_{inc} \times k \quad (4)$$

where $t_{reclose}$ is the reclose delay applied for in-range voltage on one side only, t_{fixed} is a fixed delay (typically 2-5 seconds), t_{tagged} is the tagged time, t_{inc} is a pre-selected timing increment that is much shorter than t_{fixed} (in this paper, t_{tagged} = 300 ms), and k is the tag, which is an integer between 0 and 2 that multiplies t_{inc}. Each line relay is assigned a value of the tag k, according to the following procedure:

1. Set the tag number to 0.
2. Start from each grid-forming IBR.
3. Move outward along the circuit conductors, including any branches, until a line relay is reached on each branch. If there are no branches, then this set will contain only one line relay.
4. For each set of line relays found in step 3, check to see whether any two of them are adjacent (i.e., any two line relays with no other line relay between them).
    a. For each line relay that is not adjacent to any line relay associated with another IBR, assign it the tag number k.
    b. If there are any two line relays that are adjacent as described above, assign k to one, and $k + 1$ to the other.
5. Increment the tag number by 1. If the tag number = 3, reset the tag number to zero.
6. Have all line relays been assigned a tag number? If so, stop. If not, return to Step 3.

This procedure is shown in flowchart form in Figure 26. The procedure ensures that, in the presence of multiple sources, no two adjacent relays have the same value of tagged time, and thus no two adjacent relays will ever close at the same time, preventing asynchronous connections.

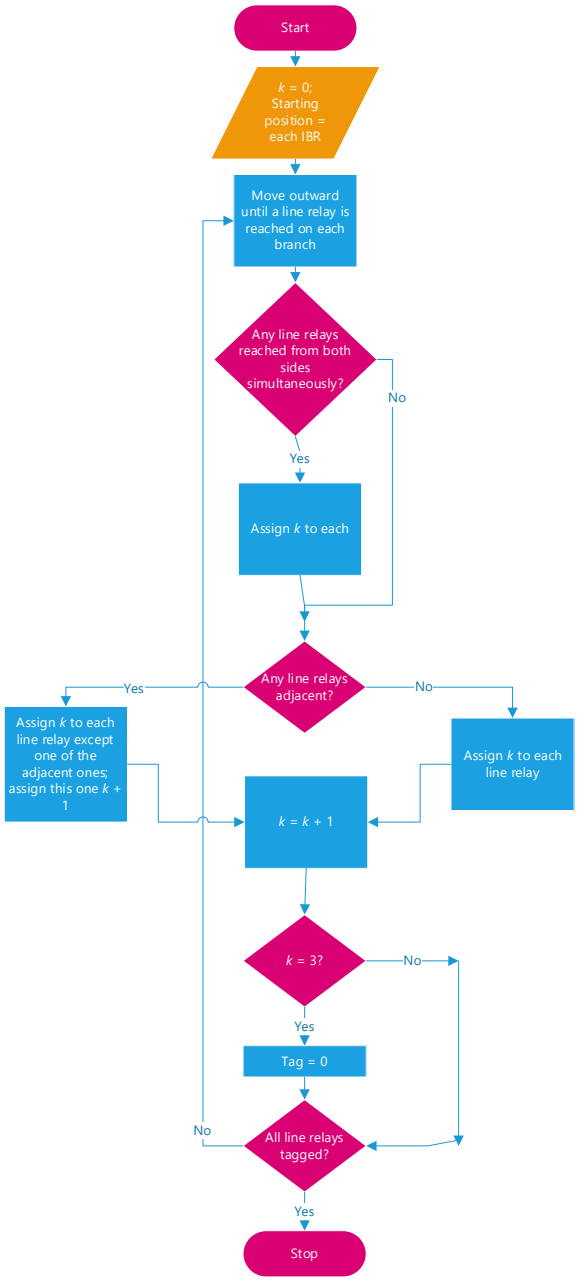

Figure 26. Flowchart of the process for assigning timer tags to the line relays.

Figure 27 and Figure 28 demonstrate the application of this process to the IEEE 13-bus distribution test circuit system shown in Figure 21. The process starts with $k = 0$, then moves outward from each IBR along each branch until we reach a line relay, as shown by the boundaries drawn in Figure 27. For IBR 633, line relay R2 is reached in this first iteration of step 3, and for IBR 675 line relay R9 is reached in this step. For IBR 671, line relays R3, R4 and R10 are reached simultaneously. Next, one checks whether any two line relays are adjacent (Step 4). In this case there is one adjacent pair : R2 and R3. One of these must be assigned $k + 1$, so in this example R2 is chosen to be tagged with $k + 1$, and the others (R3, R4, R9 and R10) are each assigned $k = 0$. The value of k is incremented to $k = 1$ (step 5), which is still less than 3.

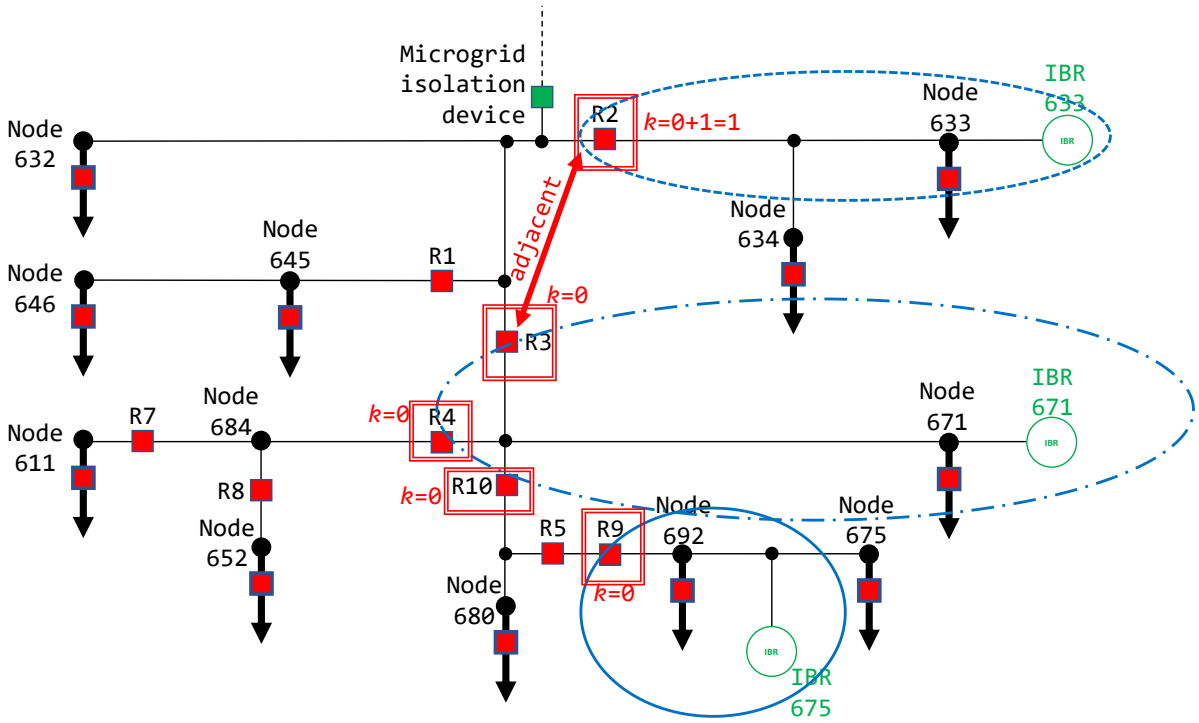

Figure 27. First step in assigning tag values to the line relays. R2 and R3 are adjacent, so one of the two (R2 is selected here) receives a tag value of *k* + 1.

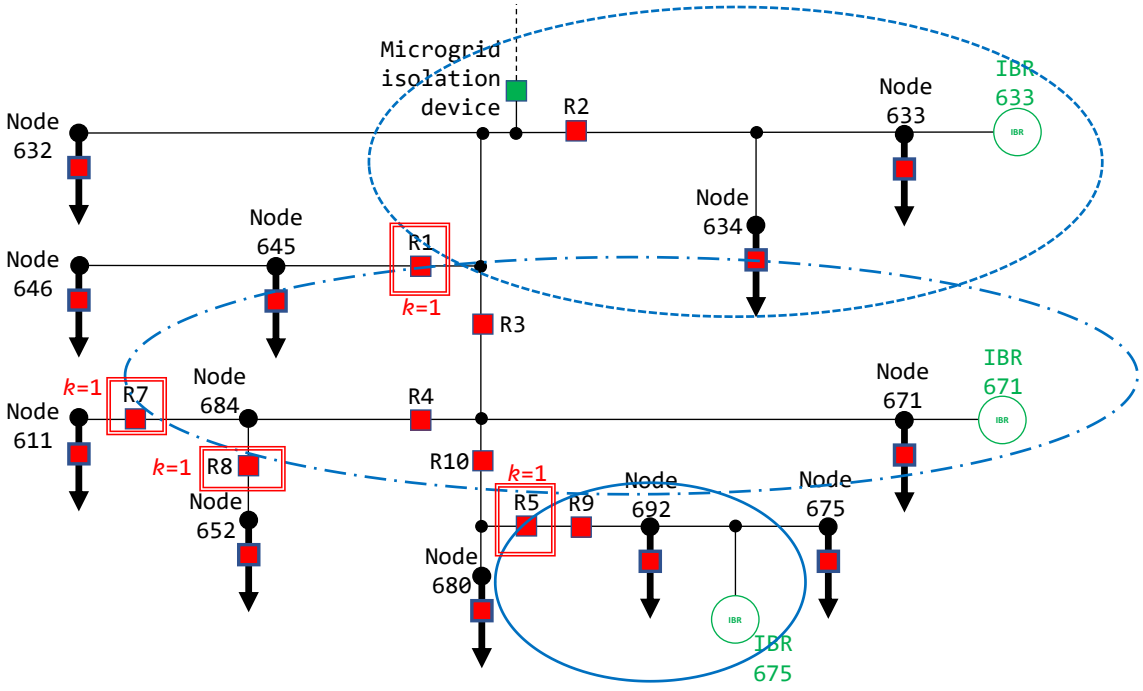

Figure 28. Second step in assigning tag values to the line relays. At this point, all relays have tag values, so this is the final step for this system.

Not all of the line relays have been assigned tag values (step 6), so the process repeats back to step 3, in which the boundaries are moved away from each IBR by one line relay, resulting in the boundaries shown in Figure 28. R1, R5, R7 and R8 each receive tag values of $k = 1$. No line relays are adjacent in this case (Step 4). The tag value is incremented to $k = 2$. At this point, all of the line relays have assigned tag values, so the process is complete.

4.2.4. Demonstration in simulation

4.2.4.1. Asynchronous connection using random timers

Figure 29 and Figure 30 show results from a PSCAD simulation in which the line relays in the IEEE 13-bus distribution test circuit (Figure 21) have fixed and random timing elements, but

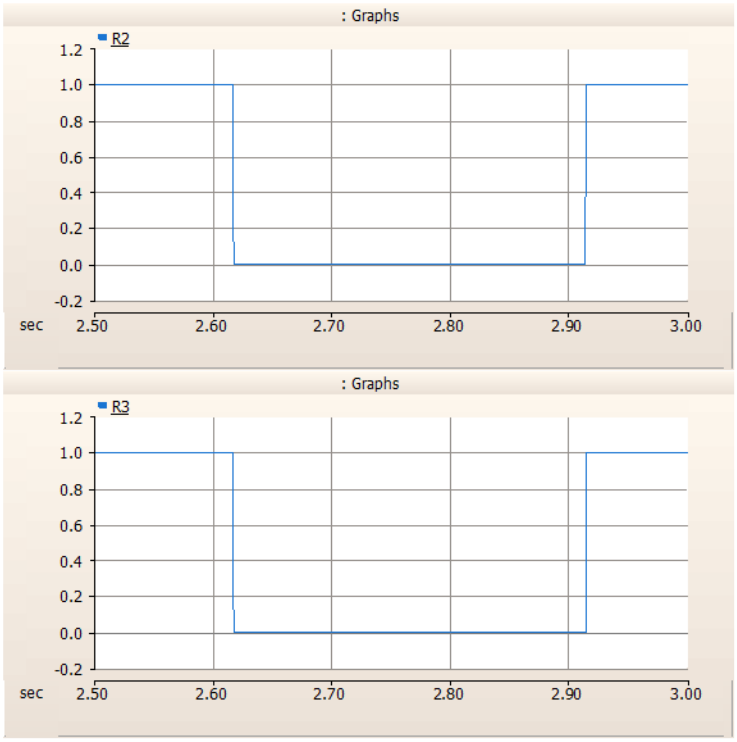

Figure 29. Breaker control signals for R2 and R3 during a black start, using the random timer element and not the tagged timer element. (In PSCAD, a 0 indicates a closed breaker, and 1 is open.)

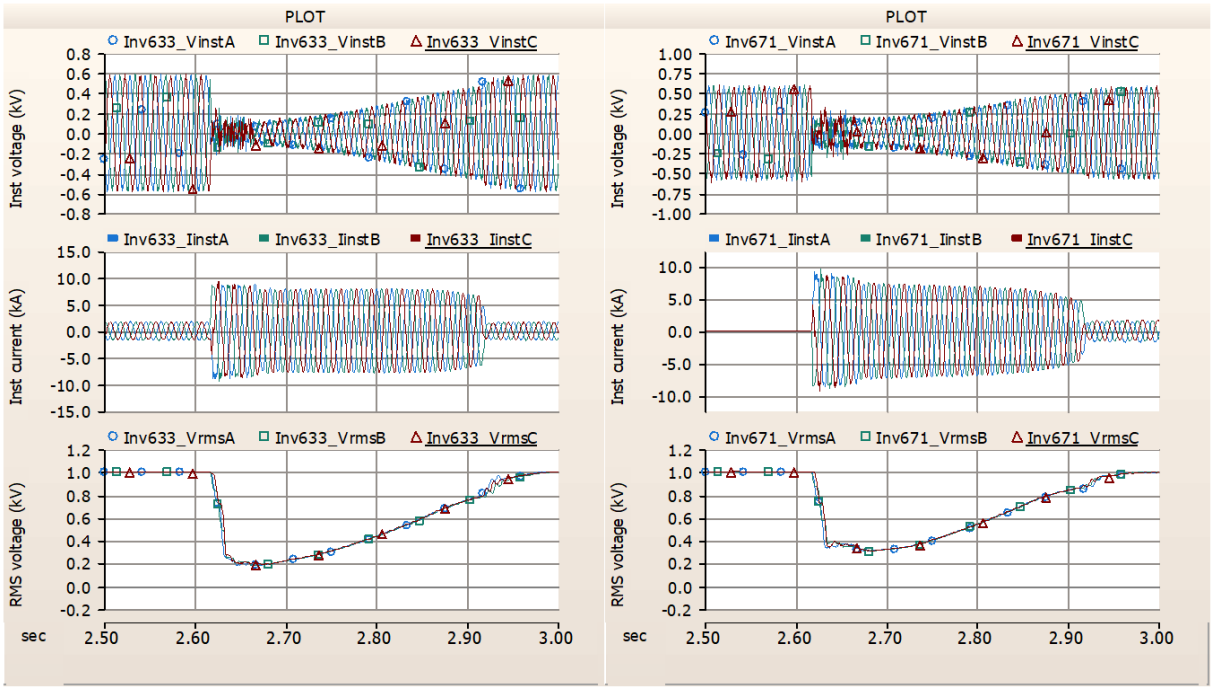

Figure 30. Instantaneous voltage (top), instantaneous current (middle), and RMS voltage (bottom) at IBRs 633 (left) and 671 (right) during an asynchronous connection of microgrids 633 and 671.

not the tagged timers. The three IBRs (Figure 1) are represented using detailed, code-based, manufacturer-supplied black-box inverter models. After a large number of simulations was run, one case was observed in which line relays R2 and R3 selected the same random time delay. During black start, both relays attempted to close at the same time (Figure 29), resulting in an asynchronous connection of microgrids 633 and 671. Figure 30 shows the instantaneous voltage, instantaneous current, and RMS voltage measured on the low-voltage buses of IBRs 633 (left) and 671 (right). The asynchronous connection leads to a voltage collapse and a large surge in current. This simultaneous voltage collapse and surge current triggers the UVOC functions in R2 and R3, both of which re-open (Figure 29) and lock out. This demonstrates the need to avoid such asynchronous connections.

4.2.4.2. Avoidance of asynchronous connection using tagged timers

Figure 31 shows results from a PSCAD simulation using the IEEE 13-bus distribution test circuit (Figure 21), using the fixed and tagged time delay elements. The left plot in Figure 31 shows the line relay closure timings during black start of the system. R2 and R3 are adjacent, and their closure times are in the red dashed circle. They are widely separated because R3 closed first ($k = 0$), after which R2 ($k = 1$) detected in-range voltage on both sides and closed on sync check roughly 11.5 seconds later. Similarly, R5 and R10 are adjacent, and their closure timings are circled in dashed green. The same situation occurs here: R10 ($k = 0$) closes first, and R5 ($k = 1$) then sees in-range voltage on both sides and closes on sync check just under 8 seconds later. The right plot in Figure 31 shows the line relay reclosure timings during system self-reassembly following a single line to ground (SLG) fault at node 633. This fault causes IBR 633 to become disconnected from the rest of the system. Line relay R3 ($k = 0$) closes first, at just after $t = 24.5$ s. Just over 2 seconds later, R2 ($k = 1$) closes on sync check, but it recloses onto the fault. The UVOC (51V) function asserts itself and R2 re-opens less than 200 ms

later, isolating the fault. (R3 does not open because the undervoltage-overcurrent combination occurs outside of its UVOC window.)

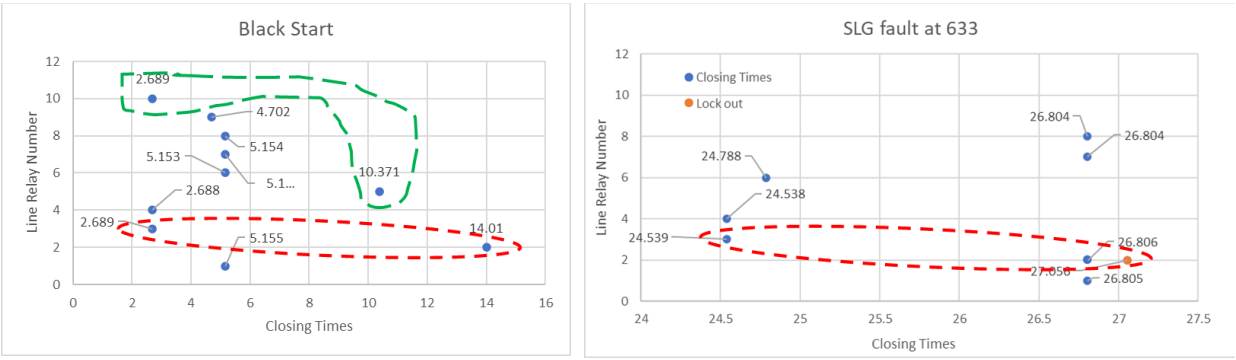

Figure 31. Closing times of the line relays in the IEEE 13-bus distribution test circuit (Figure 21), during black start (left) and reassembly after an SLG fault at node 633 (right).

4.3. Random time delays

Simultaneous closing of two or more LOAD relays may lead to greater than expected load pickup, and simultaneous closing of two LINE relays may lead to two individual microgrids attempting to connect to each other without proper synchronization or stability criteria met, i.e. asynchronous reclosure. These conditions can be avoided by adding a random element to the relay closure delay time. However, there is a finite probability that any two adjacent line or load relays may choose the same random number. The resolution (or "granularity" or "quantization" or discretization) of the random numbers affects how likely this is, and these must be selected such that there is sufficient time allowed for the relay that selected the slower random time to recognize that the other relay closed first, and respond appropriately. This section deals with a statistical analysis to quantify the risk that adjacent relays may choose the same random delay, and some means for decreasing the likelihood of this happening.

4.3.1. Problem Formulation

Random time delays for relay closure were described earlier. At the same time, even with random delays, the SHAZAM power system should not experience two or more random delays to be equal. This is illustrated in Figure 32 below. There may be several potential cases to consider:

- Two LINE relays (on each side of the line) may generate "random" time delays of equal value;
- Two line relays (ANYWHERE within the boundaries of the system) may generate "random" time delays of equal value;
- MORE than two line relays (anywhere within the boundaries of the system) may generate "random" time delays of equal value;
- Two LOAD relays corresponding to loads of different group type (Group A, B, or C) may generate "random" time delays of equal value;
- Two, three or more load relays corresponding to loads of different group type (Group A, B, or C) may generate "random" time delays of equal value;
- A combination of the above between line and load relays.

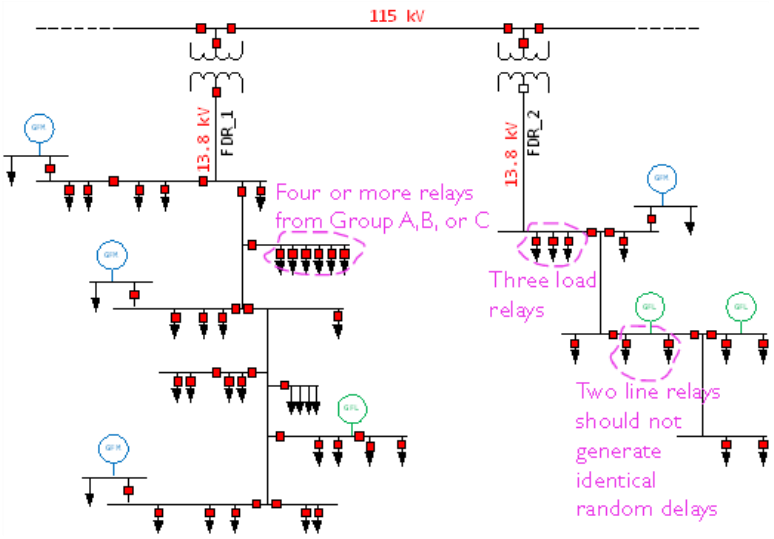

Figure 32. Illustration of the combinatorics and probability questions which need to be answered.

It is important to characterize these probabilities. Once the probabilities of these events are known, we can design optimal delay times for each relay type such that each probability is below an acceptable or desirable value, to ensure safety.

The probability of relays generating a random delay value can be calculated using traditional discrete combinatorics and probability theory.

4.3.2. Line Relays

We are mostly concerned with ensuring that no two adjacent line relays generate "random" time delays of equal value. In cases of long lines, there may be a scenario of three line relays, so we will consider this later as well, since this is a simple extension of the calculation.

After a certain condition is met (i.e. voltage has returned to a normal range), each relay will "pick" a time to close, using the following formula:

$$t_{close} = t_{fixed,c} + t_{tag} + t_{rand,c} \tag{5}$$

where $t_{fixed,c}$ is a fixed time period, t_{tag} is the tagged timer discussed in the previous section, and $t_{rand,c}$ is a random time interval that is much smaller than t_{tag}. We will analyze the probabilities of the events using discrete and continuous time approaches (seeing that continuous time is a limiting case of when the discretization time step is small). We first assume that random delays between 0 and 9 seconds will be considered, where each delay can be an integer value or decimal value. Therefore, the sample space in the discrete time may be 10 (for $\Delta t = 1$ sec) or 100 (for $\Delta t = 0.1$ sec). The 0 to 9 second interval is arbitrarily chosen, and may be sufficient for a sample microgrid system to reach electrical stability. This may not hold true for all systems, and in that case other time intervals/steps may need to be selected.

4.3.2.1. Discrete case of: what is the probability that two line relays (on each side of the line) may generate "equal "random" time delays?

The probability of any value of the delay is a uniform random variable, with a probability of:

$$P_i = \frac{1}{\mathrm{N}}$$

Calculation of this probability is equivalent to answering a question: "What is the probability of throwing any value, when rolling a fair die", except for in our case our "die" is ten-sided "die" for integer-second delay discretization, or hundred-sided for decimal-second delay discretization cases.

The next question is: what is the probability of any two relays producing an equal random delay number, for a discrete case of time steps in time within a given time interval, for example, within 10 seconds? This question is equivalent to asking: "If two fair dice are thrown, what is the probability of getting two equal faces (doubles)?".

Since for two "ten-sided dice" of 10 seconds with 1 sec time steps, the total sampling space is 10^2, and there are 10 "doubles" outcomes.

$$P_{2equal} = 10\frac{1}{10}\frac{1}{10} = 0.1$$

Hence, the probability of two similar line relays groups generating two random, but identical delays is 10%.

For a "hundred-sided die", the total sampling space is 100^2, and there are 100 "doubles" outcomes. Hence, the probability of two similar line relays generating two random, but identical delays is 1%:

$$P_{2equal} = 100\frac{1}{100}\frac{1}{100} = \frac{10^2}{100^2} = 0.01$$

We notice that there is an order of magnitude reduction in likelihood of simultaneous line relays closing if the allowed delay time is quantized in decimal steps. If further reduction of probability to less than 1% is desired, then further quantization of delay can be considered. However, here we can notice that 0.1sec corresponds to 6 cycles of a 60Hz signal. Therefore, a six-cycle time separation may not be enough in our case to ensure enough stability is reached by the microgrids one each side of the relay, and a longer delay may be needed. So, it may be logical to consider increasing the quantization time step to even greater that 1 sec, for example, 2 sec. And also allow for a longer overall time interval where the relays may close, for example, 20 sec. Results of this calculation are shown in Table I(b).

Table 14. Probabilities of line and load relays closing.

	Time step quantization of 10sec interval		
	2 sec	1 sec	0.1 sec
Two line relays closing	20%	10%	1%

(a)

	Time step quantization of 20sec interval		
	2 sec	1 sec	0.1 sec
Two line relays closing	10%	5%	0.5%

(b)

Given the results above, if a probability of no greater than 10% is required, a SHAZAM architecture designer may select $t_{rand,c}$ to be multiples of 2 s. The exact determination of an acceptable probability, time steps and max duration of the allowed time interval (i.e. total sample space) will be based on individual power system information and configuration.

Longer time horizons and shorter time steps will lead to a continuous time consideration, which we will discuss next.

4.3.2.2. Continuous time case of: what is the probability that two line relays (on each side of the line) may generate equal "random" time delays?

Previous section considered uniform random distribution of random time delay selected within a given time interval. In real life situations, it may be more practical to consider a normal distribution of these random time delays. An example of such a distribution is shown in Figure 33, where both blue distributions have the width $t_{fixed,c}$ =2 sec (blue), $t_{rand,c,mean}$ = 1 sec, and $t_{rand,c,sigma}$ = 0.5 sec, and an orange outline illustrates a continuous time normal distribution with the same parameters.

For the case of two line relays on opposite sides of the same line, and if both line relays have the same time delay parameters, it is clear that there is some non-zero possibility that both of these relays may "pick" the same random time to reclose. In order to avoid this condition, we add an additional term, t_{tag}, which was mentioned earlier, such that t_{tag} is a time that is assigned to each line relay in such a way that no two adjacent line relays have the same value of $t_{tag,}$. For example, setting $t_{tag,}$=0 to a relay on the right side of the line $t_{tag,}$=1 to a relay on the left side, will result in the probability distributions which look shifted, or staggered in time, as shown in Figure 34. (Adding an additional term $t_{tag,}$ is essentially similar to adding the same term to the mean of the normal distribution). In this case, the selection of t_{close} staggered by 1 second as in Figure 34(a) shows that there is some separation of probabilities in time. The selection of t_{close} staggered by 10 seconds as in Figure 34(b) ensures that there is a statistically significant separation of these two relay's operation in time. These illustrations explain why earlier we have mentioned that t_{tag} should be selected to be much greater than $t_{rand,c}$. More precisely, t_{tag} should be selected to be much greater than $t_{rand,c,mean} + t_{rand,c,sigma}$.

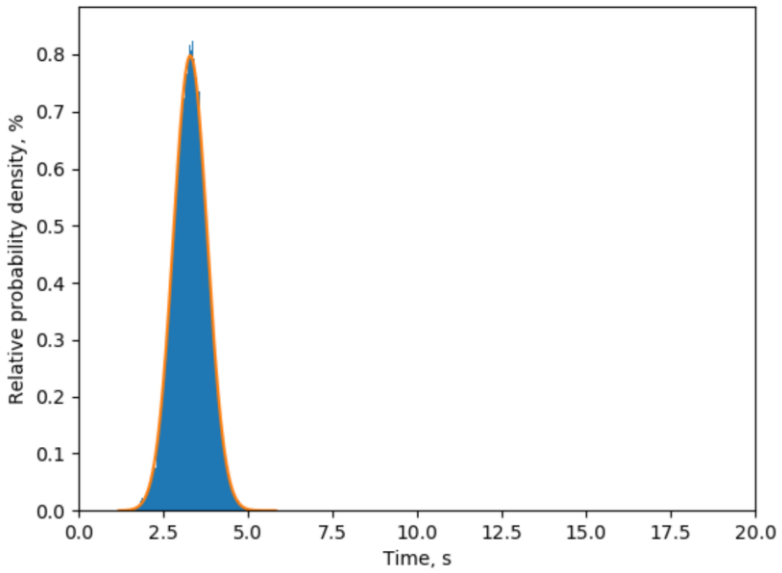

Figure 33. Illustration of a normal distribution of random closing times for sample relay with $t_{fixed,c}$ =2 sec, $t_{rand,c,mean}$ =1 s, and $t_{rand,c,sigma}$ = 0.5 s

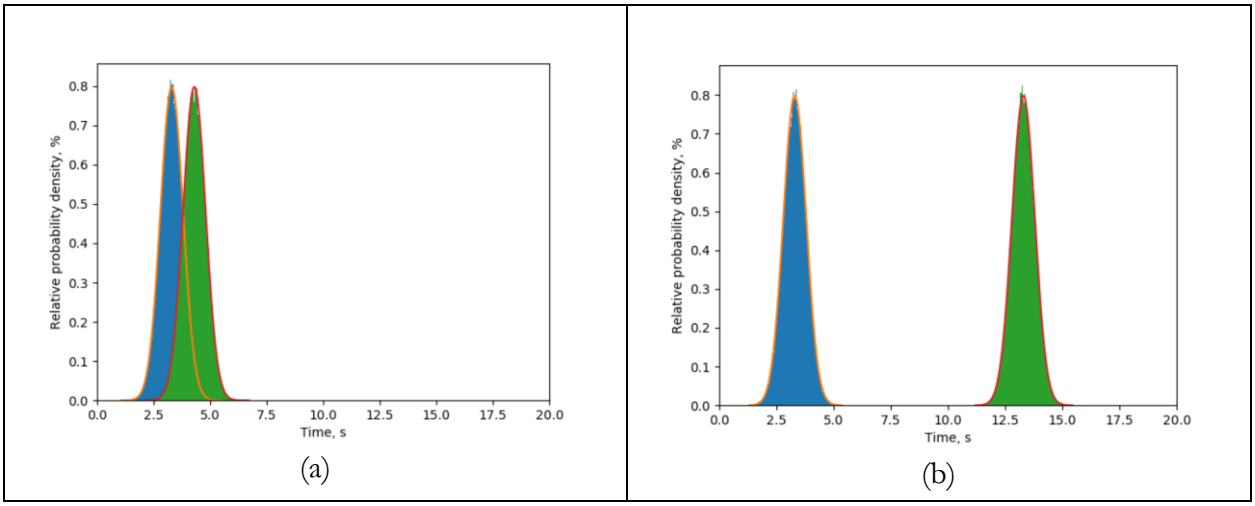

Figure 34. Illustration of a normal distribution of random closing times for sample relay in green with the same parameter as the blue, but with additional delay t_{tag} = 1 s (a) and t_{tag} = 10 s (b).

The next question: "By how much exactly greater should $t_{rand,c,mean}$ + $t_{rand,c,sigma}$ and t_{tag}. be separated by?" should be answered by examining the overlap integral of two probability densities, as shown in Figure 35. It is clear that the answer will be different for different values of $t_{fixed,c}$+ $t_{rand,c,mean}$. While it is possible to derive a generalized expression for this relationship, such a closed form derivation is outside of the scope of this project. It is, though, possible to construct a table to understand the general trend. These answers are shown in Table 15. It is important to notice that $t_{fixed,c}$, $t_{rand,c,mean}$, $t_{rand,c,sigma}$ in the table are the same for both relays – which explains the same numerical results in rows

two one and two: it is only the $t_{rand,c,sigma}$ + t_{tag} value which affects the reduction of probability in this case.

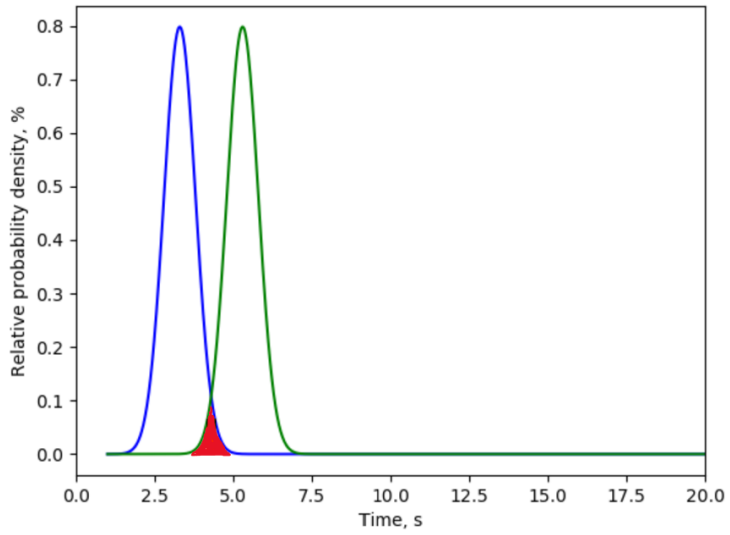

Figure 35. Illustration of a potential overlap in closing times probabilities if the delay times selection have not been staggered sufficiently.

Table 15. Probabilities of load relays closing, %, as a function of t_{fixed}, $t_{rand,c,mean}$, $t_{rand,c,sigma}$ and t_{tag}.

$t_{fixed,c}$, s	$t_{rand,c,mean}$	$t_{rand,c,sigma}$	t_{tag}, sec			
			0	1	2	3
2	2	0.5	29.66	10.91	0.5	0.003
2	3	0.5	29.66	10.91	0.5	0.003
2	3	1	14.83	11.55	5.46	1.56
3	3	1.5	9.88	8.84	6.34	3.63
3	3	2	7.41	6.96	5.77	4.22

From Table 15, two generic conclusions can be drawn:

1. If t_{tag} = 0, there is a approximately 30% probability of both of the line relays attempting to close at the same time;
2. t_{tag} selection is much more important for the cases where the random component of the delay is greater (i.e. distributions are "wider", which is characterized by $t_{rand,c,sigma}$).

The key conclusion to be taken from this is that the distribution of the random element of the delay time must be kept significantly less than t_{tag}. If this precaution is not observed, the distributions of the delay times from neighboring values of t_{tag} will start to overlap, leading to a higher possibility of adjacent relays closing too close together in time.

4.4. Generalization of the continuous time case of: Two line relays (ANYWHERE within the boundaries of the system) may generate equal "random" time delays?

Given the conclusion above that it may be challenging to arrive to a determination of a safe value for the tags without knowing additional information about the circuit, we can attempt to develop a more general approach.

Although for line relays, we are primarily concerned with the two neighboring relays not closing at the same time, for a reasonably large electrical system, closing of two not-neighboring line relays (not on the same line) may still result in instability, which, in its turn, may result in SHAZAM separating into smaller microgrids, and re-starting the re-assembly process again.

Therefore, it is still important to quantify the probability that two line relays anywhere within the boundaries of the system may "pick" the same closing time. Granted, given the statistical assembly process that SHAZAM is utilizing, it is intuitively unlikely. But we will examine this case anyway. Let's examine the same IEEE-13 system as shown in Figure 36. Tag values of "0" or "1" were initially assigned to each of the neighboring tags, as shown in Table 16.

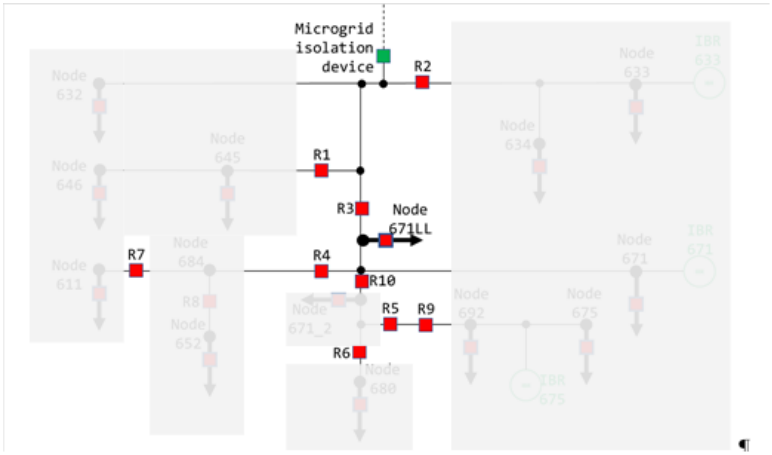

Figure 36. IEEE 13 system highlighting the locations of the line relays, with load locations greyed out for visualization purposes.

Table 16. Tag values used in each line relay.

Line Relay	R1	R2	R3	R4	R5	R6	R7	R8	R9	R10
Tag Value1	1	1	0	0	1	1	1	1	0	0
Tag Value2	3	3	0	0	3	3	3	3	0	0

To quantify the improvement in reduction of probability, we can examine the normal distributions of probability of line relays closing, taking into account the same formula as in (5):

$$t_{close} = t_{fixed,c} + t_{rand,c,mean} + t_{rand,c,sigma} + t_{tag} \qquad (6)$$

Graphs showing these probabilities are shown in Figure 5, using the following parameters: $t_{fixed,c}$ =3 s, $t_{rand,c,mean}$=3 s, $t_{rand,c,sigma}$ =1.5 s, t_{tag} as shown in Table 16, Tag Value1. These values were selected based on the values from the Table 15, row 4, to intentionally make the differentiation slightly challenging. Figure 37(a) shows probability density functions for all relays without adding any tag values, and, as expected, they are identical and cannot be distinguished. Figure 37(b) shows probability density functions for all relays after Tag Values 1 (shown in Table 16) added to corresponding locations. As can be seen, this results in separation of pdf's into two distinct groups: for those relays where Tag Value is "zero", and for those relays where Tag Value is "one". While this would indeed lead to the reduction in undesirable probability of any two neighboring line relays closing at the same time, it is clear that the separation in time does not seem to be enough. Figure 37(c) shows probability density functions for all relays using Tag Values 2. Although the temporal separation between zero-tagged relays and tagged relays has increased, we still observe that there are only two distinct groups: tagged and non-tagged relays.

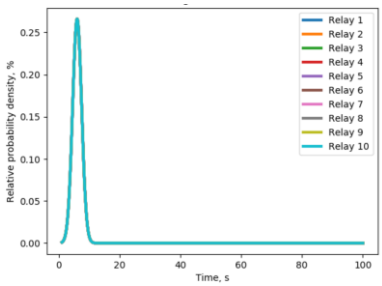

(a)

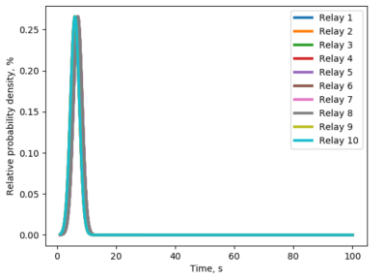

(b)

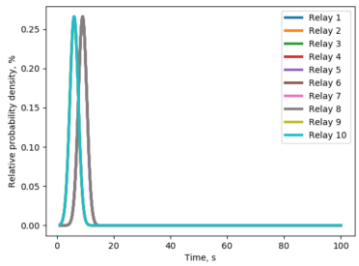

(c)

Figure 37. Illustration of a normal distribution with (a) no tags, (b) Tag Values 1, and (c) Tag Values 2.

As mentioned earlier, in a real life system, this may already be enough to provide for such statistical separation in time. However, this method relies on an important assumption that the tag values are assigned correctly to the line relays "on the left" and "on the right". One approach for assigning the tagged timer values was explained above. The next section suggests another possible approach.

4.4.1.1. Improvement of the line relay probability reduction, using approximate knowledge of the circuit topology

In order to introduce additional randomization to the total delay time for line relay reclosing, we can leverage certain knowledge of the microgrid or distribution circuit topology.

We assume that the setting on the relay will be programmed by a qualified personnel, who may be configuring these settings in field, and would like to be able to select the parameters with ease, but at the same time, making sure that these settings are mostly error-proof.

One way to introduce randomization into the delay time is to add an additional term to the equation (6), such that:

$$t_{close} = t_{fixed,c} + t_{rand,c,mean} + t_{rand,c,sigma} + t_{tag} + t_{dist} \quad (7)$$

where t_{dist} is a new time delay equal to, or proportional, to an approximate geographic (or linear circuit) distance to each line relay from a certain location. This linear distance may be estimated by the personnel in field, and only an approximate distance is needed.

To evaluate if this method provides a better randomization, we applied this method to further evaluate the pdf's shown in Figure 37.

The blue arrows in Figure 38(a) show the estimation of the approximate distance to each relay estimated from the microgrid isolation device. Figure 38(b) and (c) show the new distribution of pmf's for all the 10 line relays in the system for Tag Values 1 and Tag Values 2 correspondingly. It is clear that the spatial separation between all the relays' pmf's has increased, and each line relay pmf is now resolved. The difference between Tag Values 1 and Tag Values 2 is less pronounced, so we can conclude that the distance contribution is more pronounced than the tag value contribution.

However, we can see that relay R2 ends up with the shortest delay time, and the delay times increase as the line relay location "radiates" further away from the microgrid isolation device. For the SHAZAM architecture, it is instead desirable that the values "radiate" away from the IBRs. Figure 39 demonstrates this approach. We can see that the shortest delay times are now for relays 9 and 5, while relay 2 moved somewhere to the "middle of the pack".

This algorithm may prove a good improvement to the selection of the t_{dist} values, but it is not without a disadvantage: it may be harder for personnel in field to estimate a distance to the nearest IBR which will be providing energization. It is much easier for personnel to know the approximate distance to the microgrid isolation device. Also, note that no maximum constraint was applied, and clearly time delays well into the tens of seconds are impractical for this application.

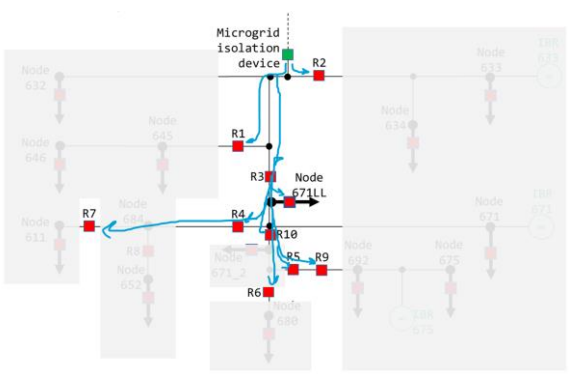

(a)

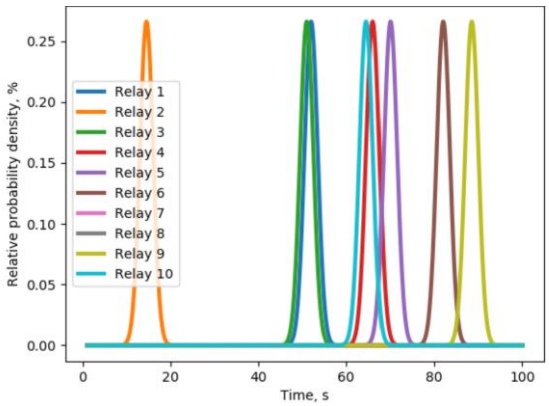

(b)

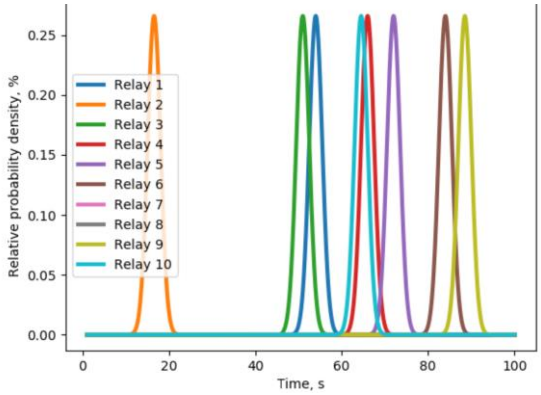

(c)

Figure 38. Illustration of a suggested linear distance estimation from the microgrid isolation device (a); pmf's for all line relays using distances from POC with regular tagsTag Values 1) (b) and 3x tags (Tag Values 2) (c).

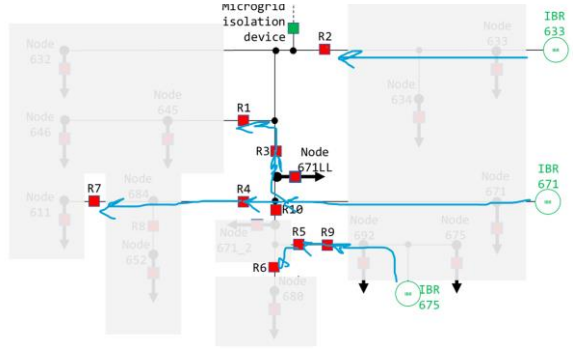

(a)

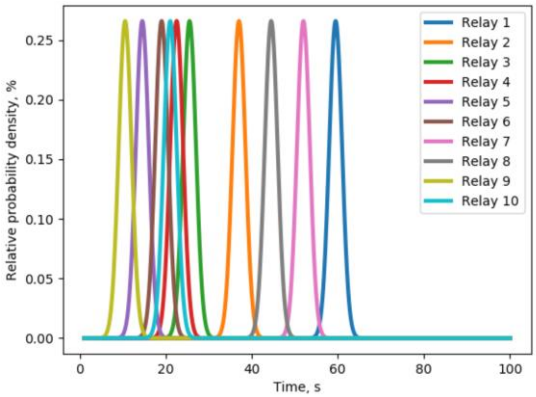

(b)

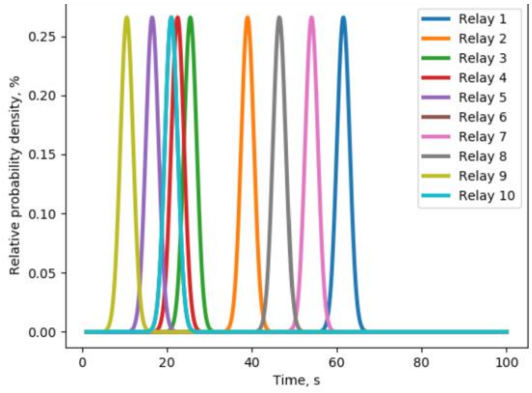

(c)

Figure 39. Illustration of a suggested linear distance estimation from the nearest IBR. (a); pmf's for all line relays using distances from POC with regular tags (Tag Values 1) (b) and 3x tags (Tag Values 2) (c).

4.5. Load Relays

As mentioned earlier, and as illustrated in Figure 40, we may expect different groups of loads "next" to each other (for example, on the same lateral). Simultaneous closing of two or more load relays may lead to greater than expected load pickup. If these loads are not the heaviest loads (in terms of rating), then such even should be treated as a normal event. Therefore, probabilities in the range of 27%- 54% do not need to be treated as alarming. However, if one such loads represents a significant or heavy load, it would be reasonable to move up such load in the classification scale (for example, upgrade classification from Group C to Group B, or Group B to Group A) in order to avoid a possibility of several heavy and/or critical loads coming on at once.

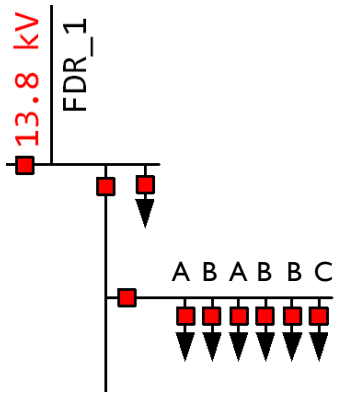

Figure 40. Illustration of several loads of different groups "next to each other" on the same lateral.

Nevertheless, it is important to be able to quantify these probabilities. First, we will calculate this probability for the case when NO information is given to us about (1) location of the line relays; (2) their locational relationship to each other (i.e. whether one of the relays is downstream from another line relay, etc).

4.5.1.1. What is the probability of any two load relays from two different GROUPS that will pick the same moment of time for reclosing?

After a certain condition is met (i.e. voltage has returned to a normal range), each relay will "pick" a time to close at, using the following formula:

$$t_{close} = t_{fixed,c} + t_{tag} + t_{rand,c} \qquad (8)$$

where $t_{fixed,c}$ is a fixed time period, t_{tag} is a time that is assigned to each line relay in such a way that no two adjacent line relays have the same value of $t_{tag,}$ and $t_{rand,c}$ is a random time interval that is much smaller than t_{tag}. As described earlier in this report, one of the primary goals of SHAZAM is to separate different priority load groups (A,B, C) in time, such that the groups are brought back into the power system according to their priority designation. This time-scheduling should be controlled by careful selection of times $t_{fixed,c}$ and $t_{rand,c}$. As previously discussed, if we want all group A loads to have been energized before any of group B loads, then it is important to select times $t_{fixed,c}$ and $t_{rand,c}$. such that, under all conditions,

$$t_{fixed,c,\ group\ A} + t_{rand,c,\ group\ A} < t_{fixed,c,\ group\ B} + t_{rand,c,\ group\ B} \quad (9)$$

and, similarly, for groups B and C:

$$t_{fixed,c,\ group\ B} + t_{rand,c,\ group\ B} < t_{fixed,c,\ group\ C} + t_{rand,c,\ group\ C} \quad (10)$$

These considerations are illustrated in Figure 41. Figure 41(a) shows the case where time delays for groups were selected such that condition in the equation (9) was not met. As a result, one can see that there is some statistical probability of load relays in different groups overlapping in time for closing procedure. Figure 41(b) shows the case where time delays for groups were selected such that condition in the equation (9) was met correctly. As a result, there is an appropriate time separation between all groups, and any loads within each group, from each other. Moreover, as in the case in Figure 41, if there are 50 loads of each group, $t_{fixed,c,\ group\ B}$ should be selected such that ALL loads of group A had enough time to be energized. So, in this case, may need to be selected as:

$$t_{fixed,c,\ group\ B} = t_{fixed,c,\ group\ A} + 50 \cdot t_{rand,c,\ group\ A} \quad (11)$$

Equation (11) does not take into account any relational information about where individual load and load relays may be located (for example, within the same lateral, or not, etc).

Therefore, the conclusion is that, with the correct selection of fixed+random closing times for each group, it is possible to select them such that there is a zero probability of load relays from different groups attempting to close at the same time. Additional information, such as knowledge of approximate number (count) of each loads in each group, their relational information (on the same lateral or not, etc), and how conservative one might want to be with time separation between each group, may be used for careful selection of individual fixed and random delay times for each group.

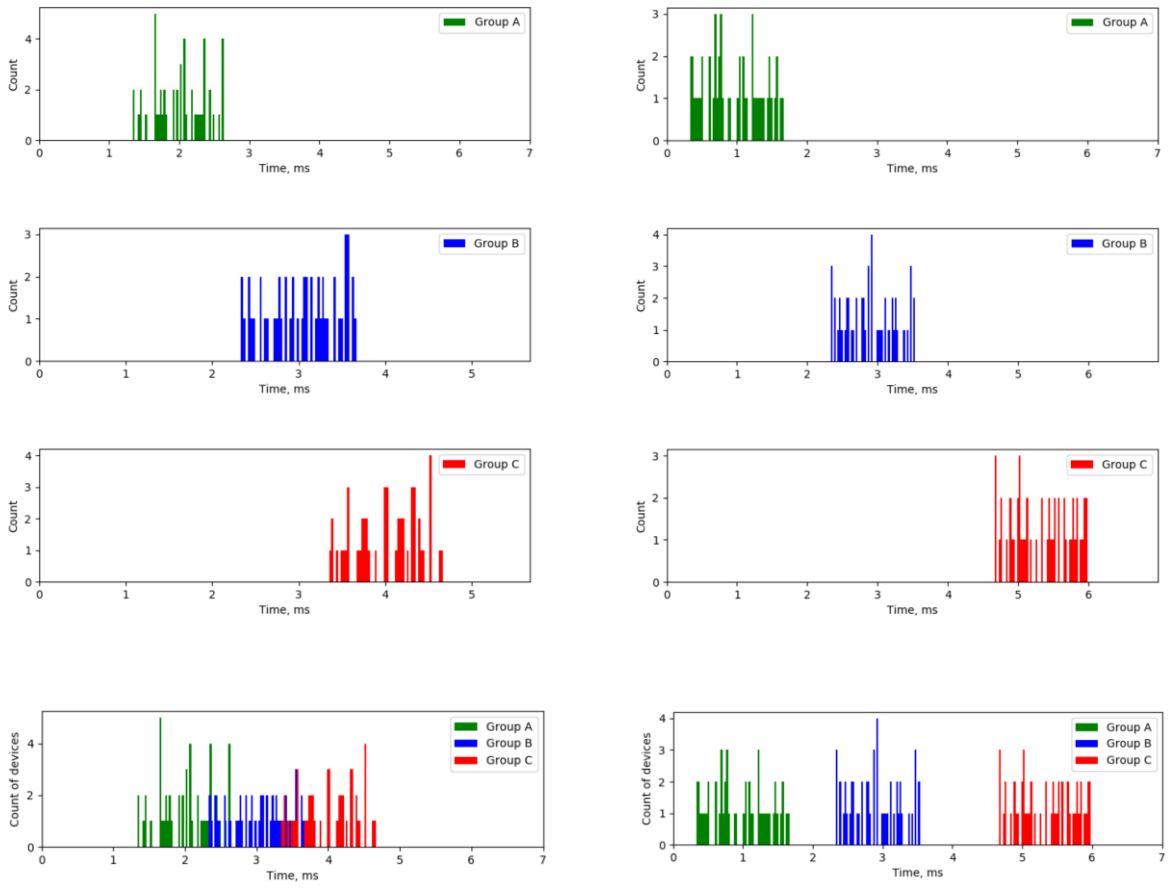

(a) (b)

Figure 41. Histogram distribution of closing delays for 50 each of group A, B, and C loads: (a) case when incorrect times $t_{fixed,c}$ and $t_{rand,c}$ were selected, resulting in overlap of possible closing times for of group A,B, and C loads; (b) case when correct times $t_{fixed,c}$ and $t_{rand,c}$ were selected, resulting in no overlap of possible closing times for of group A,B, and C loads, plus some margin.

4.5.1.2. Discrete case of: What is the probability that any two load relays within the SAME group will pick the same moment of time for reclosing?

This question is similar to the one already answered above: "Discrete case of: what is the probability that two line relays may generate "random" time delays that may produce equal value?".

The values of the answers are 10% for $\Delta t = 1.0$ s discretization and 1% for $\Delta t = 0.1$ s discretization.

4.5.1.3. Discrete case of: What is the probability that TWO or MORE load relays within the same group will pick the same moment of time for reclosing?

There may be more than two load relays protecting loads from the same load category on any given bus as shown in Figure 43. For this calculation, the question is: "What is the probability of two or more load relays from the same load category closing at once?".

In this case, the calculation of this probability reduces to calculating the binomial distribution coefficients C_k^n ("n choose k") and finding the probability of n out of k relays will "pick" the same time, during any given period of time Δt. Therefore, the actual answer to these probabilities questions will always be depend on the number "n" (the count of loads on the same lateral of the same group). Below we will show the methodology of the calculation, the actual values may be calculated for each actual microgrid topology.

If the delay is quantized in integer seconds (Δt = 1.0 s), then the probability of two out of three relays closing at the same time can be found as:

$$P_{k\ out\ of\ n\ relays} = \frac{C_2^3 \cdot n \cdot (n-1)}{10^n} = \frac{3 \cdot 10 \cdot 9}{10^3} = 0.27$$

where C_k^n is a binomial distribution coefficient ("n choose k"). If the delay is quantized in decimal seconds (Δ = 0.1 s), then the probability can be found as:

$$P_{k\ out\ of\ n\ relays} = \frac{C_2^3 \cdot 100 \cdot (100-1)}{100^n} = \frac{3 \cdot 100 \cdot 99}{100^3} = 0.0297$$

The probability of two out of four load relays closing at the same time with Δ = 1.0 s can be found as:

$$P_{k\ out\ of\ n\ relays} = \frac{C_2^4 \cdot 10 \cdot (10-1)}{10^n} = \frac{6 \cdot 10 \cdot 9}{10^3} = 0.54$$

If Δ = 0.1 s, then the probability can be found as

$$P_{k\ out\ of\ n\ relays} = \frac{C_2^4 \cdot 100 \cdot (100-1)}{100^n} = \frac{6 \cdot 100 \cdot 99}{100^3} = 0.0594$$

And lastly, probabilities for three out of four for integers with Δ = 1.0 s:

$$P_{k\ out\ of\ n\ relays} = \frac{C_3^4 \cdot 10 \cdot (10-1)}{10^n} = \frac{4 \cdot 10 \cdot 9}{10^3} = 0.36$$

and for Δ = 0.1 s:

$$P_{k\ out\ of\ n\ relays} = \frac{C_3^4 \cdot 100 \cdot (100-1)}{100^n} = \frac{4 \cdot 100 \cdot 99}{100^3} = 0.0396$$

The final results are shown in Table 17.

Table 17. Probabilities of load or line relays selecting the same random time delay.

	Delay value: $\Delta = 1.0$ s	Delay value: $\Delta = 0.1$ s
Two line relays closing	10%	1%
Two out of three load relays	27%	2.97%
Three out of four load relays	36%	3.96%
Two out of four load relays	54%	5.94%

Note that for load relays, an event of several relays of the same group closing at the same time does not necessarily constitute a bad event or a failure. This only means that the system may see several loads pick up at the same time. If these loads are not the largest loads, then it is likely that the system's sources can accommodate such an event. Therefore, probabilities in the range of 27%- 54% do not need to be treated as alarming. Additionally, the calculation above was shown for such simultaneous load closing at ANY of the selected time interval – which implies that realistic voltage levels have not changed during such time interval (i.e. extremely steady state condition). This condition is probably not realistic since the voltages will always be changing. Therefore, the probabilities calculated above are the extreme worst case scenario, and can be used as a guideline for the "no-worse-than" calculations. Further, if one of such loads represents a significant or heavy load and really MUST be avoided in potential simultaneous reclosure, it would be reasonable to move up such load in the classification scale (for example, upgrade classification from Group C to Group B, or Group B to Group A) in order to avoid a possibility of several heavy and/or critical loads coming on at once.

These statistical probabilities lead to several conclusions on both the feasibility of proposed protection algorithms and their timescales:

1. Delay value quantization of 0.1 sec seems to produce probability values low enough to be concerned about, within the scope of this project.
2. A delay of 0.1 sec at 60 Hz frequency translates into 6 electrical cycles. This indicates that we are at a "sweet spot" of trade-offs between:
    a. Time step of 0.1 sec where computational and processing times of electronics can be achieved with fairly cheap resources (such as cheap microprocessors); and
    b. Waiting for several electric cycles, which is enough for IBRs to achieve steady-state operation and interaction with the rest of the power system.

5. PREVENTION OF FORMATION OF UNINTENTIONAL MESHES

The method presented in this section is described in [23]. To the best of our knowledge, this is the first method for solving the unintentional loop prevention problem in self-assembling power systems.

5.1. Background

As noted above, one challenge SHAZAM must deal with is to ensure that the off-grid power system does not self-assemble into any configuration that is in some way undesirable. One such configuration that must typically be avoided is the creation of closed loops. Most North American distribution is designed to be purely radial, meaning that there is only one path from the grid source to each load. In off-grid systems formed from circuits designed to be operated radially, unintentional formation of closed loops can lead to operational problems, such as large circulating currents, difficulties in paralleling tap-changing voltage-regulating transformers [13], [22] or issues with protection [14], [23].

The example system shown in Figure 42 illustrates how unintentional closed loops may be formed in a SHePS. This off-grid system is formed from a section of subtransmission (SBTSM_1 at the top of the figure) and two existing distribution circuits, FDR_1 on the left and FDR_2 on the right. Grid-forming sources are labeled "GFM" and are shown in blue, and grid-following sources are labeled "GFL" and are shown in green. The red boxes indicated closed breakers, the green boxes indicate open breakers, and the heavy black arrows are loads. The breakers at either end of the subtransmission section are green, indicating that they are open and this portion of the system is operating off-grid.

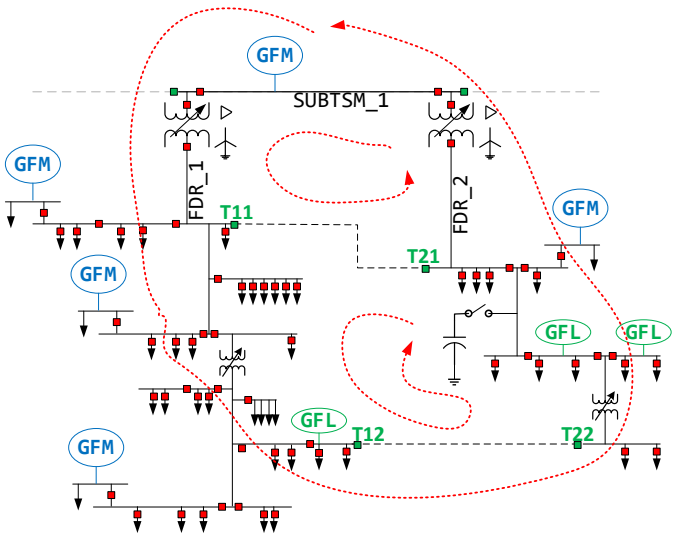

Figure 42. Example SHePS including two distribution circuits and a portion of a subtransmission circuit, showing the locations of potential closed-loop paths.

This system includes two normally-open tie lines between FDR_1 and FDR_2. These tie lines are isolated at both ends by breakers T11-T21 and T12-T22. In many situations, overall power system resilience could be significantly enhanced if the tie-line breakers could be automated as part of the SHePS scheme. However, there are three ways in which closed loops could be formed in this system, as shown by the dashed red loops. This system is designed for radial operation, so formation of any of these loops must be prevented, and in SHAZAM, this must be achieved using local measurements only.

If there is in-range voltage on one side only, then the other side is de-energized and closing of that relay cannot form a loop. Thus, the loop-prevention function will only need to operate in a situation in which an open line relay detects in-range voltage and frequency on both sides. The synchronization check function (IEEE function 25 [21]) must also be satisfied in this case. Because the difference in frequency on either side of the relay will typically be fairly small (on the order of a few tenths of a Hz at most), the sync-check function will operate slowly, possibly taking tens of seconds to reach phase matching. Thus, the loop detection function does not need to be especially fast; operation times of as much as 10 to 20 seconds or more should not cause unacceptable system performance degradation.

5.2. Theory and Proposed Method

Figure 43 shows an open line relay that is on the boundary between two small off-grid power systems x and y, and the potential transformers (PTs) that provide voltage measurements to the line relay from either side.

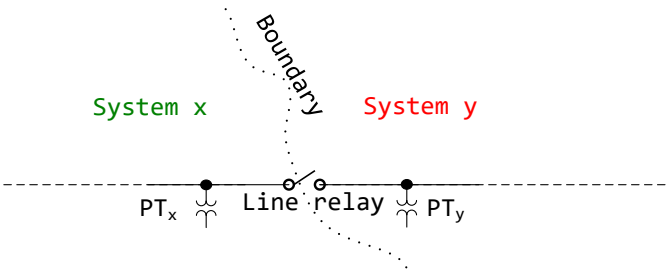

Figure 43. Example of a line relay on the boundary between two subsystems, with measurements on each side of the boundary.

If systems x and y are not connected to each other, then closing the line relay in Figure 43 will network the two systems, allowing them to share resources. This is generally a desirable situation. However, if systems x and y are already connected at some other point, closing the line relay in Figure 43 will form a closed loop through this line relay and that existing point of interconnection. Thus, the key loop-prevention challenge lies in enabling the relay in Figure 43 to determine using local measurements only whether systems x and y are already connected somewhere else.

As noted above, in SHAZAM, all of the GFM IBRs use a linear frequency droop function as shown in Figure 1, which is expressed in equation form as

$$f(t) = f_0 + m(P(t) - P_0) \tag{3}$$

where $f(t)$ is the operating frequency at time t, f_0 is the operating frequency corresponding to power P_0, $P(t)$ is the power being drawn from the source at time t (i.e., the load power at time t) and m is the desired slope of the power-frequency droop line. The load power $P(t)$ can be expressed as a combination of an average component, P_{avg}, and a randomly-varying component, P_{rand}:

$$P = P_{avg} + P_{rand}\,(t) \tag{4}$$

Substituting Eq. (4) into Eq. (3) shows that the operating frequency $f(t)$ also has a random component:

$$f_{rand}\,(t) + f_{avg} = mP_{rand}\,(t) + [f_0 + m(P_{avg} - P_0)] \quad (5)$$

Assume that the loads in systems x and y will vary independently (an assumption that will be supported via real-world data subsequently). Thus, if systems x and y are not connected at any point, then their sources will see load variations $P_{xrand}(t)$ and $P_{yrand}(t)$ that are independent. Reflecting each of these independent power vectors off of the droop curve of each source using Eq. (5) results in two $f(t)$ vectors with independent $f_{xrand}(t)$ and $f_{yrand}(t)$ components. However, if systems x and y are interconnected, then their sources share a total load, a common frequency, and a common frequency variation, as demonstrated in the house diagram in Figure 44. In this case, their $f_{xrand}(t)$ and $f_{yrand}(t)$ components will be very similar over time periods of a few seconds to a few tens of seconds.

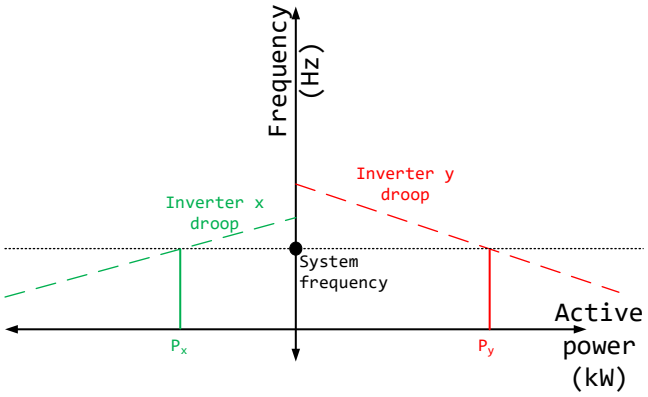

Figure 44. House diagram for the sources in systems x and y from Figure 43.

The independence or non-independence of the two frequency vectors can be identified via any of several statistical comparisons of the vectors. For example, Pearson's correlation r [24] between the two frequency vectors would be expected to yield very close to +1.0 when the two systems are connected, but would vary widely between ± 1.0 when they are independent. Similarly, it would be expected that the average error at each time step between the two frequency vectors would be much larger when the systems are independent than when they are connected. Thus, the mean absolute error (MAE) [24] between the two frequency vectors would be expected to be orders of magnitude smaller when the systems are connected than when they are independent. This provides two means for determining from local measurements only whether closure of any line relay will form a closed loop.

A flow diagram illustrating the decision-making process for the closure of the line relay in Figure 43 is shown in Fig. 4. The process starts at the center-left with the breaker open. The x- and y-side voltages are measured, and are processed in two ways: extraction of magnitude and phase for the sync check, and calculation of the correlation or MAE for the loop detector. If both the loop detector and the sync check determine that breaker closure is allowed, then the breaker closes and the process terminates until the breaker is open again.

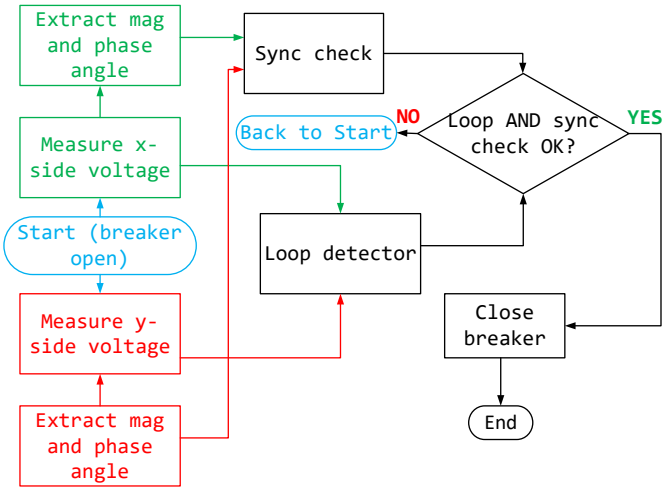

Figure 45. Flow diagram for loop detection and sync check.

5.3. Demonstration of Non-Correlation of Geographically Adjacent Loads

Either implementation of the proposed method of unintentional loop detection relies on there being an uncorrelated variation between the loads in adjacent microgrids, over a time window of a few seconds to a few tens of seconds. Because of the reliance of the loop-prevention method on this property of loads, it is important to demonstrate that real-world loads actually do have this property. Thus, to demonstrate this lack of correlation between real-world loads, two sets of 1-second load data, one measured at the individual residence level and one measured at the feeder-head level, were analyzed using MATLAB. This section presents the results of those analyses.

5.3.1. Data from Ota City, Japan

The first data set includes two years' worth of 1-second data measured at individual residence meters for 586 residences in Ota City, Japan. These residences are geographically clustered within a roughly 1 km × 1 km area, and are served by the same distribution circuit. Details of the system and the data set are found in [25]. Because summing of individual residence loads will lead to "smoothing" of their total load via load diversity and this smoothing will increase the level of correlation between aggregations of loads, two synthetic 'microgrids' were created by summing the first 260 residences (1-260) and the next 260 residences (261-520) into two aggregates. Figure 46 shows the power demand of these two synthetic microgrids for a subset of the total time period (a portion of the June 2007 data). It can be seen in Figure 46 that the microgrids' loads *do* correlate over longer intervals—for example, there is a clear diurnal correlation in the loads—but superimposed onto this is a higher-frequency noise that results from the shorter-term individual load switching referred to earlier in this paper. That higher-frequency variation is the variation on which the loop detection method will rely. The load data are measured at a 1-s interval, meaning that the Nyquist frequency is only 0.5 Hz. Some load variation that is relevant to this method will be faster than this and will be aliased to lower frequencies in these data. Figure 47 shows a zoomed-in view of Figure 46, after high-pass filtering to remove the DC offset. It is visually apparent that these loads are changing independently; short times can be found in which the loads are well-correlated, anticorrelated, and uncorrelated. Figure 48 shows the Pearson's correlation coefficient versus time between the two synthetic microgrids' active power demand, using a 7200-point buffer. As expected from the visual inspection of the data, the correlation

appears oscillatory, fluctuating over a range of almost ±0.9 with approximately zero mean. Figure 49 shows a moving-average filtered version of the correlation in Figure 48, showing that the mean value of the correlation is low.

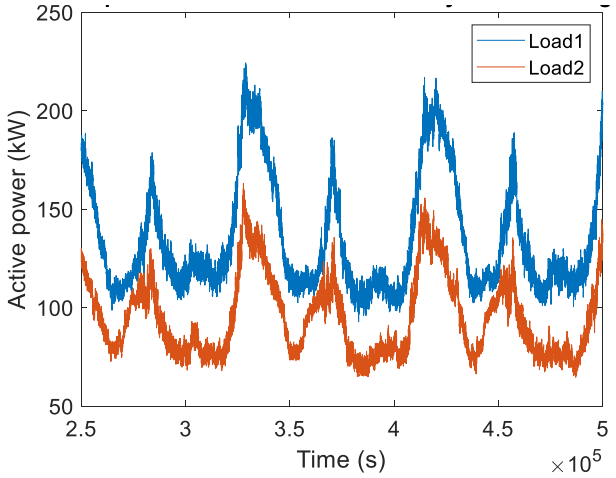

Figure 46. Active power demand vs. time at 1-s resolution of the two synthetic microgrids, using the June 2007 data from Ota City, Japan.

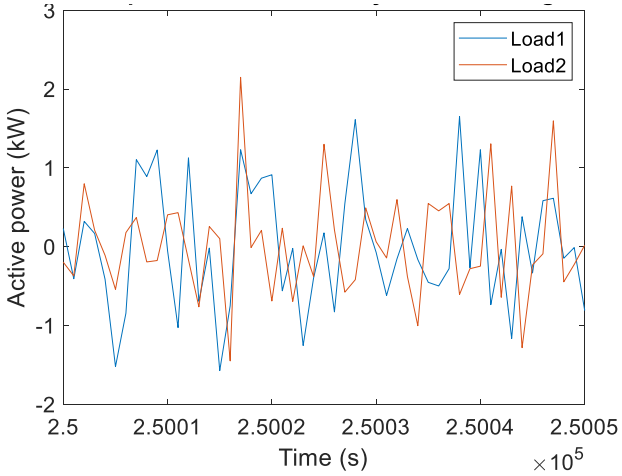

Figure 47. Zoomed-in view of the active power demand of the two synthetic microgrids, with the DC offset between them removed.

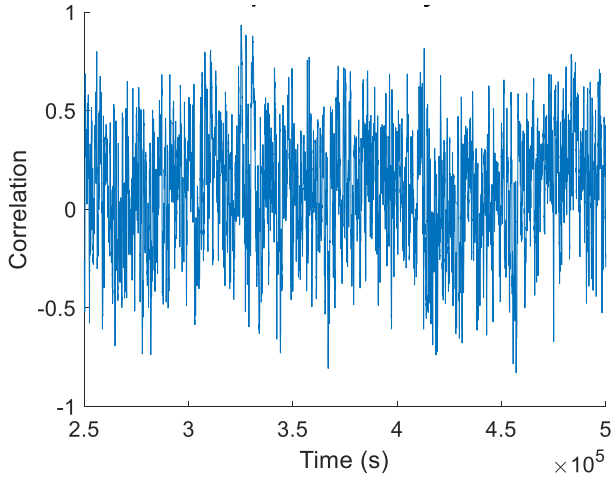

Figure 48. Pearson's correlation vs. time between the power demand of two aggregated 'synthetic microgrids' using the June 2007 Ota City data.

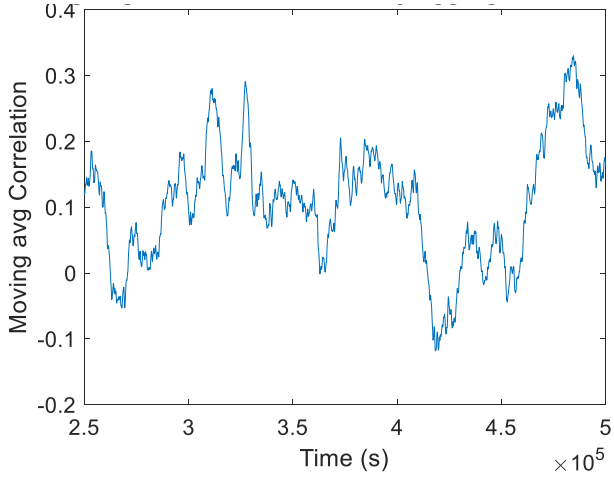

Figure 49. Moving-average correlation vs. time between the power demand of two aggregated 'synthetic microgrids' using the June 2007 Ota City data.

5.3.2. Data from Cordova, AK

A second set of data was also analyzed for this work. This data set contains two years' worth of 1-second data provided by the Cordova Electric Cooperative (CEC) system in Cordova, AK [26], measured at the feeder head-end level. There are data sets for five separate feeder head-ends fed from a common main bus. Figure 50 shows the active power vs. time at 1-s resolution measured at the head ends of two similar feeders, for a small segment of the data recorded in June 2015. Similar to the Ota City case, the CEC data show a correlated diurnal variation, with a higher-frequency uncorrelated variation superimposed on it. Figure 51 shows a zoomed-in view of a section of the data in Figure 50, highlighting this higher-frequency variation. Figure 52 shows Pearson's correlation calculated on the data set in Figure 50, and Figure 53 shows the results in Figure 52 after passage through a moving-average filter. The correlation in Figure 52 shows "noisy" behavior similar to that in Figure 48, with a low mean value as shown in Figure 53.

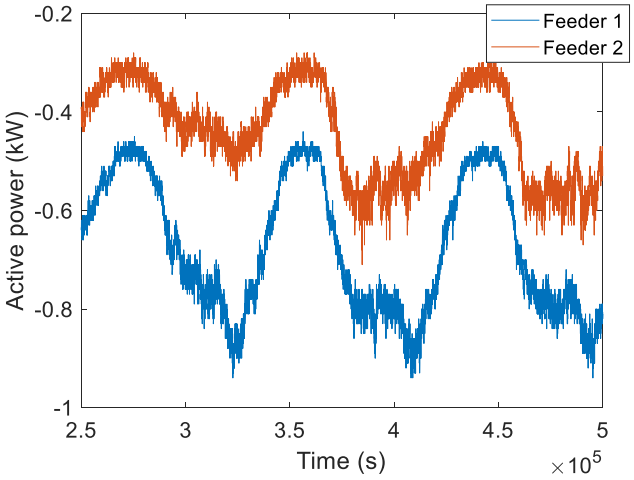

Figure 50. Active power vs. time at 1-s resolution measured at two feeder head-ends for the CEC system.

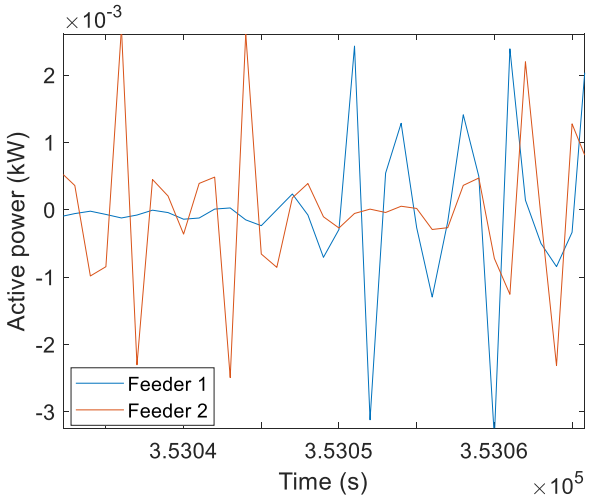

Figure 51. Zoomed-in view of the active power demand of the two feeders, after removal of the DC offset between them

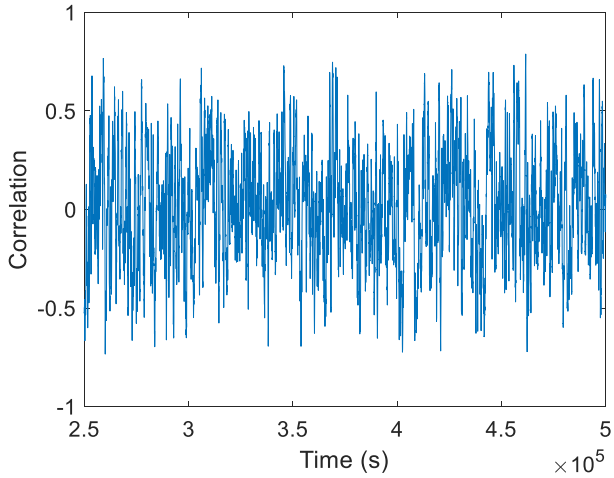

Figure 52. Pearson's correlation vs. time between the active power demand of the two CEC feeders.

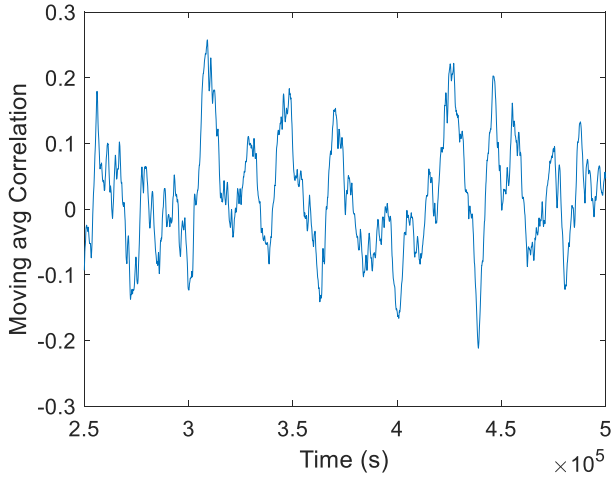

Figure 53. Moving-average correlation vs. time between the active power demands of the two CEC feeders.

5.4. Demonstration of unintentional loop formation detection via simulation

To demonstrate the operation of the unintentional loop prevention function, the IEEE 13-bus distribution test circuit [21] was partitioned into three microgrids. Figure 54 shows a simplified one-line diagram of the 13-bus system, and Figure 55 shows the actual PSCAD model of the 13-bus test circuit. The blue dashed lines in both figures indicate the boundaries between the microgrids. Microgrid Boundary Relays (MBRs), also shown in blue, connect the microgrids to one another after a user-selected time has elapsed and synchronization-check conditions are met. Each microgrid has an inverter-based source, the locations of which are indicated by the heavy black boxes along the right side of the figures. The numbers 633, 671, and 675 in the black boxes indicate the node number in the IEEE 13-bus test feeder to which each inverter is connected. For this work, two tie lines and two normally-open tie-line breakers TL1 and TL2 were added to the 13-bus model. These are shown in green. The inverters are represented in PSCAD using a generic H-bridge model switching at 3.6 kHz

with forward- and backward-rotating dq0-frame grid-forming controls. The inverters have a linear power-frequency droop characteristic as shown in Figure 1. The microgrids are numbered 633, 671, and 675, corresponding to the number of the inverter in that microgrid. In the PSCAD model in Figure 55, each microgrid includes a pseudo-random load that consists of a small parallel R-L load (about 2% of the total microgrid load) that is switched on and off at random times using the switching function generator shown in Figure 56. The simulation time step used is 20 μs, and the sampling rate of the data for post-processing is 5 kHz.

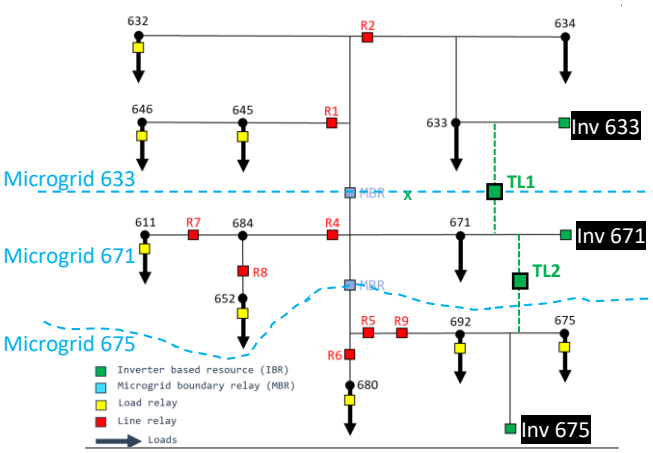

Figure 54. One-line diagram of the IEEE 13-bus system, partitioned into three microgrids each with an inverter-based source, and with two added tie lines and tie-line breakers TL1 and TL2.

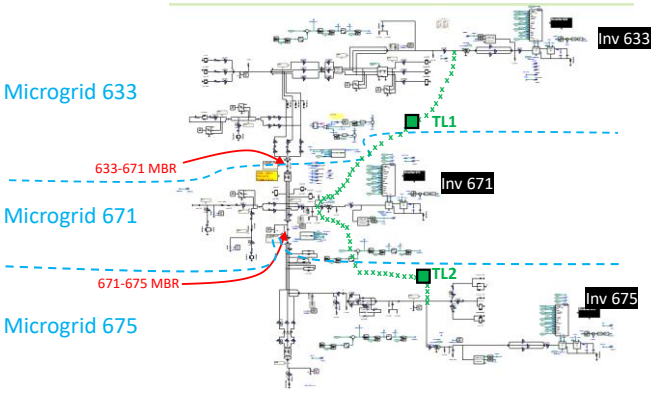

Figure 55. PSCAD model of the system in Figure 54.

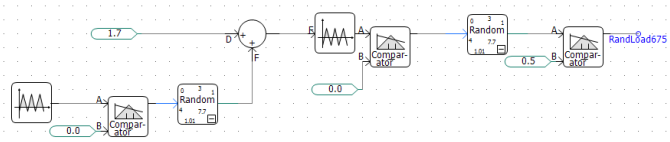

Figure 56. Block diagram of the random load switching-function generator.

The simulations start with the three microgrids all operating independently, meaning that all of the tie-line breakers and MBRs are open. At t = 15 s, the MBR between microgrids 671 and 675 is allowed to close once its synchronization check conditions are satisfied, and at t = 35 s, the MBR between

microgrids 633 and 671 is allowed to close. In each microgrid, the frequency is measured using a phase-locked loop (PLL), the output of which is then filtered using a first-order low-pass filter with a 0.5-sec time constant. Two categories of use cases were studied: 1) "unmatched" cases in which the loading is such that there is a steady-state frequency difference between adjacent microgrids; and 2) "matched" cases in which the microgrid loads were manipulated so that the steady-state frequencies between two adjacent microgrids were essentially equal. In the plots below, a red vertical dashed line marks the time at which the MBR between microgrids 671 and 675 is allowed to close, and a purple vertical dashed line marks the time at which the MBR between microgrids 633 and 671 is allowed to close. The cases presented below provide representative results.

5.4.1. Unmatched load case, using correlation

Figure 57 Figure 59 show correlation-based results for an "unmatched load case", with the correlation calculated using MATLAB's "corr" function [27] calculated over a sliding window. Figure 57 shows the 5 kHz-sampled frequency vs. time for each of the three microgrids in an unmatched load case. Until t = 15, all three microgrids are independent, and there is a steady-state difference in frequency between any two microgrids. In this period, any two microgrids could be connected without forming a loop. Just after t = 15 s, the 671-675 MBR closes, and the frequencies of those two microgrids become equal as their inverters share load according to the droop characteristic (Figure 44). Now if TL2 (Fig. 15) were closed, a closed loop would be formed. At roughly t = 37 s, the 633-671 MBR closes, and after that, all three microgrids have the same average frequency. Following this, the closure of either TL1 or TL2 would form a loop, so the closure of either tie-line relay should be blocked. Figure 58 shows the unfiltered (raw) correlations vs. time over a 50,000-point (10-second) moving buffer between each pair of frequencies. For the first 10 s of the simulation, the correlation shows as zero because the buffers are filling. The trace labeled 633-671 shows the correlation between the frequencies on either side of TL1, and 671-675 shows the correlation between the frequencies on either side of TL2. The correlation between 633 and 675 is also included. Figure 58 shows that the correlation of frequencies between any two independent microgrids is low (less than 0.5), but as soon as any two microgrids are connected at one point, such that connection at a second point would form a loop, the correlation between their frequencies rises rapidly and remains above 0.98. Figure 59 shows the correlations of Figure 58 after passing through a moving-median filter with a 50,000-point (10-second) buffer. The median-filtered results increase the margin between connected and disconnected cases while preserving a reasonable speed of response. As predicted, the independent microgrids have uncorrelated frequencies and a tie line relay between them could be allowed to close, but as soon as the microgrids are connected and a loop becomes possible, their frequencies are strongly correlated, and the closure of a relay seeing these frequencies on either side is blocked to avoid loop formation.

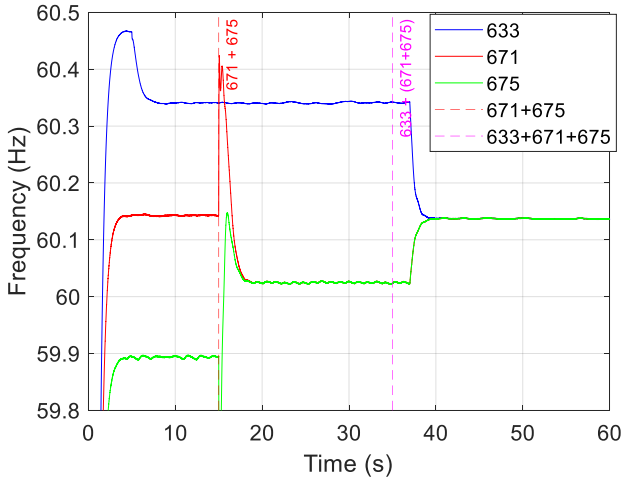

Figure 57. Measured frequencies, unmatched load case.

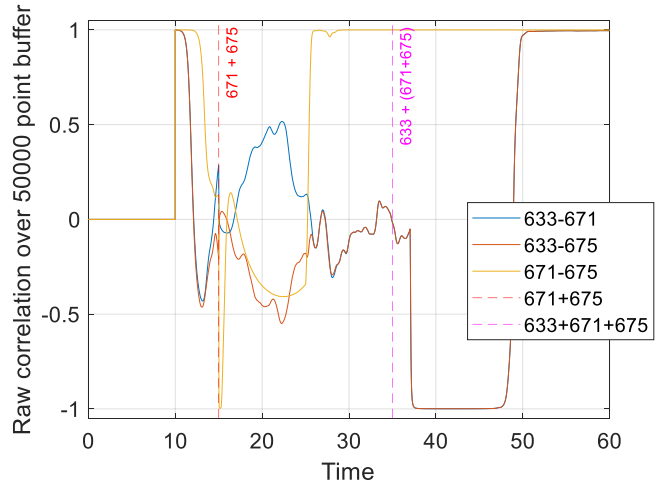

Figure 58. Raw correlations vs. time, unmatched load case.

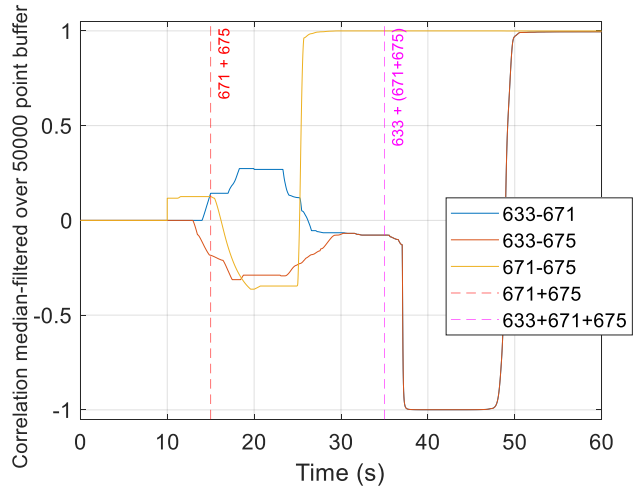

Figure 59. Moving-median-filtered correlation vs. time, unmatched load case.

5.4.2. Matched load case, using correlation

Figure 60, Figure 61, and Figure 62 show correlation-based results for a "matched load case". In this case, the load of microgrid 633 was manipulated so that after the 671-675 MBR closes, the average frequency of that 671+675 combined microgrid is equal to that of microgrid 633. Figure 60 shows the measured frequencies in the three microgrids. Once the 671-675 MBR

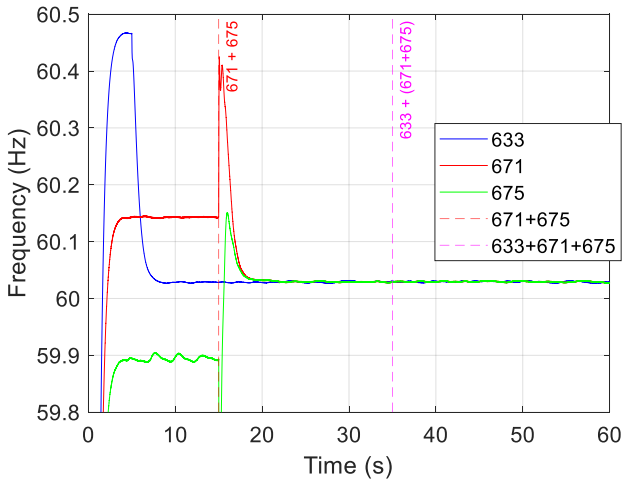

Figure 60. Measured frequencies, matched load case.

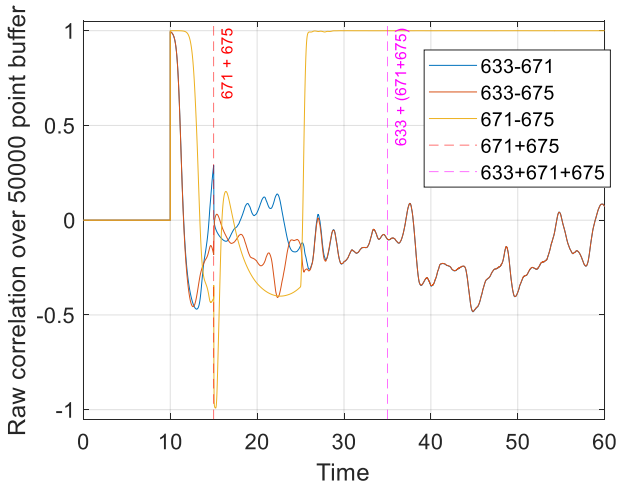

Figure 61. Raw correlations vs. time, matched load case.

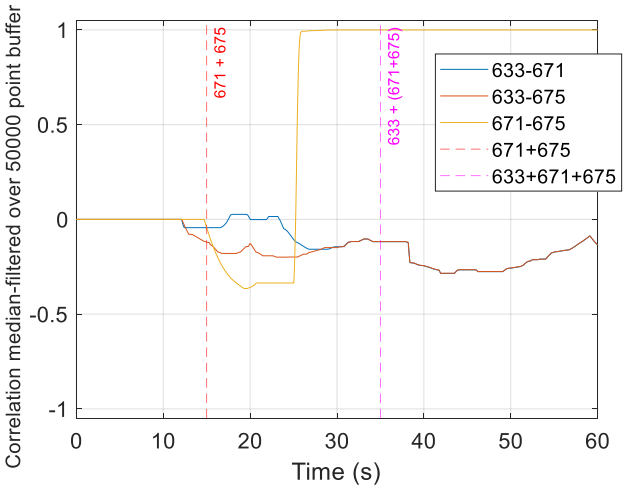

Figure 62. Moving-median-filtered correlations vs. time, matched load case.

closes (just after t = 15 s), the frequencies of those two microgrids become equal, and they align very closely with the frequency of microgrid 675, which is still independent. Under this condition, TL1 cannot be closed without forming a loop, but TL2 could be closed, and thus these conditions must be differentiated. Figure 61 shows the unfiltered Pearson's correlations between each pair of measured frequencies, calculated using MATLAB's "corr" function [27] over a sliding window, and Figure 62 shows the results from Figure 61 after passing through a moving median filter. Figure 62 shows that the 633-671 correlation is near unity after these two microgrids are connected, indicating that closing further connections between them would form loops. The 633-675 and the 671-675 correlations remain very low, indicating that the closure of a relay between these could be allowed. Thus, correlation is effective in preventing the unintentional formation of closed loops.

5.4.3. Matched load case, using MAE

Figure 63 shows MAE-based results for the matched-load case[4]. Microgrid 633 is independent throughout the simulation, and the MAE between microgrid 633's frequency and that of either of the other two microgrids hovers around 1×10^{-3} Hz. Microgrids 671 and 675 connect just after t = 15 s, and after that time the MAE between their frequencies drops to just over 1×10^{-5} Hz.

The MAE is calculated over a sliding window as

$$MAE_k = \frac{\sum_{i=k}^{k+N} |f_{1,i} - f_{2,i}|}{N} \tag{6}$$

where k is the starting index of the MAE window, MAE_k is the value of the MAE over the window starting at point k, f_1 and f_2 are the two vectors of frequency measurements, and N is the number of data points over which the MAE is calculated (here, 50,000).

[4] MAE easily detects the unmatched load case because it is sensitive to the offset in frequencies. Thus, for MAE, the matched-load case is the worst case, so that is the case shown here.

As expected, the MAE between the frequencies in the two connected microgrids is much smaller (here, two orders of magnitude smaller) than between independent microgrids. The connected versus non-connected cases are clearly distinguished, and thus MAE can also be used to prevent unintentional loop formation.

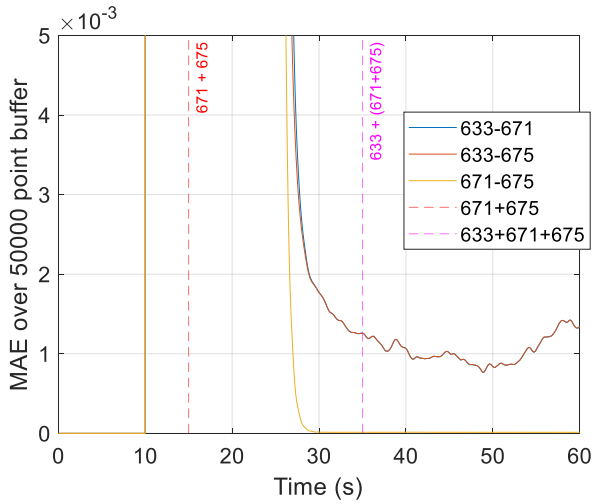

Figure 63. MAE vs time, matched load case.

5.5. Discussion

The results above show that filtered correlation and mean absolute error can both be used to reliably indicate whether the closure of a relay would lead to the formation of a loop. In the correlation-based implementation, closure of the relay can be allowed if the windowed-average correlation between the filtered frequencies of the voltages on either side of the relay is below some threshold (say, < 0.9), but closure should be blocked if that correlation is above that threshold because this indicates that closure of the relay could create a loop. It appears that filtering of the correlation results in a method that has a good margin between the two cases, and acts within a time frame suitable for this application. In the MAE-based implementation, there was a large detection margin between the two cases with no further filtering; a threshold of 1×10^{-4} Hz would allow detection and preserve a large buffer against nuisance trips.

Correlation is a nonlinear, sensitive function. This sensitivity can be advantageous in some circumstances, but it could also in some cases lead to erratic behavior. For example, Pearson's *r* is sensitive to outliners [24], so some form of outlier removal might be necessary to ensure reliable performance. The MAE, by contrast, is a well-behaved, linear function. Also, correlation by itself does not detect when there is a constant "DC" offset between the frequency vectors, so when the correlation-based implementation is used, a difference in average frequencies between the two vectors could be used as a separate indication that the relay can be safely closed without forming a closed loop. The MAE, on the other hand, intrinsically detects a "DC" offset of this type and does not require that as a separate condition.

On the other hand, because MAE has units of frequency, the MAE-based implementation may depend more strongly than the correlation-based method on the parameters of the inverter controls, such as specific droop slopes. Thus, the threshold values may be more inverter-specific for the MAE-based method than for the correlation-based method. Also, the magnitude of the frequency variation may become smaller as the system gets larger, which could reduce the margin between the case in which a

loop would not be formed and the case in which a loop would be formed. Thus, the MAE-based version could potentially be less scalable than the correlation-based version.

It is not clear how effective either method would be in a case in which the sources are under isochronous control. Detection still seems likely because there would still be small uncorrelated changes in frequency between the two intentional-island systems when they are independent, but the frequencies of connected generators under isochronous control are not necessarily linearly related and thus their relationship may not be well-detected by Pearson's correlation [24]. A different correlation, such as Kendall's tau [24], may work better in this case, but computing Kendall's tau over a sliding window would be computationally intensive. The magnitudes of the frequency differences under isochronous control may be sufficiently small that differentiation by the MAE-based method also may no longer work. However, two independent intentional-island systems with isochronous sources and relying only on local measurements would not be good candidates for paralleling in a self-assembling system, so this use case may be of minimal practical concern.

6. PREVENTION OF THERMAL OVERLOADING OF CONDUCTORS

In a self-assembling SHePS, loads may be shifted from one set of conductors to another if those conductors provide an intact path to sources. The sources may have sufficient capacity to serve the load, but the conductors may not. Thus, overloading of conductors during self-assembly can occur. The line relays have awareness of the ampacities of the conductors connected to them and of the currents flowing, so they can detect when thermal overloads occur, but load control is required to alleviate the thermal overload, and the load-control relays cannot detect thermal overloads on upstream conductors on their own. Various forms of artificial intelligence have been applied to this problem [28], [29], [30], but the large training data sets required are not available for self-assembling SHePS, particularly those relying only on local measurements.

In SHAZAM, a voltage modulation technique was created and demonstrated in simulation to address this problem. In this technique, referred to as the "tapping" method, a line relay that senses an overload is opened and closed in a series of "taps" to modulate the voltage downstream from the relay. The load-control relays in that downstream zone can detect this voltage modulation and appropriately relieve the thermal overload by switching off some loads, least-critical loads first. Methods for enabling shed loads to determine when to reconnect to the system are also proposed and demonstrated.

6.1. Theory

6.1.1. Overload detection and mitigation

Consider the example system shown in Figure 64, which is based on the IEEE 13-bus test circuit [21]. This system is separated into three microgrids by the Microgrid Boundary Relays (MBRs) shown in the figure. Each microgrid has a grid-forming inverter-based resource (IBR) indicated by the green labels at the left of the figure. Line relays are shown as red boxes, and load relays are shown as yellow boxes.

Consider an example case in which the system in Figure 64 is in the off-grid mode operating only from its inverter-based sources, and a thermal overload of the conductor between single-phase line relay R4 (near the center of Figure 64) and node 684 (to the left of line relay R4 in Figure 64) occurs. The overload is caused by there being too much load at nodes 611 and 652. Line relay R4, from its local current measurements, can detect that this conductor is loaded beyond its ampacity, but by itself the only action R4 could take would be to open and black out the entire system downstream from R4. It would be more desirable to somehow cause noncritical loads at nodes 611 and 652 to disconnect. Thus, in the method proposed here, the line relay opens and closes ("taps") in a predetermined pattern, which modulates the voltage downstream from the line relay, analogous to sending Morse code along the conductor. Downstream load relays are programmed to look for this pattern, and if it is detected, lower-priority loads are disconnected to relieve the overload.

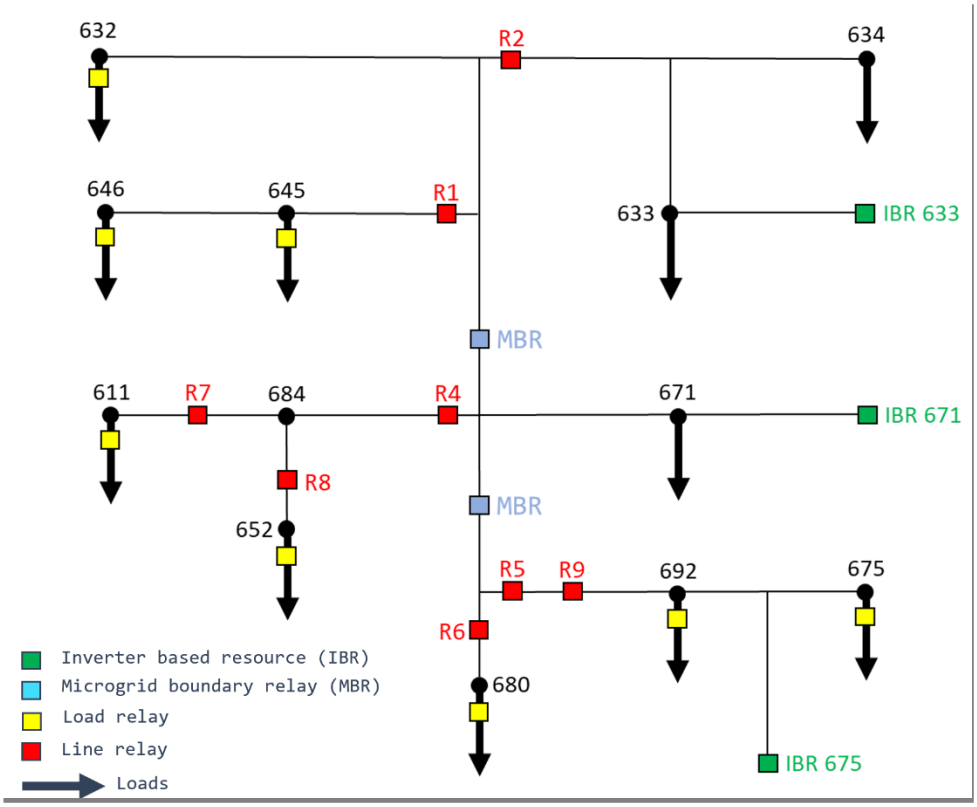

Figure 64. Single-line diagram of the modified IEEE 13-bus test circuit diagram used to describe and test the tapping method.

6.1.1.1. Reclosing Load Relays

The loads that were shed to relieve the thermal overload must be able to automatically reconnect at some point. To enable this, the load relays monitor their windowed-average voltage and are allowed to reclose if at least one of three following conditions are met:

- The voltage drops to zero. This indicates that the SHePS may have undergone a reconfiguration such that the load may not be served through the same path as before, so the thermal overload issue may no longer exist and the load could attempt to come back online.
- The voltage increases by at least two percent from its previous value. This suggests that another load in the system has switched off, freeing enough thermal capacity to reconnect the load that was disconnected to relieve the thermal overload.
- The voltage exceeds 1.0 volts per unit for a preset length of time. This also suggests a load reduction that might have freed up sufficient capacity to allow the disconnected load to reconnect without creating an overload.

If closure of the load relays causes another overload, the tapping of the line relay begins again.

6.2. Demonstration Procedure

6.2.1. Test System

The proposed tapping technique is demonstrated using a PSCAD model of the IEEE 13-bus distribution test circuit [21]. The model is separated into three microgrids, as shown in Figure 64. The system is operating in the off-grid mode. Each microgrid is energized by a grid-forming inverter, modeled here using a switching (non-averaged) three-phase H-bridge inverter with forward- and backward-rotating dq0-frame grid-forming controls, with current limiting.

6.2.2. Overload Detection and Tapping Implementation

The thermal-overload current thresholds in each line relay were set to 125% of the corresponding cable ampacity. Once a thermal overload is detected, the line relay triggers its tapping sequence. The cable between line relay R4 and node 684 in Fig. 1 has an ampacity of 120 amps, so if the current through R4 exceeds 150 amps, R4 detects a thermal overload of that conductor.

Figure 65 shows the tapping pattern used by R4 for this demonstration. At roughly t = 3 s, R4 begins its tapping sequence. R4 opens, stays open for 25 milliseconds (selected to be shorter than the zero-voltage duration allowed by the ITIC/CBEMA curve, to avoid adverse impacts on loads), and then recloses. This is one tap. The breaker remains closed for approximately 225 milliseconds before executing another tap. The entire tapping pattern of R4 lasts less than 0.5 seconds and contains three evenly spaced taps. In practice, the duration and spacing of the taps must be chosen strategically. This will be elaborated on in a later section.

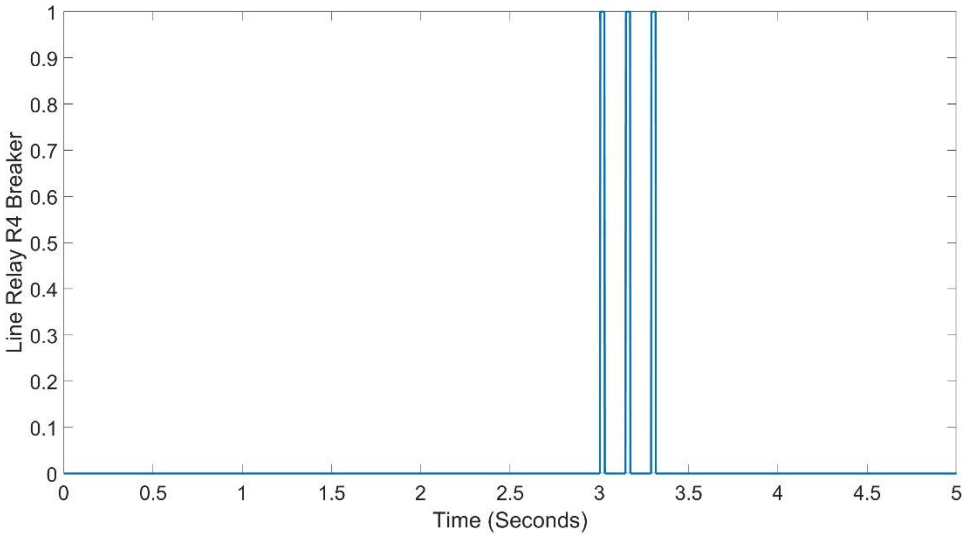

Figure 65. The tapping pattern used in relay R4 in this demonstration. Zero indicates a closed breaker and one indicates an open breaker.

6.2.3. Detection of the Tapping Signal by Load Relays

Load relays detect and interpret the tapping signal using a finite-state machine (FSM), the flow diagram of which is shown in Figure 66. The load relay counts one tap if the voltage drops below a pre-determined threshold and recovers within a specified duration. The voltage threshold and the

recovery duration are determined by the nature of the expected tapping signal. For instance, load relay 611 in the example counts a tap when the voltage drops below 0.3 volts per unit and recovers within 50 milliseconds.

Each time a tap is detected, the load relay FSM moves to the next state. It will reset if the duration between taps is longer or shorter than a predetermined value. When the highest state is reached, this means that a complete tapping signal was detected, indicating that a thermal overload on a conductor is being sensed by an upstream line relay. The load relay then opens to relieve the overload. It remains open until a separate set of logic determines that it may be safe for the load to come back online, resets the FSM, and closes the load relay. Figure 66 illustrates this process with an FSM diagram for a load relay that expects a signal to contain four taps.

In Figure 66, *State 0* transitions to *state 1* when a tap is detected. To ensure the correct signal is detected, *state* N (for $N = 1, 2, 3$) transitions to *state* $N+1$ when a tap is detected within $T_N \pm 10$ *ms*, where T_N is the expected time between taps. At state 4, the load relay is opened. It remains open until a reset signal indicates that it may be safe for the load to come back online without causing an overload.

In this example, the FSM interprets three taps as a complete tapping signal and will open load relay 611 immediately after sensing the signal. Load relay 652 will also experience the voltage drops from the tapping of R4. However, in this demonstration, the load at node 611 is designated less critical than that at 652. Thus, when the first "tapping" pattern occurs, load relay 652 will not open. If the first set of "taps" relieves the overload, no more tapping will occur as the issue is resolved. If this does not relieve the overload, line relay R4 will continue to sense an overload and will send another series of taps. This signals line relay 652 to open as well. If after a set number of attempts the thermal overload is not alleviated, then the line relay R4 will open.

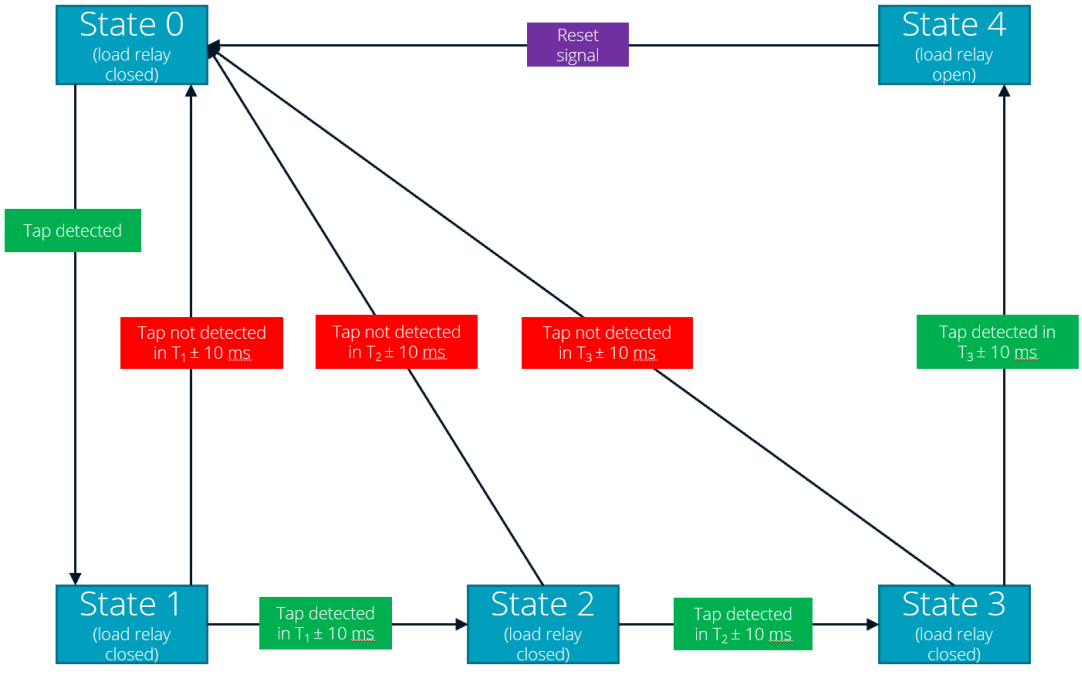

Figure 66. State diagram of the logic used in the load relays to detect tapping signals.

6.2.4. Reclosure conditions

In this demonstration, a load control relay is allowed to reclose if its voltage rises above 1.0 pu for 3 seconds. This rise in voltage indicates that at least some other load has been shed, creating the possibility that the load shed through "tapping" can now be re-energized.

6.3. Demonstration Results

Figure 67 shows a PSCAD demonstration of a thermal overload event. The top trace in Fig. 3 is the current through line relay R4. At first the current is well below the cable's ampacity, but at t = 1 s excessive load is added and the cable's ampacity is exceeded.

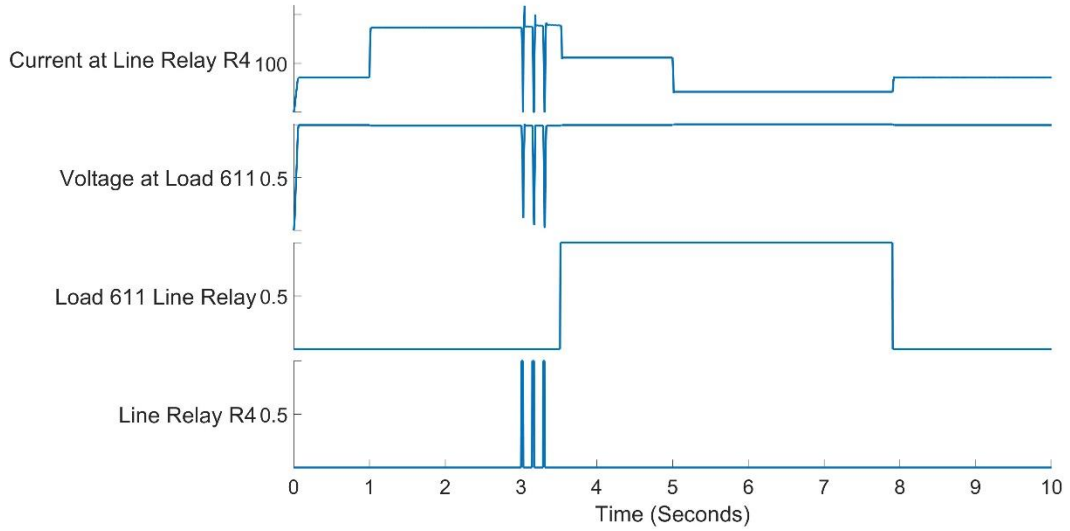

Figure 67. Current through line relay R4 (top), voltage at load control relay 611 (second from top), load-control relay 611 status (third from top); and status of line relay R5 (bottom).

After 2 s of this current, the line relay executes a "tapping" sequence. The bottom trace in Figure 67 shows the line relay status (0 = closed, 1 = open), and the tapping pattern shown in Fig. 3 is evident at t = 3 s in that bottom trace. The second trace in Figure 67 shows the voltage at the load control relay for load 611. When the line relay "taps", the load relay sees dips in the voltage, and the FSM at load control relay 611 receives and interprets this signal. Accordingly, immediately after the third "tap", load control relay 611 disconnects its noncritical load, as seen in the third trace in Figure 67 which is the status of the load 611 breaker (0 = closed, 1 = open). In this case, removal of that load was sufficient to relieve the thermal overload.

Then, at t = 5 s, another load elsewhere on the conductor disconnects. This results in a drop in the current through line relay R4 at t = 5 s (top trace in Figure 67), and a small change in voltage at load control relay 611, which is difficult to see in Figure 67 so a zoomed-in view is provided in Figure 68. The voltage exceeds 1.0, which is one of the conditions that would allow load 611 to reconnect. After the voltage has remained above 1.0 for three seconds, load control relay 611 reconnects, as shown in Figure 67 (third trace). No thermal overload results, and the system continues to operate.

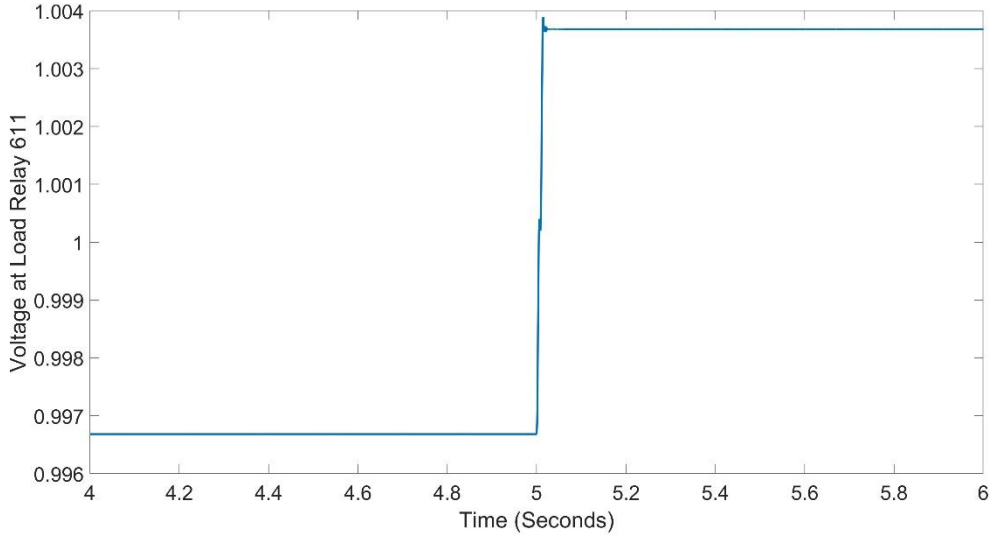

Figure 68. Voltage at load control relay 611 zoomed in on t = 5 s.

6.4. Discussion

6.4.1. Impact on Breaker Lifetime

Perhaps the biggest potential drawback to the proposed tapping method is its potential adverse impact on breaker lifetimes. Conventional electromechanical medium-voltage distribution circuit breakers can be operated somewhere on the order of 5000 times under full load, depending on several factors [31]. Tapping a breaker in this way will increase the number of operations of the breakers associated with the line relays, which will shorten their lifetimes. It is not yet clear how much their lifetimes would be shortened by this tapping method. Further investigation of this factor is needed. The tapping technique would be more suitable for use with solid-state circuit breakers, which are capable of orders of magnitude more operations [32].

6.4.2. Impact of Motor Load on Tapping Signal

Some power system elements, such as motor loads, inline transformers, and shunt capacitors, might have a filtering or smoothing effect on the voltage dips arising from tapping of the breaker. If this effect is too large, it might cause load relays to fail to detect the signal. Figure 69 and Figure 70 show results from a PSCAD simulation using the 13-bus system with a large three-phase motor load included at load 680 (bottom of Figure 64). The line relay that is tapping in this case is R6. When excessive load is applied downstream of R6 and it applies the three-tap pattern shown in Figure 65, Figure 69 shows that the first voltage dip at load 680's load-control relay is much shallower than was the case with a constant-impedance load, indicating that the motor load has had some smoothing effect on the tapping signal.

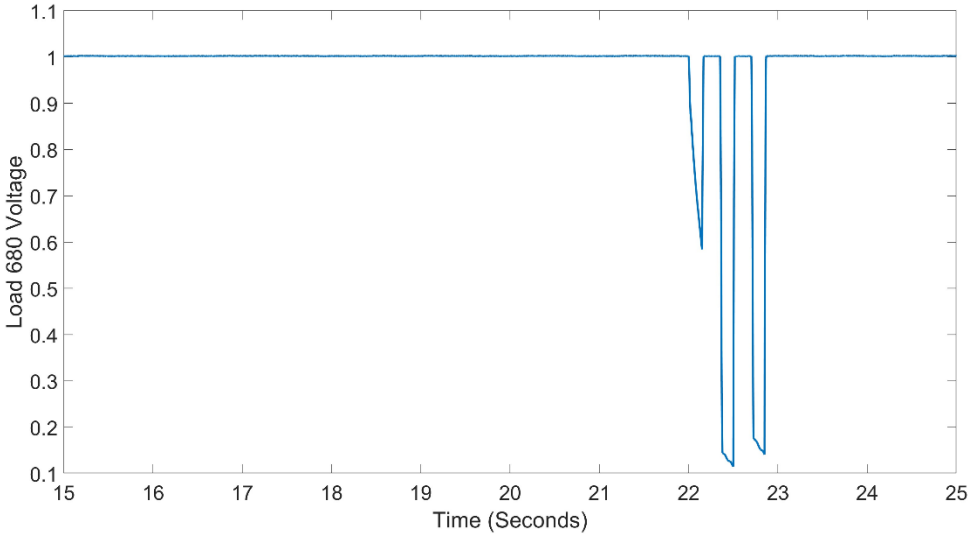

Figure 69. Voltage at load 680 during "tapping" of R6, with motor load.

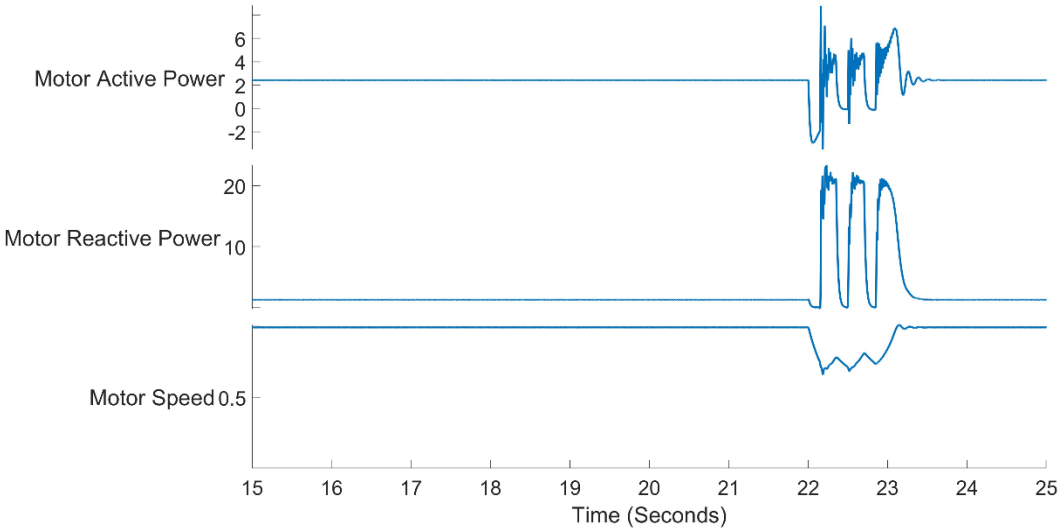

Figure 70. Motor active power (top), reactive power (middle), and speed (bottom) during application of the three-tap pattern.

Figure 70 shows the active power (top), reactive power (middle), and speed (bottom) of the three-phase motor during application of the three-tap pattern from R6. The motor's active power does briefly swing negative during the taps, indicating that the motor has briefly entered generator mode and is supplying energy from its rotating mass (as indicated by the changes in speed, bottom trace of Figure 70). Immediately following each tap, when the voltage returns to nominal, the motor exhibits a reactive current surge, akin to but smaller than a motor-start surge. Figure 71 shows the induction machine phase currents during this same event.

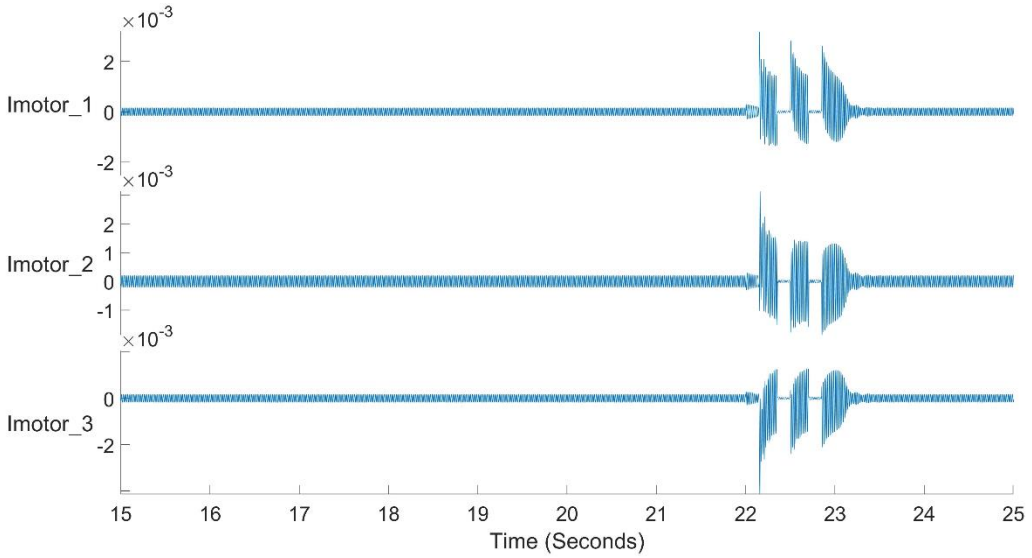

Figure 71. Phase currents drawn by the three-phase induction motor during the application of the three-tap pattern.

6.4.3. Selecting the Tapping Pattern

There is a maximum speed at which an electromechanical circuit breaker in the line relay can go from closed to open to closed again, and this will set a limit on the minimum duration of a tap. While many breakers are capable of 25 millisecond taps, this tap duration may be too short for some breakers.

The duration of each tap also cannot be too long. The repeated voltage drops caused by line relay taps are used to send a signal to downstream load relays, but they can also disrupt load function. The tapping pattern shown as an example here was designed so as to remain in the "No Loss of Function" region of the Information Technology Industry Council (ITIC) curve. Longer-duration taps might result in load malfunctions.

In addition, to avoid nuisance tripping, the tapping pattern must be chosen so that it is minimally likely to be replicated under normal conditions by other system elements.

6.4.4. Load Rejection Overvoltage Considerations

If there is little load between a line relay and a source, tapping of that line relay can result in load-rejection overvoltage. For example, in Fig. 1, line relay R9 is the closest line relay to inverter 675. Figure 72 shows the voltage on the source side of load relay 675 that results from the tapping of line relay R9. Each time R9 is tapped, there is a transient overvoltage reaching a peak of approximately 1.08 p.u. These particular load rejection overvoltages are sufficiently small in magnitude and duration that they do not lead to violations of the ITIC curve, but they are still undesirable.

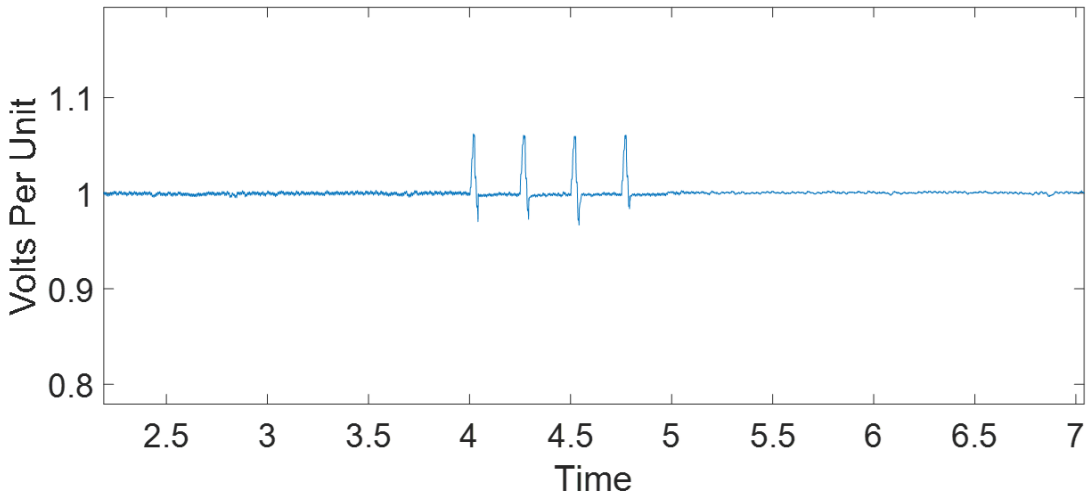

Figure 72. Voltage measured at line relay R9 during tapping, showing brief load rejection overvoltage spikes.

The practical importance of this issue is debatable, because for a SHePS, planning considerations would result in conductors close to sources being sized to carry the entire output of that nearby source. As a result, thermal overload of these conductors would result in an overload of the source itself. According to the SHAZAM logic, this would trigger undervoltage load shedding according to load Group priority until the overload is eliminated.

6.5. Future work

Future work will include implementing and testing the tapping method in larger and more complex models; investigating the impact on breaker lifetime and identifying breaker types that are most compatible with this technique; and further investigating the impacts on various types of loads.

7. INVESTIGATION OF THE USE OF SHAZAM WHEN LOAD RELAYS ARE UNAVAILABLE

7.1. Load shedding using only line relays

7.1.1. Motivation and setup

Thus far, SHAZAM has been tested on distribution circuits where each load has an individual load relay. However, real distribution systems are not guaranteed to have load relays at every load. The following case considers SHAZAM's capability without any load relays. To test this potential, a PSCAD model of the IEEE 13-bus shown in Figure 1 is tested. As discussed in sections 3 and 4, three microgrids, supplied by three IBRs, are bounded by, "microgrid boundary relays" R3 and R10. The three smaller microgrids are connected to form one larger 13-bus microgrid that operates off-grid. For a more realistic system, SMA inverters are modeled in PSCAD and are used instead of generic IBR models. The load relays are removed from the system by disabling the relay logic and setting their corresponding breakers to remain closed throughout the simulation. Without the load relays, line relays (R1-R10) will have larger load areas to control. This section will cover the challenges induced from the lessened flexibility without load relays and the proposed solutions.

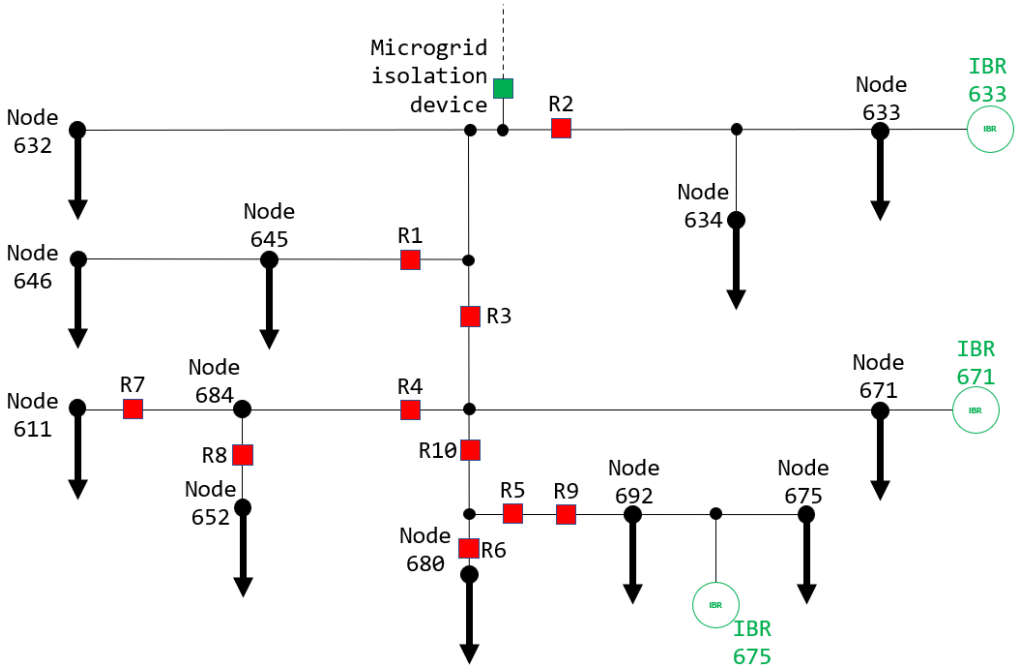

Figure 73: One-line diagram of the IEEE 13-bus system, operating off-grid, with three grid-forming IBRs (in green at the right) and without load relays.

7.1.2. Simulation of default case

In a situation without faults or overload conditions, i.e. the default case, the system is able to black start and all line relays come to steady state in about 10 seconds. The lack of load relay control does not impede the FLISR process. The relays successfully self-assemble themselves using the technique discussed in sections 3 and 4.

7.1.3. *Simulation of faulted case*

A 3LG fault is added on node 633 to test the FLISR process without load relays in a faulted system. In the PSCAD model, the fault occurs at 60s and occurs next to the 633 SMA inverter as shown in Figure 2. During the 120 second simulation, the inverters start up and all the line relays close by 30s. The system remains steady until, at 60s, when the fault triggers R3's UVOC function and R3 locks out. The rest of the line relays trip due to undervoltage and the breakers open. This isolates the upper microgrid from the rest of the system. Beginning from the line relays closest to inverters 671 and 675, R9 and R10, the line relays self-assemble the lower microgrid.

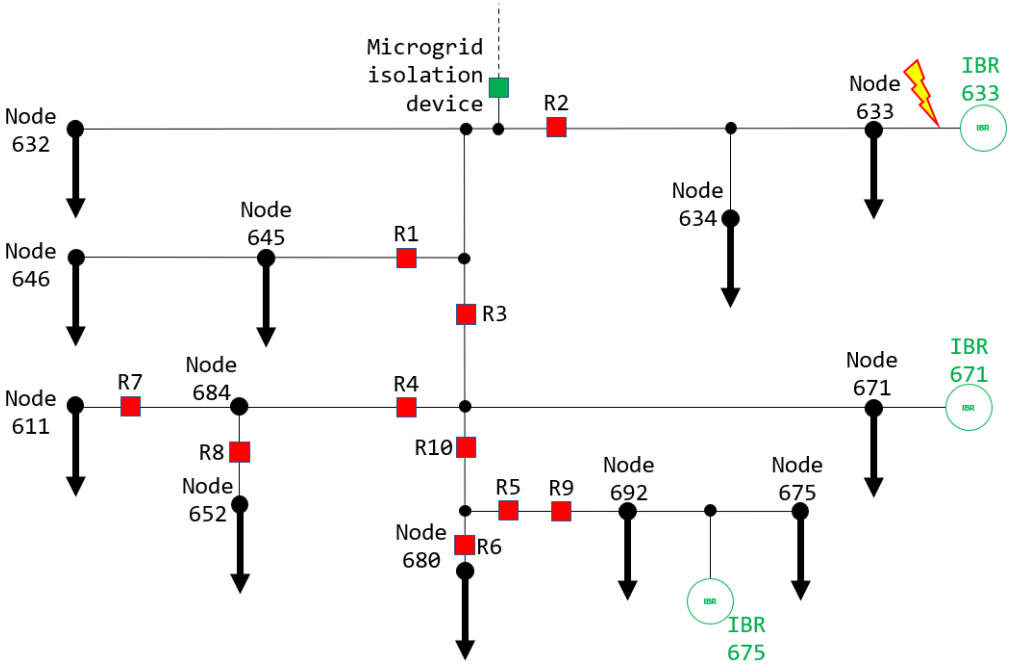

Figure 74: IEEE 13-bus distribution test circuit, without load relays, and with a 3LG fault at node 633.

In this case, the ideal response would be for R2 to lock out, so R3 and R1 can reclose and supply those load areas. However, in this simulation, the upper microgrid is left unserved. A proposed solution is investigated in the following section 7.2.

7.2. Use of "inverse tagged timers" to coordinate line relay tripping

7.2.1. *Problem statement*

Without the granularity induced by having load relays, there is significant cold load pickup for each line relay. In the IEEE 13-bus system, the line relays along the trunk, R3 and R5, experience especially large currents, about 1p.u. when closing onto the rest of the system. Additionally, without knowledge of which sources are available, there is considerable variability in the available fault current. Therefore, it is impractical to choose a UVOC current threshold when the potential fault currents and reclosing currents are inconsistent and overlapping.

7.2.2. Inverse tagged timers concept

The proposed solution is as follows, to stagger the underfrequency opening of the line relays based on the tagged timers established in section 4.2. Instead of closing in the assigned 'tagged timer' order, opening occurs in the opposite order, hence 'inverse.' Instead of relying on UVOC to trip the line relays, underfrequency tripping is used because the frequency is more consistent throughout the system than voltage or current. When the system frequency drops to 59.5Hz, the relays wait a certain delay time before opening. Using the tagged timers to order the opening of the relays helps keep the rest of the system operational while the fault is blocked off. The delay values are assigned to each line relay using:

$$\text{fdelaytag} = \left(\text{fdelay} + -0.3 * (\text{numTags} - \text{PosTag})\right)$$

where fdelay = 0.1s, numTags is the number of unique tags, and PosTag are the previously established tags. Each line relay gets the resulting time delay shown in Table 1. The tag number 1 corresponds to the relays closest to the inverters, that should remain closed as long as possible. Similarly, tag number 3 corresponds to the relays furthest from the inverters and loads that are shed first.

Table 18. Time delay values used in each line relay.

Line Relay	R1	R2	R3	R4	R5	R6	R7	R8	R9	R10
Tag Value	2	1	2	3	2	3	3	3	1	3
Time Delay	0.4s	0.7s	0.4s	0.1s	0.4s	0.1s	0.1s	0.1s	0.7s	0.1s

In addition, as discussed in section 7.1.3, the relay R3 is locking out instead of R2 during a fault on node 633. If the relay opening is staggered, relay R3 could open first on underfrequency and R2 could lock out on UVOC, since R2 is adjacent to the fault in this case.

7.2.3. Simulation of overload case using inverse tagged timers

To simulate an overload case in the IEEE 13-bus model, the IBR 671 is disconnected from the system. The system starts with all three IBRs present, but inverter 671 disconnects at 20 seconds. All the relays are closed by 20s. Immediately after 20s, relays R1, R4, R6, R7, R8, and R10 open due to undervoltage. R2, R3, R5, and R9 remain closed. Around 22s, inverter 675 shuts itself off due to its internal protection logic. Shortly after, the relays adjacent to inverter 675, R5 and R9, open due to the voltage dropping to zero. R3 eventually opens and continues to close and open every few seconds until the simulation ends as shown below in Figure 3. R1 also opens and closes continuously. When R1 or R3 closes, the voltage across the relays drops to about 0.93p.u. and causes them to reopen due to undervoltage.

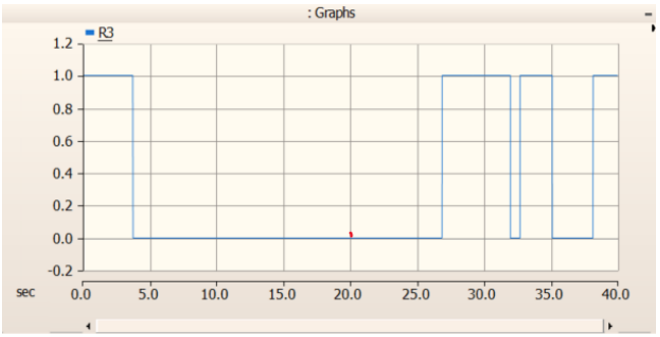

Figure 75: Line relay R3 opening and closing after loss of inverters 671 and 675.

In this simulation, the inverse tag timers successfully stagger the opening of relays. However, inverter 675 shutting off is not resolved from the tags. The opening and closing of relays R1 and R3 is another undesirable side effect caused by the loss of inverter 675.

Table 19. Sequence of events in simulation of overload case with inverse tagged timers.

Time	10s	20s	22s	24s	26s
Event	All relays close	R1,R4,R6,R7,R8,R10 open	IBR 675 turns off	R5,R9 open	R3 open

Additionally, simulations were run where inverter 671 was disconnected from the start of the run. In these tests, the system black starts with only two inverters. As in the previous case, IBR 675 turns off as well around 6s. None of the relays remain closed except R2 and R1. The upper microgrid remains active and is separated by R3, which remains open throughout the simulation. R3 stays open due to slightly low voltage, around 0.97p.u. on the 633 side.

Other solutions implemented include adding hysteresis to the frequency and voltage tripping and reclosure. At 59.5Hz, the relay trips on underfrequency and at 60Hz or higher, the relay is cleared for reclosure. The relays trip for voltage at 0.9p.u. and recloses at 0.95p.u. Another solution was replacing the internal SMA droop controls by an external droop controller. These two additions prevented R1 and R3 from bouncing between open and closed in the overload case. Figure 4 shows R1 and R3 remaining stable after inverter 671 disconnects at 20s. However, the issue of IBR 675 shutting off remains.

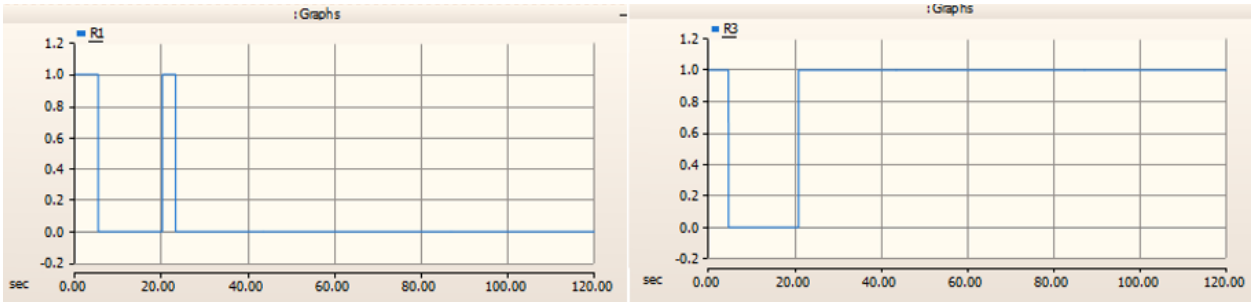

Figure 76: Line relays R1 and R3 maintaining their status after loss of inverter 671 at 20s.

7.2.4. Next steps without load relays

SHAZAM is limited without the flexibility of load relay control. The IEEE 13-bus system is stretched thin when losing an inverter and struggles to self-reassemble. As a possible solution, more line relays will be added to allow for smaller load areas to be served by each relay. To understand why IBR 675 shuts off, more information on the SMA inverter PSCAD model is needed. The manufacturer will be contacted to discuss the situation.

8. SCALING TO LARGER SYSTEMS

It is believed that there may be an upper limit on the scalability of SHAZAM because, in very large systems, inevitable small variations in timing will eventually add up sufficiently that load Groups and perhaps even load and line relay trip timings will overlap. It is thus important to explore SHAZAM using continually larger system models.

The first system model explored after the IEEE 13-bus is the IEEE 123-Bus distribution test circuit. The version of the l23-bus model used for SHAZAM is based on a model produced for other protection projects at Sandia. A one-line diagram of this system is shown in Figure 77.

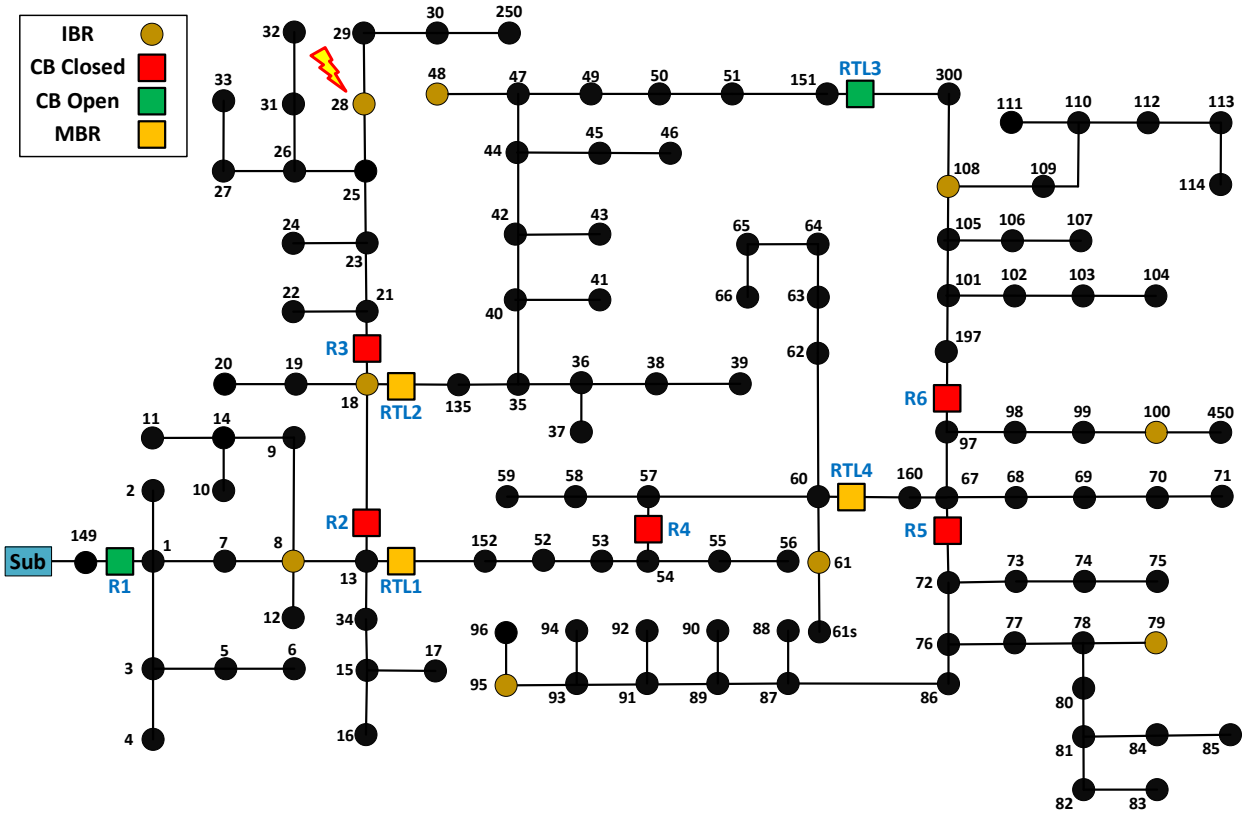

Figure 77. One-line diagram of the IEEE 123-bus distribution test circuit, as configured for this work. A fault is shown on bus 28 (upper left).

There are nine GFM IBRs in this system, six line relays, and four tie-line relays that serve as MBRs. One of the line relays, R1 (left side of Figure 77), serves as the Microgrid Isolation Device that disconnects the rest of the system from the grid. Also, if one of the MBRs is left always open, there is no way to form a closed loop in this system, and thus in this work RTL3 is always open. In this system, there is a GFM IBR in every zone between any two line relays; there are no zones that contain no sources. Furthermore, every IBR has sufficient capacity to carry its own zone, with some margin, meaning that each zone and the system overall are both generation-rich. Because there are sources on both sides of every line relay, in general all line relay closures in this system occur due to sync-check.

8.1. Initial testing

Initial testing of the SHAZAM line relays in the 123-bus system was performed using the grid source, with no GFM IBRs. Thus, for this initial step, the microgrid isolation device R1 is closed. The earliest incarnation of this model had line and load relays that initialized into a "closed" state. Thus, to initiate a reassembly, a 3LG fault at Bus 28 (upper-left portion of Figure 77) was implemented. The fault was set to occur at 5 s and persists through a 70-s simulation run time in order to check the line relay logic, including sync-check and UVOC.

8.2. Results to date

A demonstration of self-assembly in the IEEE 123 bus system *starting from the grid source*, with no IBRs, is given in Figure 78 through Figure 82. All load relays were set to Load Group C, and no tags were designated. The progress of self-assembly in this case is highlighted using **Red** bubbles. The system self-assembles correctly and isolates the fault at bus 28.

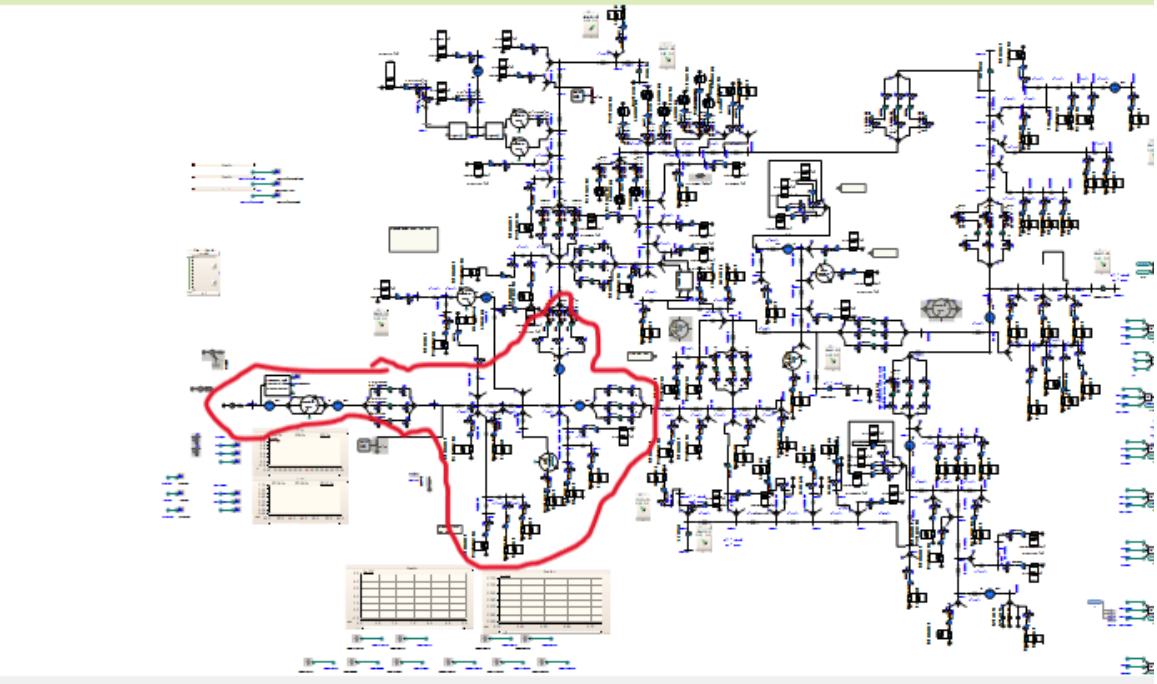

Figure 78. Initial set of line relay closures in the IEEE 123-bus system.

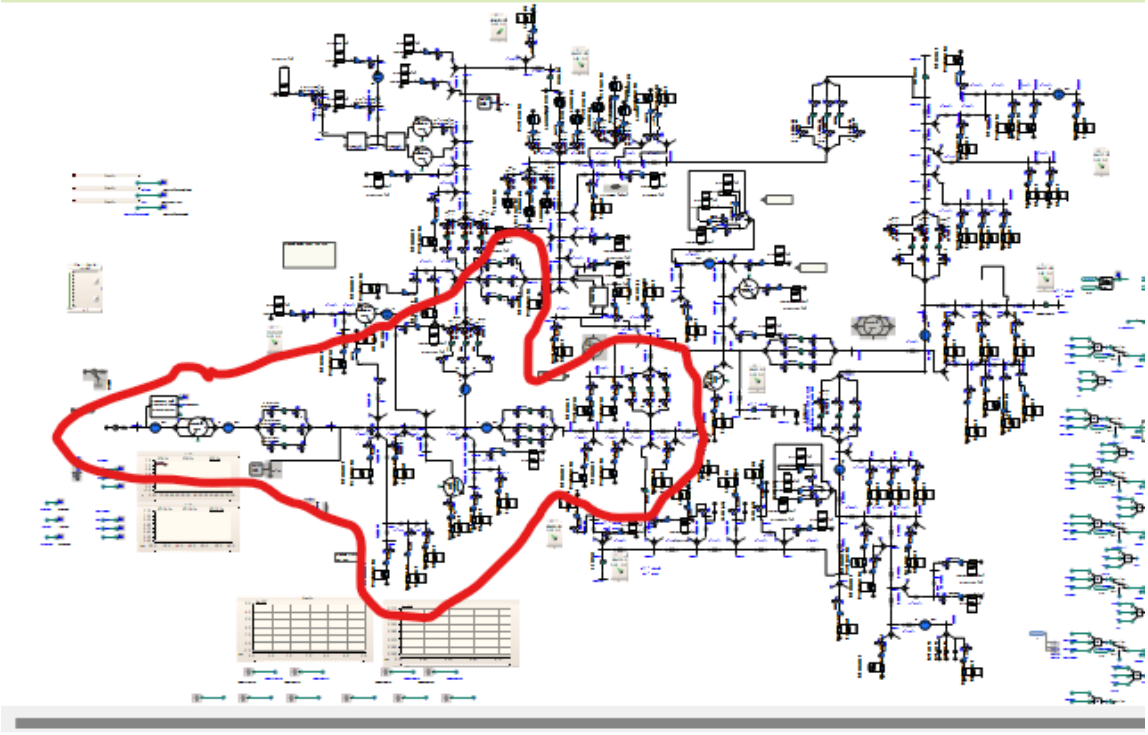

Figure 79. Second set of line relay closures in the IEEE 123-bus system.

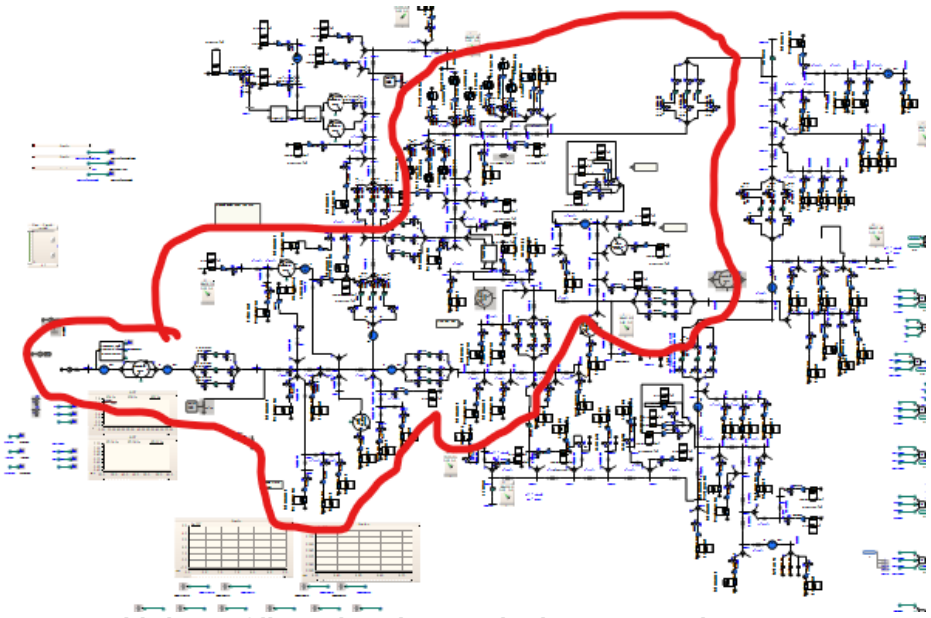

Figure 80. Third set of line relay closures in the IEEE 123-bus system.

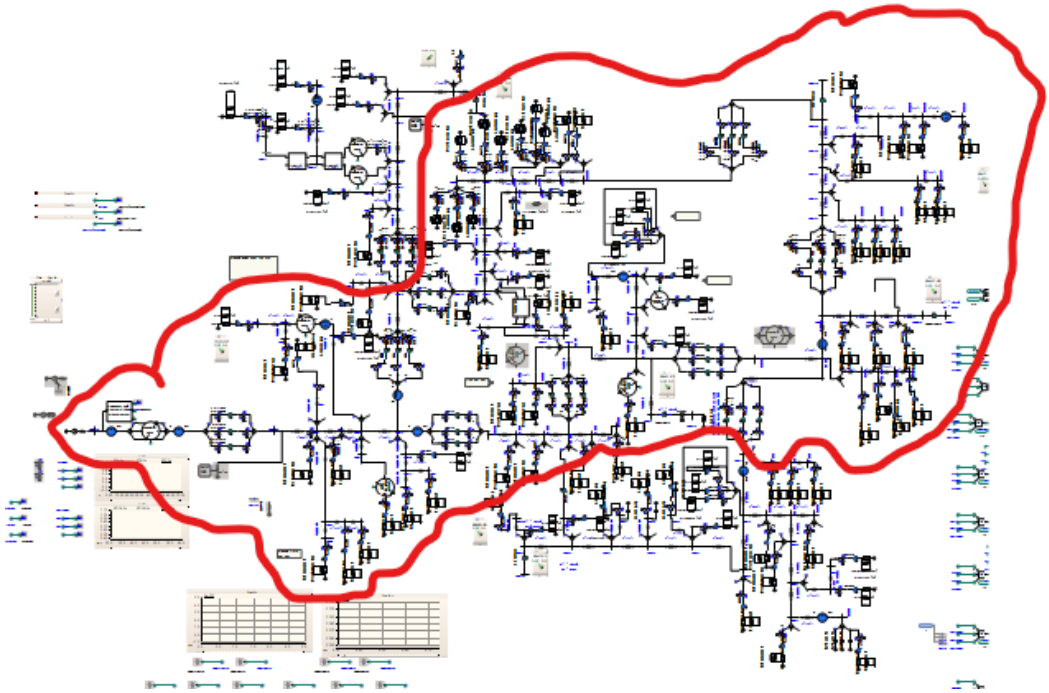

Figure 81. Fourth set of line relay closures in the IEEE 123-bus system.

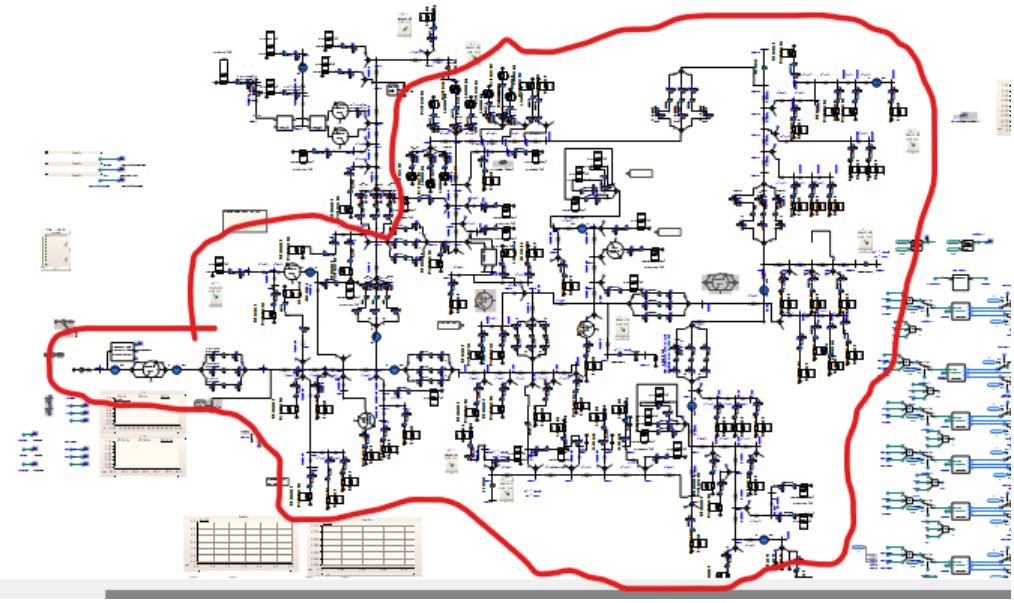

Figure 82. Final self-assembled state of the IEEE 123-bus system.

9. LACK OF NEED FOR BATTERIES IN LINE AND LOAD RELAYS

Figure 83 shows a photograph of the components in a cabinet that is part of a FLISR system. This system uses communications between the various system-reconfiguring elements of the system, and those communications must remain operational after the main power source has failed. Thus, this system includes batteries, and battery-maintenance infrastructure. In Figure 83, the components associated with the battery backup system are outlined with red boxes.

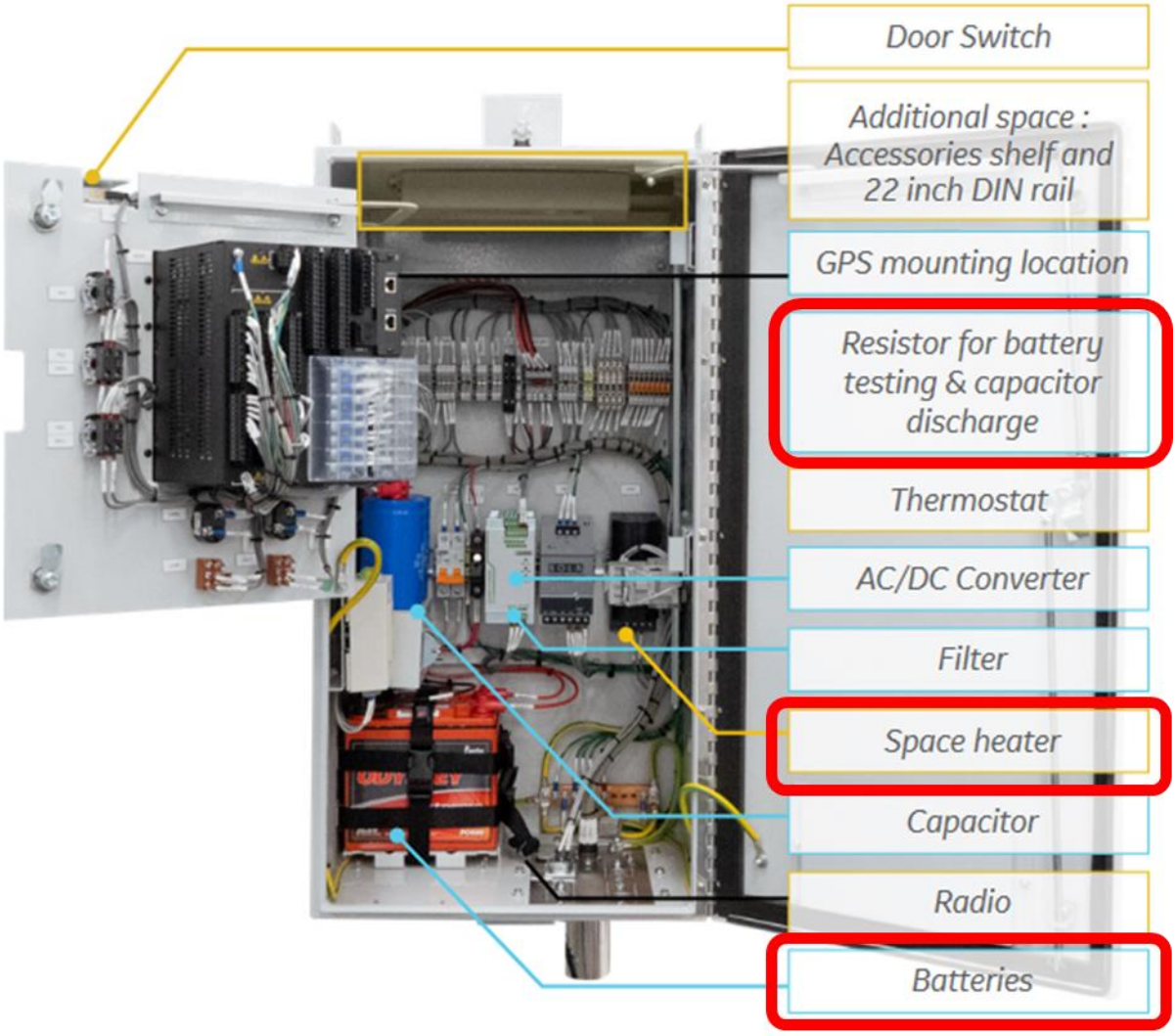

Figure 83. Annotated photograph of the contents of a cabinet used in a FLISR system.

In SHAZAM, the line and load relays use only local measurements, and the relays are not required to take any action at all until mains power reaches them. Thus, it is likely not necessary that SHAZAM relays have battery backup systems. The only requirement for a SHAZAM relay would be that the relay has to "fail open": when power is lost, the relay relaxes to an open state, and closes only when power is available.

This should be an advantage for SHAZAM, but the significance of this advantage is not yet clear. Certainly, battery backup systems are a well-known maintenance item that carries a nontrivial cost, and the batteries are responsible for a significant fraction of the size and weight of the relay cabinet. All of that would be eliminated with SHAZAM, but conversations with utility FLISR users have suggested that a) the cost of battery maintenance is not especially large (although quantitative values were not provided), and b) to date they have not experienced a FLISR system failure due to a failed or dead battery. Furthermore, conversations with relay manufacturers have indicated that configuring a relay to "fail open" is readily technically possible and does not add significant cost.

10. FUTURE WORK

10.1. Self-healing and self-assembly in systems with a combination of rotating generation and IBRs

Increasing numbers of intentionally-islanded power systems are energized solely by IBRs, but still, a significant fraction of intentional-island power systems for resilience purposes also include engine-generator sets. SHAZAM was designed to work with IBRs, but to improve its range of applicability, it is desired to work on its ability to incorporate rotating generation.

Figure 84 shows two configurations of intentional-island systems for resilience. On the left is a traditional system, in which all of the power is provided by a single, centralized engine-generator set. Historically, this is the way most power-resilience island systems were configured. In a system like this, the rotating machine provides a significant initial pulse of fault current, so protection can usually be handled by typical time-overcurrent, with proper consideration of minimum clearing times. SHAZAM is not needed in a system like this.

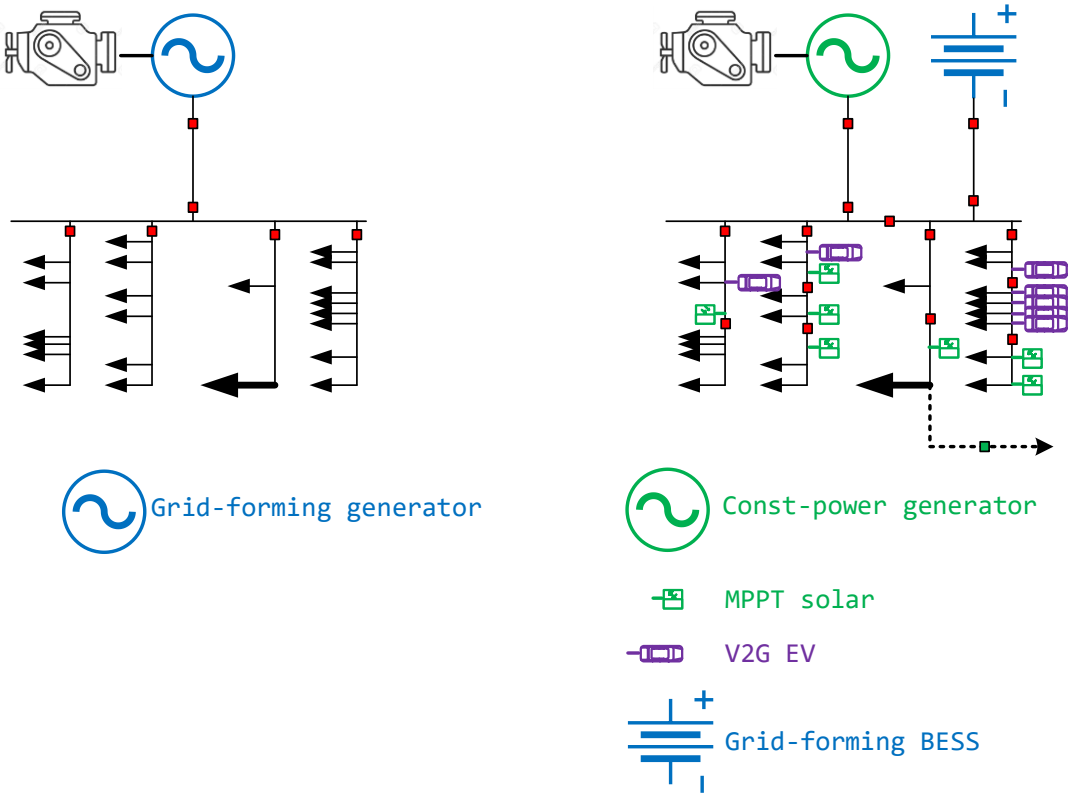

Figure 84. Two one-line diagrams of intentional-island power systems for resilience. Left: the traditional model, centered around a grid-forming engine-generator set. Right: a hybrid configuration including an engine-generator set in constant-power mode, a grid-forming battery plant, and distributed grid-following IBRs.

On the right in Figure 84 is a hybrid microgrid that includes a rotating machine, a central BESS plant, and various grid-following and grid-forming IBRs scattered across the microgrid. Often, in a system of this type the engine-generator is controlled to operate at its most efficient loading point (usually around 80% loading), and the BESS handles all voltage and frequency regulation, entering its charging

mode when the generator power exceeds the load power. When the BESS reaches a desired state of charge, the engine-generator shuts down. This is a configuration that is becoming more common, and because there are distributed IBRs, it is desirable that SHAZAM be able to work in a system like this. However, SHAZAM relies on undervoltage for much of its operation, and with the rotating generator in the system the voltage may not reliably fall when there is a fault.

With IBRs, there may be little to no gradient in voltage between the fault and the IBRs, but with a rotating generator, which does not have firm current limits, this will in general be much less true; the voltage gradient between the generator and the fault should be considerably larger then. In that case, it would be expected that the time-undervoltage function shown in Figure 2 may actually work *better*, achieving a higher degree of coordination between relays because of the voltage gradient.

The primary concern is that UVOC may no longer work to isolate the fault, because with the rotating machine there may not be enough undervoltage to trigger this function. At this time, the solution to this problem is thought to be to add time-overcurrent functions. The SHAZAM line relays will already have time-overcurrent functions because they will need these functions when the intentional-island system is grid-connected. It may be possible to

10.2. Investigation of the importance of different types of IBR fault current limiter on SHAZAM performance

The first versions of the 13-bus PSCAD model utilized a generic inverter model, based on a "Utility-grade BESS" model provided by Nayak, the PSCAD vendor. This generic model's control functions were primarily focused on the on-grid mode, so the SHAZAM team had to significantly develop the off-grid controls. This included adding both positive-rotating and negative-rotating dq0 controls to be able to obtain a very low voltage unbalance factor even when the loading is highly unbalanced; and adding a current limiter. The current limiter developed for this work operates by reducing the voltage reference when an overcurrent is detected, such that the islanded system is "browned out" until the current drawn from the IBRs is at or below the current limit. This current limiter has the advantage of maintaining highly sinusoidal voltages when current limited, but it has a key disadvantage: it is relatively slow to clamp the current to the limited value. The SHAZAM-developed current limiter requires 20-30 cycles to reduce the current to the limited value. This is much longer than the current-limiting times observed in manufacturer-specific PSCAD models and in manufacturer-supplied IBR fault current data, where current limiting may occur in just a few cycles for fast controllers or maybe on the order of 10 cycles for slower ones. It became immediately clear that the fact that the SHAZAM-developed current limiter was allowing much more overcurrent was artificially making it easier for the UVOC function to detect and isolate the fault. It was at this point that the work shifted primarily toward using manufacturer-specific code-based models.

These results made it clear that the performance of key SHAZAM functions, particularly UVOC, could be critically dependent on how the IBRs' current limiters work. Thus, future work should include use cases using other manufacturers' IBR models, and mixtures of IBR types with different current-limiting properties.

10.3. Improved means for integrating grid-following assets into off-grid SHePS

Grid-following (GFL) assets embedded into SHePS using the SHAZAM concept can create a challenge in maintaining generation-load balance under all conditions. The net load on the system, P_{net}, is:

$$P_{net} = P_{load} - P_{GFL} \tag{7}$$

where P_{load} is the total active power demand of all loads in the system, and P_{GFL} is the active power production of all GFL resources. The GFM IBRs supply P_{net}, and it is P_{net} that determines the frequency of the GFM IBRs via the P-f droop curve (Figure 1). Thus, the power provided by the GFL assets, P_{GFL}, causes the GFM IBRs to slide up the P-f droop curve to a higher frequency. Because the load relays in SHAZAM use system frequency as an indication of source loading, this frequency increase will allow more load relays to close, bringing more load onto the system. When the GFL asset then undergoes an uncontrolled change in output (e.g., a cloud passes over a solar array), the load formerly served by the GFL assets must quickly be picked up by the GFM IBRs.

If the total GFM IBR capacity in the off-grid system exceeds the total peak load (plus an acceptable margin) in all possible system configurations, and the GFM IBRs can ramp quickly enough to support the ramp rate of the load, then this situation does not necessarily present a problem. However, if the GFM IBR capacity is diminished for whatever reason, such that the total load in the system can exceed the GFM IBR capacity, then load must be shed every time a GFL output varies, or the system will go into voltage collapse. Unfortunately, the presence of sufficient GFM IBR capacity cannot always be guaranteed in a self-assembling off-grid SHePS, especially during contingency events that may make some sources unavailable. In these cases, it is necessary to suppress the operation of GFL assets by operating the system at an elevated frequency, typically above 60.5 Hz. For GFL assets compliant with either IEEE 1547-2003 or IEEE Std 1547-2018, 60.5 Hz is the overfrequency trip limit, so operation above that frequency prevents these sources from coming online. This enables the resilience benefits of SHePS even if the system does not have sufficient GFM IBRs to cover 100% of the load, but it wastes the energy that could have been generated by the GFL assets.

It is desirable to develop a better technique using only local measurements that would allow the participation of GFL assets without harming the ability of the system to maintain generation-load balancing.

REFERENCES

[1] D. Ghosh, R. Sharman, H. Rao and S. Upadhyaya, "Self-Healing Systems--Survey and Synthesis," *Elsevier Decision Support Systems,* vol. 42, pp. 2164-2185, 2007.

[2] F. Li, Z. Chen, L. Fan and P. Zhang, "Toward A Self-Healing Protection and Control System," in *40th North American Power Symposium*, September 2008.

[3] Y. Liu, R. Fan and V. Terzija, "Power System Restoration: A Literature Review From 2006 to 2016," *Journal of Modern Power Systems and Clean Energy,* vol. 4, no. 3, pp. 32-341, July 2016.

[4] R. Campos, C. Figueroa, H. Oyarzun and J. Baeza, "Self-Healing of Electric Distribution Networks: A Review," in *7th IEEE International Conference on Computers Communications and Control (ICCCC)*, May 2018.

[5] M. Elgenedy, A. Massoud and S. Ahmed, "Smart grid self-healing: Functions, applications, and developments," in *First IEEE Workshop on Smart Grid and Renewable Energy (SGRE)*, March 2015.

[6] S. Refaat, A. Mohamed and P. Kakosimos, "Self-Healing Control Strategy: Challenges and Opportunities for Distribution Systems in Smart Grid," in *12th IEEE International Conference on Compatibility, Power electronics and Power Engineering*, April 2018.

[7] J. Liu, X. Dong, X. Chen, X. Tong, X. Zhang and S. Xu, Fault Location and Service Restoration for Electrical Distribution Systems, Wiley, 2016.

[8] S&C Electric Company, "IntelliTeam® SG Automatic Restoration System," [Online]. Available: https://www.sandc.com/en/products--services/products/intelliteam-sg-automatic-restoration-system/. [Accessed 2023].

[9] Schweitzer Engineering Laboratories, Inc., "Improving System Performance Using SEL's Distribution Network Automation (DNA)," [Online]. Available: https://cms-cdn.selinc.com/assets/Literature/Publications/Case%20Studies/LCS0030_Westar%20Energy%20Case%20Study_20141103.pdf?v=20161024-215235. [Accessed 2023].

[10] D. Lagos, V. Papaspiliotopoulos, G. Korres and N. Hatziargyriou, "Microgrid Protection Against Internal Faults," *IEEE Power and Energy Magazine,* pp. 20-35, May/June 2021.

[11] L. Maurer, A. Stevens and W. Reder, "Tales From the Frontline: Keys to Successful Self-Healing Distribution Projects," *IEEE Power and Energy Magazine,* vol. 10, no. 2, pp. 100-106, March/April 2012.

[12] L. Yang, F. Xiao, H. Chen, Y. Lai and Y. Chollot, "The Experiences of Decentralized Self-Healing Grid," in *8th IEEE International Conference on Advanced Power System Automation and Protection (APAP)*, October 2019.

[13] P. Anderson, Power System Protection, IEEE Press, 1999.

[14] M. Reno, S. Brahma, A. Bidram and M. Ropp, "Influence of Inverter-Based Resources on Microgrid Protection, Part 1: Microgrids in Radial Distribution Systems," *IEEE Power and Energy Magazine,* pp. 36-46, May/June 2021.

[15] K. Sun, Y. Hou, W. Sun and J. Qi, Power System Control Under Cascading Failures, IEEE Press, 2019.

[16] J. Brombach, C. Hachmann, D. Lafferte, A. Klingman, W. Heckmann, F. Welck, D. Lohmeier and H. Becker, "“The Future of Power System Restoration”," *IEEE Power and Energy Magazine,* pp. 30-41, Nov/Dec 2018.

[17] M. Ropp, O. Lavrova, S. Ranade, A. Ramoko and C. Valdez, "Results of Late-Start LDRD Project 'SHAZAM'," *Sandia National Laboratories report SAND2021-11593,* September 2021.

[18] E. Silva, O. Lavrova and M. Ropp, "Protection Elements for Self-Healing Microgrids Using Only Local Measurements," in *North American Power Symposium (NAPS)*, October 9-11 2022.

[19] "Nature Portfolio definition of "self-assembly"," [Online]. Available: https://www.nature.com/subjects/self-assembly. [Accessed 2023].

[20] "Lumitos Industrial Portal ChemEurope," 2023. [Online]. Available: https://www.chemeurope.com/en/encyclopedia/Self-assembly.html.

[21] "IEEE PES Test Feeder," [Online]. Available: https://cmte.ieee.org/pes-testfeeders/resources/. [Accessed 2023].

[22] "IEEE Std C57.153-2017 - IEEE Guide for Paralleling Regulating Transformers".

[23] "IEEE Std C37.230-2007 - IEEE Guide for Protective Relay Applications to Distribution Lines See Clause 6.".

[24] J. Myers, A. Well and R. Lorch Jr., Research Design and Statistical Analysis, 3rd ed ed., Routledge, 2010.

[25] M. Lave, J. Stein, A. Ellis, C. Hansen, E. Nakashima and Y. Miyamoto, "Ota City: Characterizing Output Variability from 553 Homes with Residential PV Systems on a Distribution Feeder," *Sandia National Laboratories report SAND2011-9011,* November 2011.

[26] J. Vandermeer, B. Schenkman, M. Baca, M. Mueller-Stoeffels and C. Koplin, "Cordova Electric Cooperative Energy Storage Evaluation," *Sandia National Laboratories report SAND2017-13084,* November 2017.

[27] "MATLAB "corr" function description," [Online]. Available: https://www.mathworks.com/help/stats/corr.html. [Accessed 2023].

[28] D. Novosel and R. King, "Using Artificial Neural Networks for Load Shedding to Alleviate Overloaded Lines," *IEEE Transactions on Power Delivery,* vol. 9, no. 1, pp. 425-433.

[29] P. Song, Z. Xu and H. Dong, "UFPC-Based Line Overload Control for Power System Security Enhancement," *IET Generation, Transmission and Distribution,* p. 8, June 2017.

[30] L. Lenoir, I. Kamwa and L. Dessaint, "Overload Alleviation with Preventive-corrective Static Security Using Fuzzy Logic," *IEEE Transactions on Power Systems,* vol. 24, no. 1, pp. 134-145, February 2009.

[31] Schneider Electric, "How many ON-OFF operations can a circuit breaker withstand?," [Online]. Available: https://www.se.com/us/en/faqs/FA87608/. [Accessed 2023].

[32] R. Rodriguez, Y. Du, A. Antoniazzi and P. Cairoli, "A Review of Solid-State Circuit Breakers," *IEEE Transactions on Power Electronics,* vol. 36, no. 1, pp. 364-377, January 2021.

DISTRIBUTION

Email—Internal

Name	Org.	Sandia Email Address
Valerio DeAngelis	8814	vdeange@sandia.gov
Charles Hanley	8810	cjhanle@sandia.gov
Craig Lawton	8815	crlawto@sandia.gov
Matthew Reno	8813	mjreno@sandia.gov
Michael Ropp	8814	meropp@sandia.gov
Technical Library	1911	sanddocs@sandia.gov

Email—External

Name	Company Email Address	Company Name
Olga Lavrova	olavrova@nmsu.edu	New Mexico State University
Satish Ranade	sranade@nmsu.edu	New Mexico State University

This page left blank

Sandia National Laboratories

Sandia National Laboratories is a multimission laboratory managed and operated by National Technology & Engineering Solutions of Sandia LLC, a wholly owned subsidiary of Honeywell International Inc. for the U.S. Department of Energy's National Nuclear Security Administration under contract DE-NA0003525.